RICE UNIVERSITY

Harnessing Inflammatory Signaling to Promote Bone Regeneration and Mitigate Joint Damage

by

Paschalia Maria Mountziaris

A THESIS SUBMITTED
IN PARTIAL FULFILLMENT OF THE
REQUIREMENTS FOR THE DEGREE

Doctor of Philosophy

APPROVED, THESIS COMMITTEE

Antonios G. Mikos, Louis Calder Professor
Bioengineering and Chemical and
Biomolecular Engineering, Rice University

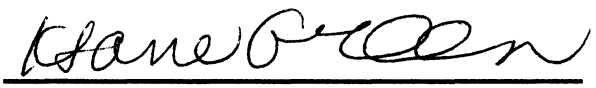

K. Jane Grande-Allen, Associate Professor
Bioengineering, Rice University

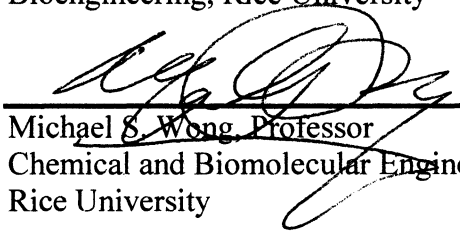

Michael S. Wong, Professor
Chemical and Biomolecular Engineering,
Rice University

HOUSTON, TEXAS
AUGUST 2011

ABSTRACT

Harnessing Inflammatory Signaling to Promote Bone Regeneration and Mitigate Joint Damage

by

Paschalia Maria Mountziaris

Inflammatory processes are infamous for their destructive effects on tissues and joints in a variety of diseases. Within the body, inflammation is a highly regulated biological response whose purpose is to promote tissue regeneration following injury. However, in certain settings, inflammation persists and leads to progressive tissue destruction. This thesis focused on modulating inflammatory signaling in both contexts. Part I investigated the effects of a model pro-inflammatory cytokine, tumor necrosis factor-alpha (TNF-α), on the *in vitro* osteogenic differentiation of mesenchymal stem cells (MSCs). In contrast, Part II describes the development and *in vivo* evaluation of the first intra-articular controlled release system for the temporomandibular joint (TMJ), which silences inflammatory signaling and thus mitigates the painful joint damage seen in inflammatory TMJ disease. The following specific aims were addressed: (1) to determine the concentration of TNF-α that enhances *in vitro* osteogenic differentiation of MSCs; (2) to determine the temporal pattern of TNF-α delivery that enhances *in vitro* osteogenic differentiation of MSCs; (3) to determine the impact of bone-like extracellular matrix (ECM) on the concentration and temporal pattern of TNF-α delivery that enhances *in vitro* osteogenic differentiation of MSCs; (4) to evaluate the biocompatibility of intra-articular microparticles in the rat TMJ; (5) to develop a microparticle-based formulation

for sustained release of a model anti-inflammatory small interfering ribonucleic acid (siRNA); and (6) to evaluate the therapeutic efficacy of intra-articular microparticles delivering siRNA in an animal model of TMJ inflammation. These studies led to the development of powerful strategies to rationally control inflammation to promote bone regeneration and mitigate joint damage in the setting of disease, both of which will ultimately improve the quality and specificity of therapies available in modern medicine.

Acknowledgments

This work would not have been possible without the constant, unwavering support and advice of my advisor, family, and friends. I faced a tremendous personal ordeal during my graduate school years, and I would not have been able to cope without you. I am very thankful to Dr. Mikos for both professional and personal advice; you have always been so supportive and encouraging, and I have really enjoyed learning and growing as a scientist in your lab. Of course, I am also extremely thankful for the encouragement and love of Rob, Yianni, Maria, Mom and Dad. I love you guys.

For their generous financial support of my graduate school career, I thank the Baylor College of Medicine Medical Scientist Training Program and Transco Energy Company M.D./Ph.D. Endowed Fellowship; the National Institutes of Health (NIH) Graduate Fellowship in Nanobiology through the Gulf Coast Consortia Consortia and W.M. Keck Center for Interdisciplinary Bioscience Training (NIH Grant No. 5 T90 DK070121-04); and the NIH Graduate Fellowship in Biotechnology (NIH Grant No. 5 T32 GM008362-19). The research described in this thesis was funded by the NIH (R01 DE17441 and R01 DE15164 to my advisor, AGM). I would like to thank Dr. Phillip Kramer for his advice and technical assistance with the *in vivo* studies described in the second part of this thesis. I would also like to thank the members of my committee for all of their advice and encouragement.

Finally, I cannot overlook my friends and lab mates in the Mikos Lab. Thank you for making me feel included, encouraging me, and providing much-needed breaks from the endless hours spent in lab. I also thank the undergraduate and high school students

that I have mentored in the lab (David Sing; Denny Lehman; Stephanie Tzouanas; Laura Ureste; and Sophia Dao) for assisting me with these studies and for brightening my day with their enthusiasm for research.

Contents

List of Figures

List of Tables

Abbreviations

ALP	alkaline phosphatase
b-FGF	basic fibroblast growth factor
BMP	bone morphogenetic protein
CD16	Fc receptor-III for IgG
CFA	Complete Freund's Adjuvant
COX	cyclooxygenase
CXCL2	chemokine (C-X-C motif) ligand 2
+dex	supplemented with dexamethasone
DLS	dynamic light scattering
ECM	extracellular matrix
EP1	prostaglandin E2 receptor type 1
FcγRIII	alternative abbreviation for CD16
FDA	United States Food and Drug Administration
HA	hyaluronic acid
IFN	interferon
IgG	type G immunoglobulin
IL	interleukin
IL-1R	interleukin-1 receptor
MSC	mesenchymal stem cell
MP	microparticle
NF-κB	nuclear factor-kappa-B

N:P ratio	Nitrogen:Phosphate ratio
NSAID	non-steroidal anti-inflammatory drug
PBS	phosphate-buffered saline
PCL	poly(ε-caprolactone)
PDGF	platelet-derived growth factor
PEG	poly(ethylene glycol)
PEI	poly(ethylenimine)
PLA	poly(DL-lactic acid)
PLGA	poly(DL-lactic-co-glycolic acid)
PLLA	poly(L-lactic acid)
PPS	poly(propylene sulphide)
RNA	ribonucleic acid
r-PEI	rhodamine-conjugated PEI
SDF-1	stromal cell-derived factor-1
SEM	scanning electron microscopy
siRNA	small interfering ribonucleic acid
STAT1	signal transducer and activator of transcription 1
TGF-β	transforming growth factor beta
TMJ	temporomandibular joint
TNF-α	tumor necrosis factor alpha
TNFR	tumor necrosis factor receptor
UV	ultraviolet light
VEGF	vascular endothelial growth factor

Chapter 1

Introduction and Objectives

Inflammatory processes are infamous for their destructive effects on tissues and joints in a variety of diseases. Within the body, inflammation is a highly regulated biological response whose purpose is to promote tissue regeneration following injury. However, in certain settings, inflammation persists and leads to progressive tissue destruction. The studies presented in this thesis focused on modulating inflammatory signaling in both contexts. Part I (Chapters 2-6) of the thesis investigated the effects of a pro-inflammatory cytokine, tumor necrosis factor-alpha (TNF-α), on the *in vitro* osteogenic differentiation of mesenchymal stem cells. In contrast, Part II (Chapters 7-10) describes the development of a novel intra-articular controlled release system to silence inflammatory signaling and prevent painful joint degeneration seen in inflammatory temporomandibular joint disease.

The goal of the studies described in Part I was to characterize the effects of a pro-inflammatory cytokine, tumor necrosis factor alpha (TNF-α), on the osteogenic differentiation of mesenchymal stem cells (MSCs). TNF-α was selected as a model inflammatory signal for these studies based on its significant impact on *in vivo* bone regeneration (1, 2). We hypothesized that delivery of TNF-α would enhance the osteogenic differentiation of MSCs. Due to the many gaps in our knowledge regarding the mechanism by which inflammatory signals trigger regeneration, the studies described in this thesis were conducted entirely *in vitro* and focused on establishing the optimal parameters for a novel tissue engineering strategy to rationally control inflammation and trigger osteogenesis at the site of a large bone injury.

In vitro osteogenic differentiation of mesenchymal stem cells typically involves the addition of dexamethasone, an anti-inflammatory agent that might mask the effects of TNF-α (3-5). Our laboratory has developed a method that supports continued *in vitro* osteogenic differentiation of MSCs without the need for dexamethasone; MSCs expanded in the presence of dexamethasone experience continued osteogenic differentiation in the absence of dexamethasone by means of a 3D porous scaffold containing pre-generated bone-like extracellular matrix (ECM) (6-11). The studies described herein established the optimal dosage and temporal pattern of delivery of TNF-α to enhance osteogenic differentiation of MSCs cultured in a 3D biodegradable polymer scaffold.

The goal of the studies in Part II of this thesis was to develop an intra-articular sustained release system to treat painful temporomandibular joint (TMJ) inflammation. TMJ disorders are a heterogeneous group of disorders that are characterized by painful, progressive joint degeneration. Although TMJ disorders are typically non-inflammatory

in origin, joint inflammation commonly appears as the disorder progresses, and this worsens the painful symptoms and also appears to accelerate destruction of TMJ tissue (12). The ultimate goal of the studies described herein was to develop a sustained release system for a model anti-inflammatory agent, a small interfering RNA (siRNA) sequence that silences inflammatory signaling.

A sustained release system was a critical component of the design because it addresses a major limitation of current intra-articular injectable formulations used to treat severe, painful TMJ degeneration: rapid clearance of injected agents, which necessitates frequent injections that carry a high risk of iatrogenic joint injury (12, 13). Although numerous drug delivery systems have been developed for various applications, including intra-articular controlled release in large joints like the knee (see summary in Table 7.1), no sustained release systems had been developed for the TMJ (13) prior to the studies described in this thesis.

The following specific aims were investigated:

Specific Aim 1

To determine the concentration of TNF-α that enhances *in vitro* osteogenic differentiation of MSCs. Osteogenic differentiation of MSCs was triggered via preculture with osteogenic supplements, including dexamethasone. MSCs were then seeded onto 3D biodegradable polymeric meshes and varying doses of TNF-α were delivered in the absence of dexamethasone (14).

Specific Aim 2

To determine the temporal pattern of TNF-α delivery that enhances *in vitro* osteogenic differentiation of MSCs. Using the optimal dosage established in Specific Aim 1, these studies established the optimal temporal pattern of TNF-α delivery (early, intermediate, late, or continuous) to promote osteogenic differentiation of MSCs. In parallel, since Specific Aim 1 indicated that TNF-α supports continued osteogenic differentiation of MSCs in the absence of dexamethasone, these studies investigated whether TNF-α was sufficient to trigger osteogenic differentiation of dexamethasone-naïve MSCs.

Specific Aim 3

To determine the impact of bone-like ECM on the concentration and temporal pattern of TNF-α delivery that enhances *in vitro* osteogenic differentiation of MSCs. The studies in Specific Aims 1 and 2 provided the optimal TNF-α delivery parameters for osteogenic differentiation of MSCs and indicated that TNF-α supports, but does not induce, osteogenic differentiation. To create a more realistic *in vitro* model of the injured bone microenvironment and explore the interplay of TNF-α and bone-like ECM, varying doses of TNF-α were delivered to osteogenically differentiating MSCs cultured *in vitro* on 3D biodegradable microfiber scaffolds containing pregenerated bone-like ECM.

Specific Aim 4

To evaluate the biocompatibility of intra-articular microparticles in the rat TMJ. We were particularly cautious in the development of a sustained release system for the TMJ due to the lack of previous data regarding TMJ tissue response and also because of the terrible history of early alloplastic (Proplast-Teflon) TMJ implants; their susceptibility to mechanical failure gave rise to Teflon microparticles that induced severe foreign body immune reactions and massive TMJ damage (15). Thus, the first step was to evaluate the *in vivo* biocompatibility of the carrier material, poly(DL-lactic-co-glycolic acid) microparticles (PLGA MPs), and determine the impact of PLGA MP concentration on healthy TMJ function (16).

Specific Aim 5

To develop a microparticle-based formulation for sustained release of a model anti-inflammatory small interfering ribonucleic acid (siRNA). As the next step in the development of an intra-articular controlled release system to treat painful TMJ inflammation, we developed several PLGA MP formulations encapsulating polyplexes consisting of siRNA and branched poly(ethylenimine) (PEI), which is a common polymeric transfecting agent. The effect of siRNA loading, as well as the effect of the relative amounts of PEI and siRNA, on the release kinetics of siRNA-PEI polyplexes was determined. The size and the relative PEI-to-siRNA content of the polyplexes released over time were also characterized (17).

Specific Aim 6

To evaluate the therapeutic efficacy of intra-articular PLGA MPs delivering siRNA-PEI polyplexes in an animal model of TMJ inflammation. Although several inflammatory mediators, including TNF-α and type G immunoglobulins (IgGs) are elevated in the TMJs of patients and animal models with painful inflammation (18-20), injection of these agents does not reproduce the severe inflammation seen in TMJ disorders. For example, intra-articular injection of TNF-α yields only mild inflammation in animal models, requiring the injection of an irritant to establish an animal model of joint inflammation (21). In this study, we used Complete Freund's Adjuvant (CFA), a severely irritating water-in-oil emulsion containing killed *Mycobacterium tuberculosis* and paraffin oil, to induce inflammation in the rat TMJ. This is an established, optimized method of establishing a model of TMJ inflammation (22-27). This joint disease model then received PLGA MPs loaded with anti-inflammatory-siRNA-PEI polyplexes, to evaluate the efficacy of the first intra-articular sustained release system for the TMJ.

Part I:
Harnessing Inflammatory Signaling to Promote Bone Regeneration

Chapter 2

Background: Modulation of the Inflammatory Response for Enhanced Bone Tissue Regeneration[1,2]

Abstract: Pro-inflammatory cytokines are infamous for their catabolic effects on tissues and joints in both inflammatory diseases and following the implantation of biomedical devices. However, recent studies indicate that many of these same molecules are critical for triggering tissue regeneration following injury. This review will discuss the role of inflammatory signals in regulating bone regeneration and the impact of both

---

[1] This chapter was published as: Mountziaris PM, Mikos AG. Modulation of the inflammatory response for enhanced bone tissue regeneration. Tissue Eng Part B Rev 2008;14(2):179-186.

[2] A second manuscript detailing advances in the field from 2008-2011 is included in the next chapter.

[3] This chapter will be published as: Mountziaris PM, Spicer PP, Kasper FK, Mikos AG. Harnessing and

[2] A second manuscript detailing advances in the field from 2008-2011 is included in the next chapter.

immunomodulatory and anti-inflammatory pharmacologic agents on fracture healing, to demonstrate the importance of incorporating rational control of inflammation into the design of tissue engineering strategies.

2.1. Introduction

The limitations of current bone reconstruction techniques have led to increased interest in bone tissue engineering. Bone has the remarkable capacity to heal without scar formation, but this regenerative process fails in patients with large bone lesions or impaired wound healing, requiring clinical intervention. Autologous bone grafts are the current gold standard solution to repair critical size bone defects, but their use is limited by the availability of suitable donor tissue. Another problem is the necessity for a second surgery to harvest graft tissue, with potentially severe complications such as hemorrhage, nerve damage, infection, and deformity. Bone tissue engineering has emerged as a new interdisciplinary strategy to promote healing of large bone defects using bioactive implantable materials. Cells and bioactive factors are incorporated into these scaffolds to provide temporal and spatial cues guiding bone regeneration (28, 29). The rational design of these scaffolds is informed by cell and developmental biology, which provide increasingly detailed knowledge of the cellular and molecular signals directing bone healing.

Fracture healing involves complex molecular signaling and induces significant changes in the expression of several thousand genes (30, 31). To develop an effective tissue engineering strategy for bone regeneration, the "master switches" controlling this process must be identified and incorporated (32). The importance of osteogenic factors,

including bone morphogenetic proteins, in bone regeneration is well known, and they are consequently widely used in bone tissue engineering systems, though with limited success. However, the critical role of pro-inflammatory cytokines in initiating regeneration remains poorly recognized in both biology and tissue engineering (33, 34). As such, to our knowledge, limited work has been done in tissue engineering to harness inflammatory signaling. This review will discuss the role of inflammatory signals in regulating bone regeneration and the impact of anti-inflammatory and immunomodulatory pharmacologic agents on fracture healing, to demonstrate the importance of incorporating rational control of inflammation into the design of tissue engineering strategies.

2.2. Bone Regeneration Following Injury: An Overview of Molecular Signaling

Bone fractures heal by either a direct (primary) or an indirect (secondary) mechanism. Primary healing refers to direct tunneling of remodeling units from the cortex across the fracture line and into the cortex on the other side. This type of healing is rare, as it requires that fracture fragments be restored to their original anatomic location and rigidly stabilized at the site. Since typical treatments, e.g. plaster cast placement, do not completely immobilize the injured bone, fractures typically heal by secondary healing (35, 36). This process involves overlapping phases of inflammation, renewal, and remodeling.

2.2.1. Inflammatory Phase

Bone fracture is an injury, and thus incites an inflammatory response, which peaks 24 hours following the injury and is complete by the first week (37). During this time, a complex cascade of pro-inflammatory signals and growth factors are released in a temporally and spatially controlled manner (38). Levels of several inflammatory mediators, including IL-1, IL-6, IL-11, IL-18, and TNF-α, are significantly elevated within the first few days (30, 38). These signals recruit inflammatory cells and promote angiogenesis (38, 39). Platelets are activated by injury to blood vessels at the fracture site, and release TGF-β1 and PDGF. Osteoprogenitor cells at the fracture site express bone morphogenetic proteins (37, 40). These factors, along with inflammatory mediators, recruit mesenchymal stem cells and then guide their differentiation and proliferation (35, 41, 42).

2.2.2. Renewal Phase

At the periphery of the fracture site, stem cells differentiate into osteoblasts. As a result, bone forms via intramembranous ossification 7-10 days after injury (35). Chondrogenesis occurs in the bulk of the injured tissue, which is mechanically less stable (37, 42). Inflammatory mediators are absent during this phase. TGF-β2 and -β3, bone morphogenetic proteins, and other molecular signals induce endochondral bone formation in the cartilaginous callus (37, 38). The cartilage calcifies, and then is replaced with woven bone (39, 41).

2.2.3. Remodeling

Osteoprogenitor cells differentiate into osteoblasts, which express IL-1, IL-6, and IL-11, and other factors that promote osteoclast formation (41). The renewing and

resorptive actions of these two cell types replace the initial woven bone with lamellar bone. This remodeling phase is regulated by several pro-inflammatory signals. In addition to IL-1, IL-6, and IL-11, elevated levels of TNF-α, IL-12, and IFN-γ are also detectable at the fracture site (30, 38). Rodent and porcine models indicate that growth hormone and parathyroid hormone also play key roles in this phase, speeding healing and strengthening the fracture callus (43-46). Although the original structure and mechanical properties of the skeleton are restored within several weeks of fracture, molecular and cellular signaling can take up to several years to return to its normal state. In human patients, hormones regulating bone metabolism remain at elevated levels for up to one year after hip fracture (47). Bone turnover is significantly accelerated in humans for at least 6 months following bone fracture, and does not return to baseline for several years (47-51).

2.2.4. Comparison to embryonic bone development

Although fracture healing is very similar to skeletogenesis in the developing embryo, there are key differences in the regulation of each process. Mechanical stimulation has a unique effect in fracture healing. An unstable environment promotes chondrogenesis, while a stable environment promotes osteogenesis (52). The inflammatory response is also unique to fracture healing. Since bone fracture is an injury, it incites an inflammatory response. Inflammatory signals result in a local increase in macrophages, which in turn release factors and cytokines that promote healing. In contrast, bone formation occurs throughout the skeleton in a developing embryo, so systemic osteogenic signals prevail (52). Although tissue engineering strategies typically involve materials that mimic the structure and function of healed bone, recent progress in

developmental biology suggests that rapid regeneration may be achieved via scaffolds that simply trigger the "master switch" for regeneration (32). A growing body of evidence suggests that inflammatory signals are critical for the initiation of the fracture healing response.

2.3. Role of Pro-inflammatory Molecules in Fracture Healing

Pro-inflammatory cytokines are best known for their destructive effects on bone in a number of clinical contexts, and as such have not been extensively explored as potential initiators of regeneration in bone tissue engineering strategies. In biomaterials research, TNF-α, IL-1, and other pro-inflammatory cytokines are best known as mediators of the foreign body reaction, an inflammatory response that can cause both severe tissue damage and premature failure of implanted materials (53). Pro-inflammatory molecules are also infamous for their catabolic effects on bone in patients with rheumatic diseases. High circulating levels of TNF-α and IL-1 in arthritis patients are directly linked to joint and bone destruction (54). In a mouse model of arthritis, absence of IL-1 due to a genetic mutation prevents bone and joint disease (55). Although it seems paradoxical, these same pro-inflammatory factors promote bone fracture healing.

Unlike the unregulated, prolonged inflammation seen in severe foreign body reactions and bone pathologies like rheumatoid arthritis, inflammatory signaling in fracture healing is highly regulated and brief. Although inflammatory cells, mainly neutrophils and macrophages, are found at the site of an injury, their absence does not adversely affect tissue repair in mice (56). Recent studies in cell and developmental biology suggest that the pro-regenerative function of inflammatory signals is a

consequence of changes in the tissue microenvironment (e.g. expression of cell-surface receptors) triggered by injury. TNF-α, IL-1, and other inflammatory molecules are resilient molecules that readily diffuse through the extracellular matrix and are thus ideally suited for transmission of signals guiding regeneration. As discussed in this section, altered levels of TNF-α, IL-1, and other pro-inflammatory molecules have a major effect on the healing of bone fractures (57).

2.3.1. Tumor Necrosis Factor (TNF-α)

TNF-α and related molecules can either trigger cell death or promote cell survival depending on the specific cell-surface receptor they bind, the cell type, and the intracellular signaling cascade that is subsequently activated (58). In fracture healing, the expression of TNF-α and its receptors, TNFR1 and TNFR2, follows a biphasic pattern. As shown in Figure 2.1, TNF-α concentration peaks 24 hours after bone injury in mouse models, returning to baseline levels within 72 hours. During this period, TNF-α is mainly expressed by macrophages and other inflammatory cells (38, 59). This brief TNF-α signaling is believed to induce the release of secondary signaling molecules and to exert a chemotactic effect, recruiting cells necessary for bone regeneration. TNF-α concentration rises again approximately two weeks later, during endochondral bone formation (see Figure 1). During this period, TNF-α is expressed by osteoblasts and other cells of mesenchymal origin, including hypertrophic chondrocytes undergoing endochondral bone formation (30, 59). Absence of TNF-α impairs fracture healing in mice, delaying endochondral bone formation by several weeks. However, TNF-α-deficient mice have normal skeletons, suggesting that TNF-α signaling is unique to post-natal fracture repair (1).

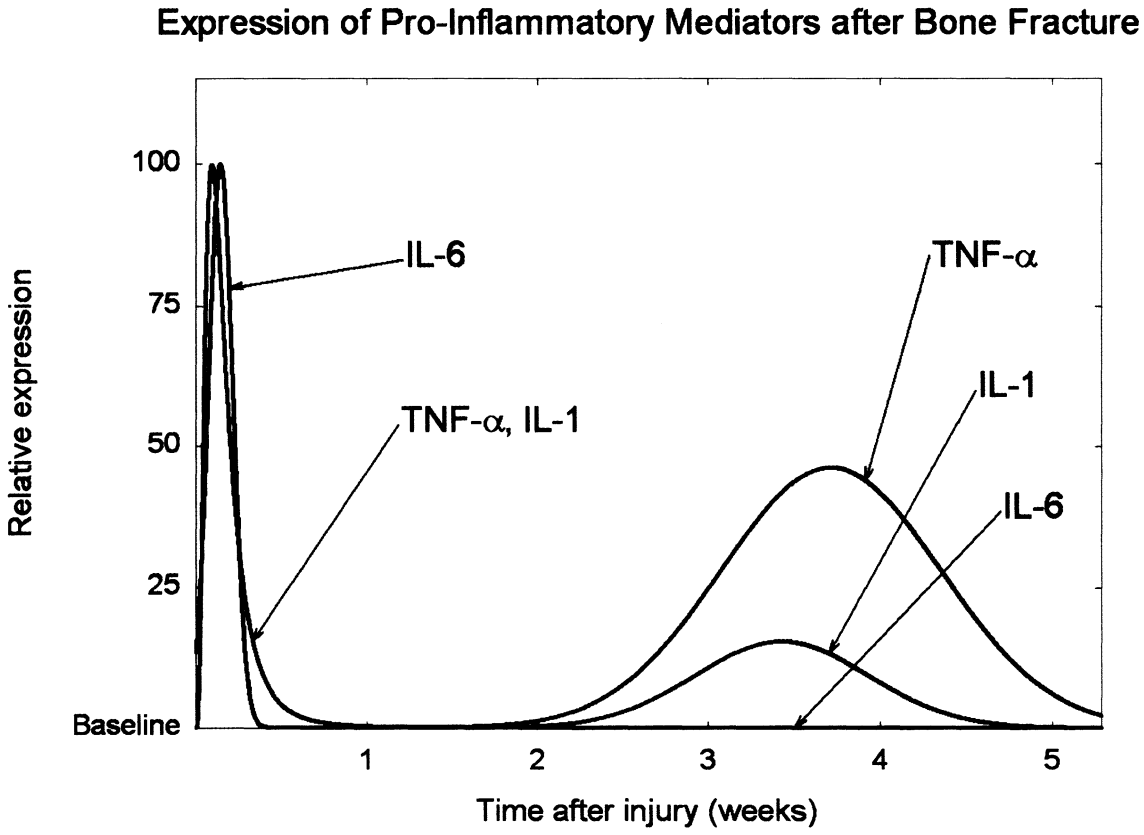

Figure 2.1: Expression of pro-inflammatory mediators after bone fracture. Schematic depicting the temporal pattern expression of three pro-inflammatory signals, tumor necrosis factor alpha (TNF-α), interleukin-1 (IL-1), and IL-6, after bone injury. The levels of each molecule are expressed as a percentage of the maximal level observed over the time period indicated. This graphic representation does not indicate concentrations of one molecule relative to another. Schematic is based on quantitative analysis of in vivo mRNA expression following bone injury (37, 59).

Although the effects of TNF-α on bone have been studied for decades, it has only recently been recognized that this molecule can exert opposite effects depending on the context in which it is released (58). Stimulation of the molecular signaling pathway responsible for TNF-α production induces osteogenic differentiation of mesenchymal stem cells *in vitro*, while signals that suppress TNF-α release decrease osteogenic

differentiation (60). TNF-α regulates the differentiation and function of both osteoblasts and osteoclasts via TNFR1 and TNFR2, the two cell-surface receptors for TNF-α (61). TNFR1 is always present in bone tissue. In contrast, TNFR2 is only expressed following bone injury (59). In an *in vitro* culture system, TNF-α signaling promoted bone formation in cells from both normal and TNFR1-deficient mice. However, the opposite effect was observed with TNFR2-deficient cells, where TNF-α signaling stimulated osteoclast differentiation and bone resorption (62). Secondary signals arising from the activation of TNFR2 receptor likely mediate the pro-regenerative effects of TNF-α in fracture healing (59, 62).

2.3.2. Interleukin-1 (IL-1)

Although it acts through a distinct molecular signaling pathway, the effect of IL-1 on bone largely overlaps with that of TNF-α (61). Like TNF-α, IL-1 expression follows a biphasic pattern. In a mouse model of fracture healing, its concentration rises immediately after bone fracture, peaking after 24 hours and returning to undetectable levels by 72 hours, as shown in Figure 1. The main source of IL-1 during this inflammatory phase is macrophages (37, 59). IL-1 triggers release of IL-6, prostaglandins, and other pro-inflammatory secondary signals (63). It also stimulates angiogenesis and promotes formation of the cartilaginous callus that stabilizes the fracture site (39). A second peak in IL-1 expression occurs approximately three weeks following the injury (see Figure 1). During this period, IL-1 is mainly expressed by osteoblasts and facilitates bone remodeling by stimulating proteases to degrade callus tissue (39, 59).

The diverse functions of IL-1 during fracture healing can be attributed to the differential expression of the two IL-1 receptors, IL-1RI and IL-1RII. In a murine model of fracture healing, the expression of IL-1RII follows the same biphasic pattern as its ligand, IL-1. In contrast, IL-1RI is only detectable during the inflammatory phase (59). IL-1RI-deficient mice have decreased bone mass and two-fold increased levels of osteoclasts (64), which underscores the importance of this molecular signal in bone homeostasis.

2.3.3. Interleukin-6 (IL-6)

IL-6 is produced by osteoblasts, in response to stimulation by IL-1 (39). In mouse models of bone regeneration, levels of IL-6 rise immediately after injury and return to baseline by the end of the first week (see Figure 1) (38). IL-6 regulates the differentiation of both osteoblasts and osteoclasts, and also promotes angiogenesis by stimulating release of VEGF (65). Unlike TNF-α and IL-1, IL-6 expression is limited to the inflammatory phase. Levels of IL-6 remain at baseline in the remodeling phase of fracture healing (38). Absence of IL-6 significantly delays the early stages of fracture healing, including mineralization and remodeling of the fracture callus. Two weeks after bone fracture, IL-6-deficient mice have reduced mineralization and increased cartilage content at the fracture site; four weeks after the injury, fracture healing is comparable to that of IL-6-replete mice (65). In human patients, IL-6 remains elevated for up to several months following fracture. Higher levels correlate with decreased load-bearing capability at injury site (66, 67).

2.3.4. Additional Cytokines

The increasing recognition of the central role and unique function of pro-inflammatory signals in bone regeneration has stimulated research on the effects of other interleukins. There is a growing amount of evidence that a large number of cytokines play an important role in bone regeneration.

2.3.4.1. Interleukin-4 (IL-4)

IL-4 is a so-called "inhibitory cytokine," a term used by immunologists to describe molecules that tend to counteract the pro-inflammatory effects of TNF-α and IL-1 (63). IL-4 targets both osteoclasts and osteoblasts, inhibiting *in vivo* bone remodeling. Genetically modified mice that overproduce IL-4 develop severe osteoporosis; their bones have reduced stiffness and a propensity for failure when subjected to mechanical loads (68).

2.3.4.2. Interleukin-5 (IL-5)

IL-5 has only recently been recognized as having a role in osteogenesis. A mouse model genetically engineered to express high levels of IL-5 developed ectopic ossification in the spleen. Splenic bone nodules were indistinguishable from normal bone by histology, exhibited osteoblast-specific gene expression, and had mineral content consistent with that of bone matrix (69). Additionally, bone formation was significantly increased in the long bones of these mice. When normal mice were transplanted with bone marrow from the transgenic mice, they developed identical pathology, including

formation of splenic bone nodules and increased cancellous bone formation in the long bones (69).

2.3.4.3. Interleukin-12 and Interleukin-18 (IL-12 and IL-18)

IL-12 inhibits *in vitro* osteoclast differentiation. This anti-resorptive effect is magnified when IL-18, which is produced by osteoblasts, is simultaneously administered to murine osteoclast progenitors *in vitro* (70). The mechanism of IL-12 and IL-18 remains unclear. Their effect on osteoclast progenitors is indirect and involves increased production of IFN-γ (71). Overproduction of IL-18 stimulates IFN-γ production and suppresses IL-4 *in vivo*, resulting in cortical thinning and decreased bone volume in a mouse model (72).

2.3.4.4. Interferon-γ (IFN-γ)

IFN-γ levels rise in response to bone injury and remain elevated throughout most of bone healing, returning to baseline late in the remodeling phase (38). Research on the mechanism of this cytokine has been complicated by its opposite effects on bone resorption *in vitro* and *in vivo* (63). IFN-γ stimulates alkaline phosphatase activity in human osteoblasts (73), while suppressing the *in vitro* differentiation of osteoclasts (74). IFN-γ-receptor deficient mice have increased osteoclast formation in the presence of bone inflammation, indicating that IFN-γ has a protective, anti-resorptive effect (74). However, systemic administration of IFN-γ to rats for eight days triggers severe osteopenia (75). IFN-γ stimulates bone resorption in human patients with osteopetrosis, a disease associated with osteoclast dysfunction (63).

The effect of inflammatory cytokines on bone depends on the timing and context of their expression. A single cytokine can have both pro-regenerative and pro-resorptive effects on bone. Further research on the mechanism of these molecules will enable their incorporation into tissue engineering strategies to rationally control inflammation and induce regeneration.

2.4. Effect of Drugs that Modulate the Inflammatory Response

The number of studies documenting the effects of drugs that modulate the inflammatory response on fracture healing has grown rapidly within the past few years. This likely reflects increasing awareness amongst clinicians and pharmacologists of the key role of inflammatory signaling. However, these insights are not yet widely recognized in the field of tissue engineering, and thus few studies have attempted to integrate this knowledge into a bone tissue engineering strategy. Recent advances in molecular and cell biology have enabled researchers to specifically target bone tissue, avoiding potentially severe side effects, including systemic inflammation or, conversely, immunosuppression (76). This section summarizes the effects of pharmacologic modulation of the inflammatory response on bone regeneration *in vivo*, and the limited cases in which this knowledge has already been incorporated into tissue engineering strategies.

2.4.1. Cytokine-Specific Agents

Four inhibitory agents that specifically target pro-inflammatory molecules are currently used in human patients; infliximab (Remicade®), adalimumab (Humira®), and

etanercept (Enbrel®) are antibodies that block the function of TNF-α, while anakinra (Kineret®) blocks binding of IL-1 to its receptor. These selective anti-cytokine therapies do not impair bone fracture healing in human patients, which likely reflects the low dosages used clinically, since higher dosages increase the risk of severe infections, particularly tuberculosis (77, 78). However, in an *in vitro* model of bone healing, addition of anti-TNF-α antibodies obliterated the dose-dependent increase in bone formation triggered by TNF-α (62).

Stimulation of the signaling pathways activated by TNF-α, IL-1, and other pro-inflammatory mediators also enhances fracture healing. A recent study indicates that the synthetic peptide TP508, which enhances *in vivo* bone regeneration in a variety of animal models, activates the same signaling pathways stimulated by TNF-α, IL-1, and other pro-inflammatory cytokines during fracture healing (79). A single injection of TP508 into a femoral fracture increased the strength of the healed bone by over 30% in a rat model (80). Molecular analysis of this same model indicated that TP508 altered protein expression for 7 days, even though the half-life of TP508 at the fracture site was less than 12 hours. The differentially expressed proteins belonged to molecular signaling pathways that regulate osteoclasts and osteoblasts (79). Similar effects on bone healing in rabbits have been reported with controlled release of TP508 from PLGA microspheres and poly(propylene fumarate) scaffolds (81, 82). A recent placebo-controlled phase I/II study indicates that TP508 significantly accelerates the healing rate of human diabetic foot ulcers (83).

2.4.2. Corticosteroids

Numerous studies have indicated that corticosteroids suppress *in vivo* fracture healing in rodents and rabbits (84-86). However, corticosteroids are known to promote *in vitro* osteogenic differentiation of mesenchymal stem cells (3). A recent study reported that intramuscular injections of methylprednisolone improved *in vivo* osteogenesis in tissue engineering scaffolds subcutaneously implanted in New Zealand white rabbits. The scaffolds were seeded with autologous chondrocytes, and the authors suggest that corticosteroids stimulated the chondrocytes to undergo endochondral bone formation (87). In human patients, prolonged corticosteroid treatment is known to cause bone necrosis (88). In fact, corticosteroids are clinically used to reduce osteogenesis in patients with *fibrodysplasia ossificans progressiva*, a disease associated with excessive bone formation (89, 90). Further studies of the effect of these agents are necessary to establish their effects on the various phases of bone healing.

2.4.3. Prostaglandins and Non-Steroidal Anti-inflammatory Drugs (NSAIDs)

Prostaglandins are pro-inflammatory molecules that enhance bone regeneration by promoting angiogenesis and stimulating both osteoclasts and osteoblasts (91). The rate-limiting step in their synthesis is catalyzed by the enzyme cyclooxygenase (COX), which exists in two forms, COX-1 and COX-2. COX-1 is present in normal bone, and triggers the production of low levels of prostaglandins. COX-2 expression is triggered by bone injury and results in high levels of prostaglandin synthesis (76, 92). Absence of COX-2, due to genetic mutation, impairs fracture healing in mice (93, 94).

Non-steroidal anti-inflammatory drugs (NSAIDs), the most common class of anti-inflammatory medication, reduce inflammation by inhibiting prostaglandin synthesis. Numerous publications over the past three decades have reported that both non-selective NSAIDs, which target both COX-1 and COX-2, and selective COX-2 inhibitors (e.g. celecoxib) delay or inhibit *in vivo* fracture healing [recently reviewed by (76, 91)]. A recent study indicates that indomethacin, a non-selective NSAID, delays *in vivo* femoral fracture healing in rats, while celecoxib (Celebrex®) and rofecoxib (Vioxx®), both COX-2 selective inhibitors, cause osseous nonunion (93). A significant increase in the proportion of nonunions, along with a significant decrease in fracture callus strength, is evident after just five days of celecoxib therapy (95). The effect of these drugs is limited to the initial period of fracture healing, corresponding to the inflammatory phase; giving celecoxib either prior to fracture or 14 days after fracture has no effect on fracture healing (95). The inhibitory effect of these drugs on fracture healing is reversible. Rats given valdecoxib (Bextra®), another COX-2 selective inhibitor, for 21 days following femur fracture had significantly increased incidence of osseous nonunion; two weeks after treatment was stopped, there were no differences between experimental and control groups (96).

Clinical studies of human patients support the experimental findings in animal models. Use of NSAIDs after long bone fracture significantly increases the risk of either delayed union or nonunion (97, 98). NSAIDs are consequently used to prevent heterotopic bone formation after hip surgery. Just 5-7 days of post-operative treatment with NSAIDs effectively prevents ectopic bone formation (99). As expected from these findings, in hip surgery patients with simultaneous long bone fractures, NSAIDs

significantly increase the risk of nonunion at long bone fracture sites. Incidence of nonunion increases by as much as four-fold, suggesting that these patients should be treated with alternative methods to suppress ectopic bone formation (100).

2.4.4. Selective Prostaglandin Agonists

Increased bone formation is a known side effect of prostaglandins, which are commonly used to maintain a patent *ductus arteriosus* in infants with congenital heart disease (101). However, they have not been pursued as a therapeutic agent to promote fracture healing because of the risk of severe side effects, including systemic inflammation (76). Recent studies indicate that there are several prostaglandin receptors, each with a distinct tissue distribution and secondary signaling cascade. The main effects on bone are exerted via the EP2 and EP4 receptors (91). Selective EP2 and EP4 receptor ligands may be used for bone repair, while avoiding systemic side effects. A recent study indicates selective EP2 receptor agonists stimulate *in vivo* fracture healing in rodents and dogs (102). For the dog studies, EP2 agonists encapsulated in a PLGA carrier enhanced *in vivo* healing of critical-size radial defects and tibial bone defects (102). A similar effect has been reported for EP4 agonists in rat femoral defects (103).

2.5. Conclusions

The impact of TNF-α, IL-1, and other pro-inflammatory signals on bone regeneration underscores the importance of incorporating rational control of inflammation into the design of tissue engineering strategies. Modulation of the inflammatory response is a new direction in the field of tissue engineering. To our

knowledge, few studies have attempted to integrate inflammatory modulation into tissue engineering strategies to enhance bone regeneration. Novel strategies that exploit inflammatory signals have the potential to induce greater regeneration than current systems, which only deliver growth factors. In bone tissue engineering, a better combination of renewal signals will decrease the required dose of factors like BMP-2, limiting their release to the injury site and thus minimizing ectopic effects likely in current systems. Rational control of the inflammatory response will provide a powerful strategy to induce healing of engineered tissue.

Chapter 3

Background: Harnessing and Modulating Inflammation in Strategies for Bone Regeneration[3]

Abstract: Inflammation is an immediate response that plays a critical role in healing after fracture or injury to bone. However, in certain clinical contexts, such as in inflammatory diseases or in response to the implantation of a biomedical device, the inflammatory response may become chronic and result in destructive catabolic effects on the bone tissue. Since our previous review three years ago[4], which identified

[3] This chapter will be published as: Mountziaris PM, Spicer PP, Kasper FK, Mikos AG. Harnessing and Modulating Inflammation in Strategies for Bone Regeneration. *Tissue Engineering Part B: Reviews* 2011; In Press (available online ahead of print: doi:10.1089/ten.teb.2011.0182).

[4] Included in the preceding chapter of this thesis.

inflammatory signals critical for bone regeneration and described the inhibitory effects of anti-inflammatory agents on bone healing, a multitude of studies have been published exploring various aspects of this emerging field. In this review, we distinguish between regenerative and damaging inflammatory processes in bone, update our discussion of the effects of anti-inflammatory agents on bone healing, summarize recent *in vitro* and *in vivo* studies demonstrating how inflammation can be modulated to stimulate bone regeneration, and identify key future directions in the field.

3.1. Introduction

Inflammation is a highly regulated biological response that plays an immediate and crucial role in promoting regeneration following bone fracture or injury (104, 105). However, in certain clinical contexts, such as in inflammatory diseases or severe foreign body reactions to implanted materials, the normal inflammatory response fails to resolve, resulting in chronic inflammation that has destructive effects on bone tissue. A tremendous amount of effort has been invested in developing pharmacologic agents to disable this uncontrolled inflammatory signaling and thus prevent bone damage (106, 107). In the process, a growing body of evidence has emerged that indicates that a complex balance exists between bone tissue and the immune system, which is responsible for the inflammatory response, and that obliterating inflammation also has damaging effects on bone (104, 106, 108). We previously published a review (104) that introduced this information to the bone tissue engineering community by identifying inflammatory signals critical for bone regeneration and describing the inhibitory effects of anti-inflammatory agents on bone healing. Since our previous review, a multitude of studies

have been published exploring new strategies to harness and modulate inflammation to facilitate bone regeneration.

The objectives of this review are to: (1) distinguish between regenerative and damaging inflammatory processes in bone; (2) identify anti-inflammatory agents that inhibit bone healing; (3) summarize recent *in vitro* and *in vivo* studies to demonstrate how inflammation can be modulated to stimulate bone regeneration; and (4) combine this information to identify key future directions in the field.

3.2. Regenerative vs. Damaging Inflammatory Processes in Bone

3.2.1. Inflammatory signaling during bone regeneration

Inflammation is an immediate response to bone injury, and a growing body of evidence indicates that the signaling cascades initiated during the week-long acute inflammatory response play a critical role in priming bone regeneration (104, 105, 108). Bone fracture stimulates expression of several dozen inflammatory cytokines, including interleukin-1α (IL-1α), IL-1β, IL-6, IL-18, and tumor necrosis factor alpha (TNF-α) (30, 37, 59). In murine models, TNF-α, IL-1α, IL-1β, and IL-6 signaling peaks 24h following bone injury and returns to baseline levels after a few days (37, 59). Together with a variety of growth factors, including proteins from the transforming growth factor beta (TGF-β) and bone morphogenetic protein (BMP) families, fracture-induced inflammatory mediators recruit inflammatory cells, promote angiogenesis, and guide mesenchymal stem cell (MSC) differentiation (30, 37, 59). Several cytokines, including TNF-α, IL-6, and stromal cell-derived factor-1 (SDF-1), have been shown to directly impact the *in vivo*

migration of MSCs (109-112). Levels of most inflammatory mediators return to baseline following the week-long acute inflammatory phase (30, 37, 59).

Fracture healing involves overlapping phases of inflammation, renewal, and remodeling. During the renewal phase, the fracture site is stabilized by a cartilaginous callus, which then calcifies and undergoes endochondral bone formation. At this point, the remodeling phase begins. Levels of TNF-α and several other cytokines rise for a second time as the mineralized fracture callus is remodeled into lamellar bone by the renewing and resorptive actions of osteoblasts and osteoclasts, respectively (37, 39, 59, 104). *In vivo* studies have identified cytokines from both the inflammatory and remodeling phases that are critical for bone regeneration. For instance, mice lacking either IL-6 or TNF-α have severely impaired fracture healing, with bone formation being delayed by several weeks (1, 65). Emerging strategies to harness this signaling and use it to stimulate bone regeneration are discussed in a separate section of this review.

3.2.2. Role of inflammatory cells in bone regeneration

Although inflammatory cells, mainly neutrophils and macrophages, are immediately recruited to the injury site and release a cascade of cytokines and growth factors, *in vivo* studies have not yet identified a crucial inflammatory cell type for fracture healing. Inflammatory cells are primarily present at the fracture site during the initial week-long inflammatory phase of bone healing (105, 113). Within 3-7 days of injury, and continuing during the subsequent renewal and remodeling phases of healing, native bone cells in the regenerating fracture callus, mainly osteoblasts and chondrocytes, are the primary source of inflammatory cytokines such as TNF-α (59). This overlapping inflammatory signaling by native bone cells may explain the normal bone healing seen in

the absence of inflammatory cells. For instance, absence of neutrophils and macrophages does not adversely affect *in vivo* tissue repair (56). Absence of lymphocytes significantly accelerates *in vivo* fracture healing and remodeling, resulting in a mineralized fracture callus with superior biomechanical properties (114, 115). In a unique chimeric animal model, transplantation of inflammatory cells from aged mice with impaired bone regeneration into otherwise healthy juvenile mice did not affect *in vivo* fracture healing. However, in the inverse case, consisting of a middle-aged mouse with inflammatory cells derived from a juvenile mouse, fracture callus healing and remodeling were accelerated (116). It is possible that the beneficial effect of acute inflammation following bone injury may not be attributable to a particular cell type, but the relative proportions of the cells recruited to the injury site. A recent study in a sheep model indicated that the composition of the injury-induced inflammatory infiltrate is tissue-specific (113). For instance, 1h after injury, a bone fracture hematoma contained fewer neutrophils than a hematoma taken from a muscle injury site. However, by 4h after injury, this difference was no longer apparent, and the relative proportions of neutrophils, macrophages, and lymphocytes at the fracture site were identical to those seen in circulating blood (113). Any variation in the number and type of inflammatory cells, even for just a few hours, directly affects the balance between bone tissue and the immune system by altering the local concentration of growth factors and inflammatory cytokines that regulate bone healing.

3.2.3. Aberrant inflammation results in bone damage

The normal inflammatory response can be disrupted by many factors, including massive trauma and inflammatory diseases (106, 107). Aberrant inflammatory signaling

has been implicated as a significant factor in bone injuries that fail to heal. Osteoblasts taken from human patients with fracture nonunion had anomalous expression of 281 genes, including sets of genes that regulate growth factor activity, osteogenesis, angiogenesis, cytokine activity, and the inflammatory response (117). Similar results were seen in an animal model of delayed osseous union; at several timepoints following bone injury, the tissue from the nonunion site had reduced expression of several growth factors, including BMP-2, BMP-4, BMP-7, and TGF-β1, as well as the cytokine TNF-α (118). These findings underscore the importance of regulated acute inflammatory signaling in priming bone regeneration.

The impact of inflammatory diseases on bone is not a direct effect of inflammatory cells. In a model of rheumatoid arthritis, mice with reduced osteoclast numbers were protected from bone damage, despite the infiltration of high numbers of inflammatory cells into the bone (119). However, osteoclast-deficient mice were not protected from other destructive effects of inflammatory arthritis, like cartilage damage (119).

When acute inflammation fails to resolve, e.g., due to the presence of an underlying inflammatory disease like rheumatoid arthritis, the resulting prolonged, unregulated inflammatory signaling has damaging effects on bone. For example, although TNF-α and IL-6 have been shown to be critical for *in vivo* bone regeneration in murine models (1, 65), chronic exposure to high levels of these cytokines has damaging effects on bone. In murine models, prolonged, systemic exposure to high levels of TNF-α triggers tissue damage and symptoms resembling those of rheumatoid arthritis, including chronic inflammation, decreased bone volume, and reduced bone mechanical strength

(120). In a recent study of a mouse model of type 1 (i.e., autoimmune) diabetes, impaired fracture healing was attributed to excessive callus remodeling triggered by elevated expression of several inflammatory mediators, including TNF-α (121). Systemic treatment with a TNF-α inhibitor starting 10 days after bone fracture significantly improved fracture healing in the diabetic mice (121). Abnormally elevated levels of IL-6 also have damaging effects on bone. In human patients, abnormally high serum IL-6 levels in the days and even months following bone fracture correlate with decreased load-bearing capability of the injured bone (66, 67). In a recent study, serum from human patients with polyarticular juvenile idiopathic arthritis, an autoimmune disorder that causes chronic joint inflammation, significantly suppressed *in vitro* osteogenesis of human osteoblasts, as determined by comparing their alkaline phosphatase (ALP) expression, osteocalcin protein level, and calcified matrix deposition to that of osteoblasts cultured in serum from healthy controls (122). Analysis of the arthritic serum indicated that IL-6 was the only cytokine that was abnormally elevated (122). This highlights the difference between the highly regulated acute inflammation that occurs during bone fracture healing, compared to the unregulated chronic inflammation seen in arthritis and autoimmune disease.

3.3. Effects of Anti-Inflammatory Drugs on Bone Healing

A tremendous amount of effort has been invested in developing pharmacologic agents to disable uncontrolled inflammatory signaling and thus prevent bone damage in patients with inflammatory diseases (106, 107). A wide variety of anti-inflammatory medications are available to treat ailments ranging from musculoskeletal pain to chronic

inflammation associated with autoimmune disease. However, therapeutic strategies have been complicated by the complex balance that exists between bone and the immune system, which is responsible for the inflammatory response; a growing number of studies indicate that anti-inflammatory medications have predominantly negative effects on bone healing (76, 104). In most cases, instead of recommending the discontinuation of anti-inflammatory medications, current clinical guidelines instruct physicians to assess the risk/benefit ratio for each individual patient (123). For researchers, considering the effects of the anti-inflammatory medications discussed in this section will aid in the design of more effective bone regeneration strategies.

3.3.1. Corticosteroids

Although corticosteroids are commonly used *in vitro* to induce osteogenic differentiation of mesenchymal stem cells (MSCs) (3), they are known to have negative effects on *in vivo* bone homeostasis and regeneration. In human patients taking corticosteroids, e.g., to treat the chronic inflammation associated with rheumatoid arthritis, monitoring for adverse effects on bone, including reduced bone density and bone necrosis, is part of standard clinical practice (124, 125). Numerous studies have shown that corticosteroids suppress *in vivo* fracture healing in rodents and rabbits by reducing osteogenesis, angiogenesis, and mechanical strength at the fracture site (84-86, 126, 127). Studies of genetically altered mice have demonstrated that baseline native corticosteroid signaling in osteoblasts is necessary for bone morphogenesis, but not for bone regeneration (128). Mice lacking corticosteroid signaling in osteoblasts had normal bone healing following tibial fracture (128). In recognition of their negative effects on bone, corticosteroids are not prescribed to human patients with bone injuries (76). In fact,

corticosteroids are a common therapeutic agent for human patients with fibrodysplasia ossificans progressiva, a disease associated with excessive bone formation (129).

Although long-term treatment with corticosteroids inhibits bone regeneration, the effects of short-term *in vivo* exposure remain unclear. Recent tissue engineering studies have reported a wide variety of effects of short-term corticosteroid exposure, ranging from no effect to substantial, beneficial effects on bone regeneration. Two recent studies have reported that 3D poly(DL-lactic-co-glycolic acid) (PLGA)-based scaffolds delivering dexamethasone stimulated *in vivo* bone regeneration in critical-size defects after 4-8 weeks, compared to empty defects (130, 131). However, neither study demonstrated a clear benefit of dexamethasone delivery, since equivalent bone regeneration was seen with dexamethasone-free scaffolds in each case (130, 131). The effect on *in vivo* osteogenesis may depend on the method and temporal pattern of corticosteroid delivery. In a study of rat MSC-seeded titanium fiber meshes implanted in critical-size rat cranial defects for 4 weeks, MSC preculture in media supplemented with dexamethasone for 4 days resulted in superior bone regeneration compared to MSCs cultured without dexamethasone. However, exposure to dexamethasone for 16 days resulted in much less bone formation than seen with untreated MSCs (132). In another study, MSCs precultured with dexamethasone for 1 week and seeded onto hydroxyapatite scaffolds resulted in increased ectopic bone formation in a rat subcutaneous implantation model; greater bone formation occurred when dexamethasone was supplied through a nanoparticle-based delivery system added to the preculture medium rather than as a free drug in solution (133). In a rabbit model, systemic injection of the corticosteroid methylprednisolone increased ectopic bone formation in subcutaneously implanted

chondrocyte-seeded PLGA scaffolds compared to rabbits not treated with corticosteroids (87).

In contrast to the diverse effects of corticosteroids in these animal models, a recent case study reported that implanting a dexamethasone-loaded gelatin scaffold in human patients with osseous nonunion stimulated bone regeneration (134). Autologous bone marrow and bone fragments were collected from the non-injured femur of each patient and incubated *in vitro* in a high concentration (10^{-5} M) of dexamethasone for 1-2h. The liquid portion of the mixture was then absorbed into a gelatin scaffold, which was packed into the site of osseous nonunion, and then surrounded by the dexamethasone-treated bone fragments. After 6-8 months, only 1/13 patients had persistent nonunion, and 6/13 had achieved complete union (134). Additional research is necessary to establish the role of corticosteroids in the various phases of bone regeneration and better understand the mechanism of the diverse effects seen in humans and animals with bone injuries.

3.3.2. Cytokine-specific antagonists

To avoid the negative effects of non-specific agents like corticosteroids, the chronic inflammation seen in auto-immune diseases is increasingly being treated with medications that specifically target a portion of the immune system. For instance, rheumatoid arthritis is treated using monoclonal antibodies and other synthetic biologic agents that target TNF-α, IL-1, and IL-6. These cytokine-specific inhibitors are a new class of medications, having only been approved for use in humans within the past 10 years (77, 78). Seven agents that antagonize specific cytokines are currently approved for use in human patients: infliximab, adalimumab, etanercept, golimumab, and

certolizumab-pegol inhibit TNF-α, while anakinra and tocilizumab antagonize IL-1 and IL-6, respectively (135). Only a small number of studies have reported the effects of these agents on bone healing, and the results have been inconclusive. Most studies have focused on the oldest cytokine-specific antagonists, the TNF-α blockers infliximab, adalimumab, and etanercept. Several studies of human patients undergoing orthopedic surgery have shown no significant impact of TNF-α antagonists on the incidence of adverse events or wound healing complications (136, 137). In contrast, other studies have shown that patients treated with TNF-α antagonists had a statistically significant increased risk of orthopedic surgical site infection and other complications (138, 139). Since absence of TNF-α has been shown to be detrimental to bone regeneration in an animal model (1), the inconsistent inhibition of bone healing seen in human patients is believed to stem from the very low doses of these medications that are prescribed, since higher doses suppress the immune system and increase the risk of severe infections like tuberculosis (77, 135). However, the specific mechanism of each agent may also play a role. A recent *in vitro* study of human osteoblasts exposed to therapeutic doses of two TNF-α antagonists indicated that infliximab had a negative effect on osteoblast proliferation, while etanercept had no effect (140).

3.3.3. Non-steroidal anti-inflammatory drugs (NSAIDs)

Non-steroidal anti-inflammatory drugs (NSAIDs), a large group of medications ranging from over-the-counter pain relievers like ibuprofen to prescription-only anti-inflammatories like celecoxib (Celebrex®), are the most widely studied anti-inflammatory medications in bone biology. The detrimental effects of various NSAIDs

on bone regeneration have been documented in both human patients and animal models for several decades (recently reviewed by (141, 142)).

NSAIDs target the cyclooxygenase (COX) enzymes, which catalyze the rate-limiting step of prostaglandin synthesis. There are two forms of COX; COX-1 is constitutively expressed in bone and results in low levels of prostaglandin synthesis, while COX-2 is triggered by bone injury and results in high levels of prostaglandin production (76). Recent studies have identified COX-2 as a critical enzyme in bone regeneration. In mouse models, absence of COX-1 due to genetic mutation did not affect bone regeneration, while absence of COX-2 impaired fracture healing and increased the risk of osseous nonunion (93, 94). Consistent with these results, studies in rodent and rabbit models have shown that selective COX-2 inhibitors cause greater reductions in bone mineral density and mechanical properties at the injury site than nonselective NSAIDs, which inhibit both COX-1 and COX-2 (96, 143, 144).

The detrimental effects of COX-2 inhibition are most profound in the initial inflammatory phase of fracture healing. In rat models, administration of COX-2 inhibitors for 5-7 days immediately after bone injury resulted in measurable effects 4-8 weeks later. COX-2 inhibition significantly reduced fracture callus mechanical strength and bone mineral density, and also increased the incidence of osseous nonunion (95, 143, 145). However, treating the rats with a COX-2 inhibitor either prior to bone fracture or starting 14 days after fracture had no effect on bone healing (95). Systemic COX-2 has been shown to be critical for *in vivo* bone regeneration; local delivery of COX-2 within a bone graft in mice lacking COX-2 could not compensate for the detrimental effects on bone healing (146).

Studies of NSAID effects in human patients with bone injuries support the results of these animal studies. NSAIDs have been shown to significantly increase the risk of delayed union or nonunion following long bone injury (97, 98). As with corticosteroids, NSAIDs are consequently used to prevent and treat ectopic or excessive bone formation in human patients (99, 129, 147). For instance, NSAIDs are used to prevent heterotopic bone formation after hip surgery, with as little as 5-7 days of postoperative NSAID administration being sufficient to inhibit ectopic bone formation (99). However, in hip surgery patients who also have long bone fractures, NSAID use increases the risk of nonunion in the long bone by fourfold (100). This underscores the fact that excessively suppressing inflammation can disrupt normal bone healing. In light of these findings, current clinical guidelines recommend that NSAIDs be avoided for the two weeks following a bone fracture, particularly in patients with a higher risk of osseous nonunion (123, 141).

3.4. Harnessing Inflammation to Stimulate Bone Regeneration

Stimulation of bone inflammation has not been extensively studied *in vivo* due to the risk of systemic inflammation and subsequent tissue damage. However, increasing awareness of the importance of certain inflammatory signals in priming bone regeneration has led to several recent *in vitro* and even some *in vivo* studies.

3.4.1. Prostaglandin E2 Receptor Agonists

Among the various prostaglandin types, prostaglandin E2 has been shown to have the most profound effects on bone homeostasis. Injury-induced increased prostaglandin

E2 production is critical for bone regeneration (148, 149). The specific bone cell types that respond to prostaglandin E2 remain unclear, although both osteoclast progenitors and mature osteoblasts have been implicated based on *in vitro* studies (144, 150). *In vivo*, signaling via the prostaglandin E2 type 1 (EP1) receptor has been shown to negatively regulate bone regeneration, while signaling via the EP2 and EP4 receptors stimulates bone formation (150). Synthetic molecules selectively targeting these latter receptors have consequently been used in bone regeneration strategies. Local injection of selective EP2 agonists improved *in vivo* fracture healing in rodent models (102, 151). In addition, implantation of a PLGA matrix encapsulating an EP2 agonist into a critical-size canine ulnar defect stimulated osseous union after 24 weeks (102). Delivery of selective EP4 receptor agonists has also shown promising results. In rodent models, both local and systemic delivery of EP4 selective agonists stimulated *in vivo* osteogenesis and angiogenesis, resulting in accelerated fracture healing (103, 151). Dual delivery of BMP-2 and an EP4 agonist from a PEG-based hydrogel stimulated bone formation in a critical-size murine cranial defect model; bone regeneration was greater with dual delivery than with delivery of either agent alone (152).

3.4.2. Leukotriene Antagonists

Modulation of leukotriene signaling is a very new bone regeneration strategy (153). Leukotrienes are a group of inflammatory signaling molecules that have the same metabolic precursor, arachidonic acid, as prostaglandins. However, unlike COX-2, which is the rate limiting enzyme in prostaglandin synthesis and has been shown to play a critical role in bone regeneration, the key enzyme in leukotriene synthesis, 5-lipoxygenase, is detrimental to fracture healing (153). One proposed mechanism for the

impaired fracture healing seen with COX-2 inhibition is increased arachidonic acid availability to 5-lipoxygenase (153), which results in abnormally elevated leukotriene levels at the fracture site (154). In a rat model, administration of a 5-lipoxygenase inhibitor for 3 weeks following femoral fracture resulted in faster fracture bridging and superior mechanical properties at the fracture site compared to untreated rats (155). Similar accelerated fracture healing was reported in mice genetically altered to lack 5-lipoxygenase (154, 155). Two clinically available leukotriene antagonists, montelukast sodium (Singulair®), a cysteinyl leukotriene type-1 receptor antagonist, and zileuton (Zyflo®), a 5-lipoxygenase inhibitor, also have beneficial effects on femoral fracture healing in a mouse model (156). Both agents are currently approved by the United States Food and Drug Administration (FDA) for the treatment of inflammatory airway diseases such as asthma. Systemic administration of either leukotriene antagonist significantly accelerated bone regeneration compared to fracture healing in untreated controls (156). Further mechanistic analysis indicated that the leukotriene antagonists enhanced fracture healing by directly affecting chondrocyte activity within the fracture callus (156). These recent results highlight the promise of modulating leukotriene synthesis as a new strategy to stimulate bone regeneration.

3.4.3. Modulating Cytokine Activity

Direct modulation of cytokine activity to promote bone regeneration is a new strategy that remains largely at the cell culture testing stage, though a few *in vivo* studies have been recently published. The most commonly studied cytokines are TNF-α, IL-1, and IL-6.

3.4.3.1. TNF-α

Since the mechanism of TNF-α in bone regeneration remains unknown, studies to date have been mainly conducted *in vitro*. These studies have revealed weaknesses in the typical *in vitro* culture conditions used to study MSC osteogenic differentiation and necessitated changes to standard cell culture protocols. TNF-α does not affect *in vivo* embryonic skeletal development (1), but plays a critical role in bone regeneration. Mice lacking TNF-α have severely impaired fracture healing, with bone formation being delayed by several weeks (1, 2). Exposure to TNF-α significantly affects the *in vitro* protein expression, proliferation, and migration of undifferentiated human MSCs, but has not been reported to induce differentiation (111, 157). Thus, in order to study the effects of TNF-α on osteogenically differentiating MSCs, supplements must be added to induce MSC osteogenic differentiation. Studies of the effects of TNF-α on osteogenic differentiation have been complicated by the fact that two supplements typically used to stimulate *in vitro* MSC osteogenic differentiation, dexamethasone and ascorbic acid, antagonize TNF-α signaling (14, 62, 158). While commonly used in *in vitro* MSC cultures, dexamethasone, an anti-inflammatory corticosteroid, is not present in the *in vivo* bone fracture environment (104). Additionally, as discussed above, corticosteroids have been implicated in impaired bone fracture healing. One strategy to overcome this limitation and create a more realistic *in vitro* model of the fracture healing environment has been to preculture MSCs in osteogenic medium to trigger differentiation and then use medium without dexamethasone to study the effects of TNF-α (14). In the absence of dexamethasone, treatment of osteoprogenitors with TNF-α resulted in dose-dependent increases in ALP activity and mineralized matrix deposition, which are, respectively,

early and late markers of osteogenesis (14, 112, 159-161). In contrast, when added to dexamethasone-containing osteogenic medium, TNF-α had the opposite effect on MSCs (162, 163). The pro-regenerative effects of TNF-α seen in dexamethasone-free *in vitro* MSC cultures were recently confirmed *in vivo* through repeated injections of TNF-α into a fracture healing model. Daily local injections of TNF-α during the first two days after injury resulted in significantly increased fracture callus mineralization four weeks later (112). These findings for TNF-α emphasize the importance of developing clinically realistic *in vitro* culture models to improve the predictions of the *in vivo* effects of various cytokines.

3.4.3.2. IL-1

Unlike TNF-α, which does not affect skeletal development but is required for normal bone regeneration, absence of IL-1 does not affect *in vivo* fracture healing (164). However, mice lacking IL-1α and/or IL-1β, the two forms of IL-1, have significantly higher bone mineral density and femoral bone mass than normal mice, which has been attributed to impaired osteoclast development (165). *In vitro* studies of the effects of IL-1α and IL-1β on osteogenically differentiating MSCs have shown that these cytokines have similar effects as TNF-α (160, 162, 166). MSCs precultured to induce osteogenic differentiation and subsequently exposed to IL-1β (in dexamethasone-free medium) had significant dose-dependent increases in early and late markers of osteogenic differentiation (160), while simultaneous exposure to IL-1β and dexamethasone had the opposite effect (162). Simultaneous delivery of IL-1β and TNF-α had synergistic effects on *in vitro* MSC deposition of mineralized matrix (160). A recent study reported that daily local IL-1β injections during the first 3 days after bone fracture resulted in slightly

accelerated *in vivo* bone regeneration(164). When compared to the results of *in vitro* studies, this finding once again emphasizes the need to deliver cytokines to MSCs under culture conditions simulating the *in vivo* fracture healing environment (e.g., no dexamethasone) in order to effectively predict *in vivo* results.

3.4.3.3. IL-6

IL-6 is required for both normal skeletal development and for bone regeneration. Mice lacking IL-6 have reduced bone mineral density and also have impaired fracture healing (65). *In vitro* studies of osteogenically differentiating cells have indicated that exposure to IL-6 for 3-6 days increases gene expression of osteogenic markers RUNX2 and osteocalcin (167). In an *in vivo* fracture healing model, repeated local injections of parathyroid hormone fragments and IL-6 in the first two weeks after injury significantly increased fracture callus mechanical strength and accelerated osseous union (168). However, this treatment reduced the mechanical strength of non-injured bones, which was attributed to a systemic effect of the injected agents (168). This underscores the need for controlled release systems to provide targeted cytokine delivery to the site of bone injury.

3.4.3.4. IL-4

Although abnormally elevated IL-4 levels have long been known to inhibit *in vivo* bone remodeling and result in extremely weak, osteoporotic bones (68), absence of this cytokine due to genetic mutation was recently shown to have no effect on *in vivo* fracture healing (169). However, in a study of *in vivo* ectopic bone formation stimulated by implantation of xenogeneic demineralized bone matrix, absence of IL-4 and IL-13

reduced angiogenesis (169), a finding that may have implications for the development of bone tissue engineering strategies.

3.4.3.5. Interferon-γ

Many studies of the effects of IFN-γ on bone regeneration have focused on signal transducer and activator of transcription 1 (STAT1), an intracellular signal that is a component of the IFN-γ pathway. Absence of IFN-γ signaling, due to absence of either STAT1 or the IFN-γ receptor, increases the number of osteoclasts in bone *in vivo*, but also increases bone mass (170, 171). Absence of STAT1 also accelerates *in vivo* fracture healing and subsequent bone remodeling (171). Gelatin scaffolds loaded with fludarabine, a STAT1 inhibitor, stimulated *in vivo* ectopic bone formation when implanted subcutaneously in a mouse model. Dual delivery of BMP-2 and fludarabine revealed an additive effect of the two agents on *in vivo* ectopic bone formation (171).

3.4.3.6. Stromal cell-derived factor-1 (SDF-1)

SDF-1 is a new target in bone regeneration strategies. In animal models with reduced SDF-1 signaling, new bone formation two weeks after injury was 60-80% less than normal (109). In another study, porous PLGA scaffolds loaded with SDF-1 triggered MSC chemotaxis both *in vitro* and *in vivo*, resulting in MSC migration toward, and subsequent attachment to, the scaffold (110). SDF-1 delivery from subcutaneously implanted PLGA scaffolds significantly reduced *in vivo* fibrotic encapsulation and inflammatory cell accumulation near the scaffold (110), demonstrating the potential of this cytokine as a component of future immunomodulatory strategies to prevent foreign body reactions to biomedical implants.

3.4.3.7. TP508

TP508 (rusalatide acetate; Chrysalin®) is a synthetic peptide that stimulates the same signaling pathways activated by cytokines like TNF-α and IL-1 (79). This peptide has been shown to be a very potent stimulator of *in vivo* bone regeneration, with a single injection into a rat femoral fracture increasing the strength of the healed bone by over 30% (80). In rabbit models, TP508 has been shown to stimulate bone regeneration of critical-sized defects when incorporated into a PLGA microparticle-based controlled release system (81, 82). However, in a recent Phase III clinical trial of this agent, a single injection of TP508 into the site of a radius fracture failed to significantly improve (vs. placebo) the primary measure of success, which was the total time that the fracture required immobilization (172). However, further analysis revealed that in a subset of the clinical trial participants, i.e., female patients with osteopenia, TP508 was successful; it significantly reduced the amount of time that the fractures required immobilization, and also accelerated fracture healing (172). Further studies are needed to clarify the efficacy of TP508 in patients with impaired bone regeneration capacity.

3.4.4. Modulating Inflammatory Cell Activity

Another emerging strategy is to directly target and modulate inflammatory cell function in bone. Small molecule inhibitors of cathepsin K, an enzyme specific to osteoclasts and other bone cells of the monocyte lineage, effectively reduced *in vivo* bone resorption and uncontrolled joint inflammation in a rat model of rheumatoid arthritis (173). Although the inherent immunomodulatory properties of MSCs have been recognized for approximately a decade, clinical strategies utilizing these cells have

focused on systemic injection of culture-expanded MSCs to treat immune diseases (174). A recent study indicates a strategy through which native MSC function can be modulated via local delivery of cytokines. MSCs exposed to IFN-γ and either TNF-α, IL-1α, or IL-β have been shown to secrete factors that suppress T lymphocyte function *in vitro* (175). The MSCs also recruited additional T lymphocytes to the area, which were then also inactivated (175).

3.5. Concluding Points

Harnessing and modulating inflammatory signaling is a promising new strategy for bone regeneration. Since our previous review (104) three years ago, which introduced this topic to the bone tissue engineering community by identifying key inflammatory cytokines that prime bone regeneration and describing the inhibitory effects of anti-inflammatory agents on bone healing, a multitude of *in vitro* and *in vivo* studies have focused on this topic. These studies have provided crucial information, as well as identified important questions to be answered in future work.

The initial week-long inflammatory phase of fracture healing is characterized by the influx of inflammatory cells, i.e., neutrophils, lymphocytes, and macrophages, and the release of a variety of cytokines and growth factors. However, the mechanism by which these complex signaling cascades trigger scar-less bone regeneration remains unknown. Several cytokines, including TNF-α and IL-6, have been shown to play a critical role in bone healing and have even been successfully harnessed to trigger regeneration in animal models of massive bone trauma. Although they are the primary source of inflammatory cytokines immediately after bone injury, no particular inflammatory cell type has been

identified as critical for bone regeneration. In fact, lymphocytes have been shown to impair bone healing, suggesting that the native bone cells are the most promising targets for rational control of bone inflammation.

Engineering strategies to rationally control inflammatory signaling are necessary because of the complex balance that exists between bone tissue and the immune system, which is responsible for the inflammatory response. Precise spatial and temporal control is necessary when delivering cytokines because both prolonging and obliterating this signaling impairs bone healing. For instance, complete absence of TNF-α delays regeneration, while prolonged exposure to high levels of this cytokine stimulates bone destruction.

A tremendous amount of effort has been invested in developing pharmacologic agents to treat uncontrolled, chronic inflammation and prevent bone damage. In the case of non-steroidal anti-inflammatory drugs (NSAIDs), the negative effects on bone regeneration are clear. However, leukotriene antagonists, which are currently FDA-approved to treat chronic airway inflammation, have shown immense potential as agents to stimulate bone healing. The role of corticosteroids in this field remains unclear. *In vivo*, they have been shown to have a wide range of effects depending on factors including the method and temporal pattern of administration. This is a particularly important lesson for the development of future tissue engineering strategies, as the composition of the implanted material can profoundly affect the immune, and therefore inflammatory, response.

Another very important lesson is the need for clinically realistic *in vitro* models of bone regeneration. Historically, bone tissue engineers have commonly used

dexamethasone, an anti-inflammatory corticosteroid, to stimulate *in vitro* osteogenic differentiation of MSCs and thus generate models of bone healing. However, comparison of *in vitro* results with the available *in vivo* studies of cytokine delivery has indicated this osteogenic supplement cannot be used when studying cytokine delivery. Concurrent delivery of corticosteroids and cytokines such as TNF-α to MSC cultures has resulted in findings that are completely opposite to those seen *in vivo*. Pre-treatment of MSCs with corticosteroids to stimulate *in vitro* osteogenic differentiation, followed by cytokine delivery alone, has yielded more realistic results. Important future directions for *in vitro* studies in this field include studies to elucidate the mechanisms underlying inflammatory signaling, additional optimization of cell culture models, as well as studies of the interplay between various cytokines and growth factors found at the fracture site. Learning to rationally control inflammation will provide a wealth of new directions in the development of bone tissue engineering strategies, and will ultimately improve the quality and specificity of therapies available to stimulate bone regeneration in patients with impaired healing or severe bone injuries.

Chapter 4

Dose Effect of Tumor Necrosis Factor-α on *In Vitro* Osteogenic Differentiation of Mesenchymal Stem Cells on Biodegradable Polymeric Microfiber Scaffolds[5]

Abstract: This study presents a first step in the development of a bone tissue engineering strategy to trigger enhanced osteogenesis by modulating inflammation. This work focused on characterizing the effects of the concentration of a pro-inflammatory cytokine, tumor necrosis factor alpha (TNF-α), on osteogenic differentiation of mesenchymal stem cells (MSCs) grown in a 3D culture system. MSC osteogenic differentiation is typically achieved *in vitro* through a combination of osteogenic supplements that include the anti-

[5] This chapter was published as: Mountziaris PM, Tzouanas SN, Mikos AG. Dose Effect of Tumor Necrosis Factor-<alpha> on In Vitro Osteogenic Differentiation of Mesenchymal Stem Cells on Biodegradable Polymeric Microfiber Scaffolds. *Biomaterials* 2010; 31: 1666-1675.

inflammatory corticosteroid dexamethasone. Although simple, the use of dexamethasone is not clinically realistic, and also hampers *in vitro* studies of the role of inflammatory mediators in wound healing. In this study, MSCs were pre-treated with dexamethasone to induce osteogenic differentiation, and then cultured in biodegradable electrospun poly(ε-caprolactone) (PCL) scaffolds, which supported continued MSC osteogenic differentiation in the absence of dexamethasone. Continuous delivery of 0.1 ng/mL of recombinant rat TNF-α suppressed osteogenic differentiation of rat MSCs over 16 days, which was likely the result of residual dexamethasone antagonizing TNF-α signaling. Continuous delivery of a higher dose, 5 ng/mL TNF-α, stimulated osteogenic differentiation for a few days, and 50 ng/mL TNF-α resulted in significant mineralized matrix deposition over the course of the study. These findings suggest that the pro-inflammatory cytokine TNF-α stimulates osteogenic differentiation of MSCs, an effect that can be blocked by the presence of anti-inflammatory agents like dexamethasone, with significant implications on the interplay between inflammation and tissue regeneration.

4.1. Introduction

The limitations of autologous bone grafting and other available surgical reconstructive techniques have led to increased interest in bone tissue engineering, an interdisciplinary strategy to promote healing of large bone defects using bioactive implantable materials. Cells and bioactive factors are incorporated into these scaffolds to provide temporal and spatial cues guiding bone regeneration (176). However, osteogenesis involves complex molecular signaling and induces significant changes in the

expression of several thousand genes (8, 30, 31). To develop an effective tissue engineering strategy for bone regeneration, the key regulators of this process must be identified and incorporated. Informed by cell biology research, efforts to date have focused on inducing bone regeneration via delivery of various bioactive molecules and osteoprogenitor cells. However, recent insight into the critical role of pro-inflammatory cytokines, including tumor necrosis factor alpha (TNF-α), in bone healing has heralded a new direction in the rational design of bone tissue engineering constructs (104, 163).

Although the impact of unregulated TNF-α signaling on mature bone in osteoporosis, rheumatoid arthritis, and other pathologies has been studied, the role of TNF-α signaling during bone healing is not well understood (104, 120, 159, 160, 162). Recent studies suggest TNF-α plays an important role in priming bone renewal. Expression of TNF-α rises immediately following bone injury, and is elevated again in later stages of bone regeneration (38, 59, 104). Absence of this TNF-α signaling impairs *in vivo* bone fracture healing in a mouse model, delaying endochondral ossification, but it has no effect on skeletal development, suggesting that TNF-α plays a unique role in post-natal osteogenesis (1, 2). We selected TNF-α as a model inflammatory signal for our studies based on its significant impact on *in vivo* bone regeneration.

Our ultimate goal is to develop a novel bone tissue engineering strategy that harnesses inflammation to trigger osteogenesis in large bone defects. However, due to the many gaps in our knowledge regarding the mechanism by which inflammatory signals trigger regeneration, we are first focusing on developing a 3D *in vitro* strategy to better characterize the role of TNF-α on mesenchymal stem cells (MSCs) undergoing osteogenic differentiation. Here we present the results of a study that aimed to establish

the effect of TNF-α concentration on osteogenic differentiation of MSCs cultured *in vitro* on biodegradable microfiber scaffolds.

MSCs are a component of the bone marrow stroma, and have the capability to differentiate into various connective tissues, including bone (3). *In vitro* osteogenic differentiation of MSCs typically requires the addition of dexamethasone (3, 5, 9), an anti-inflammatory corticosteroid that is not found in the *in vivo* fracture healing microenvironment and that suppresses *in vivo* bone regeneration (104, 177). Further, dexamethasone is known to antagonize the *in vitro* effects of TNF-α on osteoblasts (62). Recent efforts have resulted in 3D materials that support *in vitro* differentiation of MSCs without the need for dexamethasone, for instance, by means of a microfiber mesh scaffold coated with pre-generated bone-like extracellular matrix (6, 8, 9).

In this study we used polymer electrospinning to generate porous mesh scaffolds made of poly(ε-caprolactone) (PCL), a biocompatible and biodegradable polymer (178, 179). By modulating key processing variables, including the PCL concentration, flow rate, collector distance, and applied voltage, PCL microfiber scaffolds with a specific pore size, porosity, and fiber diameter can be reproducibly generated (179). Scaffold pore size and porosity are key determinants of cell attachment and migration, and also of nutrient transport, all of which affect cell function, proliferation, and differentiation (180-182). Electrospun PCL fibers with sub-micron diameters have been shown to enhance MSC adhesion and spreading (179). MSCs were pre-cultured to induce osteogenic differentiation, and then cultured on electrospun PCL microfiber meshes, which we assumed would continue to support MSC osteogenic differentiation even in the absence of dexamethasone.

This study addresses the following questions: (i) What is the impact of continuous TNF-α delivery for 4, 8, and 16 days, and (ii) what is the impact of TNF-α concentration, on osteogenic differentiation of MSCs cultured *in vitro* in 3D biodegradable PCL microfiber scaffolds? MSC-seeded scaffolds were exposed to varying concentrations of TNF-α, which we hypothesized would enhance osteogenic differentiation in a dose-dependent manner. Our ultimate goal was to determine the impact of TNF-α concentration on *in vitro* 3D osteogenic differentiation of MSCs.

4.2. Materials and Methods

4.2.1. Experimental Design

A design with 6 groups and 3 time points was used to evaluate the impact of TNF-α dose on rat MSC osteogenic differentiation on electrospun poly(ε-caprolactone) (PCL) scaffolds. Low (0.1 ng/mL), medium (5 ng/mL), and high (50 ng/mL) rat TNF-α concentrations were continuously delivered over a 4, 8, or 16-day culture period. Three control groups were included: cell/scaffold constructs cultured without added TNF-α or dexamethasone; a positive control where constructs received dexamethasone (i.e., complete osteogenic media), but did not receive TNF-α; and an acellular control, where cell-free PCL scaffolds were cultured in the absence of both TNF-α and dexamethasone, in order to account for any non-cell-specific scaffold calcium accumulation.

4.2.2. Electrospun Scaffold Generation

The PCL (inherent viscosity = 1.22 dL/g; Lactel, Pelham, AL) had a number-average molecular weight (M_n) = 72,100 ± 1400 Da, weight-average molecular weight

(M_w) = 115,000 ± 2200 Da, and polydispersity index (M_w/M_n) of 1.60 ± 0.02, determined via gel permeation chromatography (Phenogel Linear Column with 5 μm particles, Phenomenex, Torrance, CA; Differential Refractometer 410, Waters, Milford, MA) using a calibration curve created from polystyrene standards (Fluka, Switzerland). The PCL was dissolved at 18 w/w% in 5:1 (by vol) chloroform:methanol. This solution was used to generate electrospun meshes of PCL microfibers using a previously described apparatus consisting of a syringe pump (Cole Parmer, Vernon Hills, IL), power supply (Gamma High Voltage Research, Osmond Beach, FL), 19 cm diameter copper wire (18 gauge) ring, and a square grounded copper plate (11×11×0.3 cm) (179). Briefly, 9 mL of PCL solution were loaded into a 10 mL syringe to which a 16 gauge blunt-tip needle (Brico Medical Supplies, Inc., Metuchen, NJ) was attached. The syringe was positioned in the electrospinning apparatus such that the needle tip was 33 cm from a glass collecting plate, placed immediately in front of the grounded copper plate, and 4 cm from the copper ring used to direct the spinning fibers onto the plate. The positive lead from the power supply was split and connected to both the needle tip and the copper ring. A voltage difference of 33 kV was applied and the PCL solution was pumped out of the needle tip at 40 mL/h using the syringe pump. Disks with a diameter of 8 mm were cut from each resulting PCL microfiber mesh using an arch punch (C.S. Osborne & Co., Harrison, NJ). Those disks with thickness 0.90-1.10 mm, as measured using digital micro-calipers (Mitutoyo, Aurora, IL), were used as scaffolds for the study. Two electrospun PCL meshes were required to generate a sufficient number of scaffolds for this study. The meshes were prepared on consecutive days from the same lot of PCL, and using the same electrospinning parameters.

4.2.3. Scaffold Morphology

For scanning electron microscopy (SEM), samples were mounted onto aluminum stubs and sputter-coated with 30 nm of gold. Fiber diameters at the top (n = 45 fibers) and bottom (n = 45 fibers) of each mesh were measured via SEM (FEI Quanta 400 Environmental, Hillsboro, OR) at a 7.31 kV accelerating voltage and 3.0 spot size. The bottom of each mesh was defined as the side adjacent to the glass collecting plate, i.e., the first layer of electrospun PCL microfibers to be deposited. The top of the mesh (the side seeded with MSCs) was thus the final layer of microfibers to be deposited. Several methods were used to minimize bias in the fiber diameter measurements. Scaffolds for SEM imaging (n = 3) were blindly punched from widely separated regions of each PCL mesh. The coordinates of the areas to be imaged on each scaffold (n = 3 on the top, n = 3 on the bottom) were established prior to SEM, as was the (previously described) procedure for selecting and measuring fibers (n = 5 per field of view) (179).

4.2.4. Scaffold Porosity

The porosity of n = 50 scaffolds from each mesh was determined via an established gravimetric analysis protocol (179). Briefly, the porosity, ϵ, was calculated based on the apparent density of the scaffold, $\rho_{scaffold}$, and the density of PCL, ρ_{PCL}, according to the equation: $\epsilon = 1 - \rho_{scaffold}/\rho_{PCL}$. To determine $\rho_{scaffold}$ for each scaffold, mass and volume were measured. To calculate volume, each scaffold was approximated as a cylinder with 8 mm diameter and with height equivalent to the scaffold thickness measured with digital micro-calipers.

4.2.5. Mesenchymal Stem Cell Isolation

Rat MSCs were isolated from the pooled femoral and tibial bone marrow of 8 male syngeneic Fischer 344 rats weighing 150-175 g, according to established methods (8, 9). Bone marrow suspensions were cultured for 7 days in 75 cm^2 flasks using complete osteogenic media, which consists of α-MEM containing 10% v/v fetal bovine serum (Gemini Bio-Products, West Sacramento, CA), 50 mg/L gentamicin, 1.25 μg/mL amphotericin-B (Sigma, St. Louis, MO), as well as 3 osteogenic supplements: 10^{-8} M dexamethasone, 0.01 mM β-glycerophosphate, and 50 μg/mL ascorbic acid (all from Sigma), to induce osteogenic differentiation (5, 8). Culture media was changed on days 1, 3, and 5 to remove non-adherent cells. In this study, the adherent cells are designated as "mesenchymal stem cells," based on the established osteogenic potential of this cell population under appropriate *in vitro* conditions (3, 183).

4.2.6. TNF-α Reconstitution and Dilution

Rat TNF-α was used for this study to better model the *in vivo* biology of the rat MSCs, since combining TNF-α from one species (e.g., human TNF-α) with MSCs from another species (e.g., murine MSCs) has been reported to result in TNF-α receptor binding selectivity not seen with native TNF-α (184). Lyophilized recombinant rat TNF-α (R&D Systems, Minneapolis, MN) was reconstituted on the day of scaffold seeding using sterile phosphate-buffered saline (PBS) containing 0.1 w/w% bovine serum albumin (Sigma), according to the manufacturer's instructions. Aliquots were taken from this 100 ng/μL stock TNF-α solution and further diluted to concentrations of 0.1, 5, and 50 ng/μL. All reconstituted TNF-α solutions were split into aliquots, to minimize the number of

freeze/thaw cycles, and stored at -20°C in a manual defrost freezer, according to the manufacturer's instructions. For experiments, 4 μL of diluted solution were added to 4 mL of media used for construct culture, resulting in the desired experimental group concentrations of 0.1, 5, and 50 ng/mL TNF-α.

4.2.7. Scaffold Preparation

Electrospun PCL scaffolds were prepared for MSC seeding according to established protocols (179). The scaffolds were sterilized via exposure to ethylene oxide gas for 14h, and then passed through a decreasing ethanol gradient (from 100% to 70%) to expel air from the scaffold pores. Centrifugation was used to ensure complete prewetting. The ethanol was exchanged with sterile milliQ water, and the scaffolds were then immersed in dexamethasone-free osteogenic media and left in an incubator overnight. Prior to MSC seeding, the scaffolds were press-fit into seeding cassettes and placed into 6-well plates (1 cassette/well). Ultra-low attachment 6-well plates (Corning Incorporated Life Sciences, Lowell, MA), consisting of a neutral, hydrophilic hydrogel covalently bound to a polystyrene well-plate, were used based on the results of a pilot study indicating increased retention of MSCs on electrospun PCL scaffolds (i.e., reduced adhesion of MSCs to the bottom of the well) without any impact on MSC osteogenic differentiation.

4.2.8. Scaffold Seeding and Culture

Nearly confluent MSCs were detached from the cell culture flasks with 0.25% trypsin/EDTA (Sigma, St. Louis, MO), counted with a hemocytometer, centrifuged, and resuspended at 1.25 million cells/mL in dexamethasone-free osteogenic media, which is

identical in composition to complete osteogenic media, except that it lacks dexamethasone. Although dexamethasone is typically used as an osteogenic supplement *in vitro* (5, 9), it was not included in the media used for MSC/scaffold culture because this portion of the study involved TNF-α supplementation, and dexamethasone has been shown to antagonize the *in vitro* effects of TNF-α on osteoblasts (62). For seeding, 200 μL of the resuspended MSCs were added drop-wise to each scaffold, which had already been press-fit into a seeding cassette and placed in a 6-well plate (Corning), as detailed above. MSCs were allowed to attach to the scaffolds for 4h, and then each well was filled with dexamethasone-free media as well as supplemental TNF-α or dexamethasone, as appropriate. After 24h, cell/scaffold constructs (n = 15 per group) were transferred to new ultra-low attachment 6-well plates (1 construct/well). 4 mL of dexamethasone-free media were added to each well, and relevant groups also received supplemental TNF-α (0.1, 5, or 50 ng/mL per well) or dexamethasone (10^{-8} M/well). Thereafter, media and supplements were changed every two days for a total of 4, 8, or 16 days of culture.

4.2.9. Cellularity Measurement

Construct cellularity was quantified according to an established protocol (9). At each timepoint, n = 4 constructs from each group were rinsed twice with PBS and placed in 1 mL of sterile milliQ water. The cells were lysed and cell contents were extracted with 3 freeze/thaw/sonication cycles (10 min at -80°C, 10 min at 37°C, 10 min sonication). The dsDNA content of each resulting solution was quantified using the fluorometric PicoGreen assay (Molecular Probes, Eugene, OR) with an excitation wavelength of 490 nm and an emission wavelength of 520 nm, as detailed elsewhere (9).

Samples and dsDNA standards were run in triplicate. The results were converted to cells per construct using the previously established DNA content of rat MSCs (9).

4.2.10. Alkaline Phosphatase Activity Assay

Alkaline phosphatase (ALP) activity of MSC-seeded scaffolds was used as an early marker of osteogenic differentiation (9). An established colorimetric assay was used to quantify ALP activity based on the rate of conversion of a colorless substrate, *p*-nitrophenyl phosphate disodium salt hexahydrate (Sigma), to a yellow product, *p*-nitrophenol (9). The assay was prepared in a 96-well plate using aliquots of the same cell lysate used to measure cellularity, according to an established protocol (9). Samples were run in triplicate, and diluted to fall within the range of the *p*-nitrophenol standards. After 1h incubation at 37°C, the reaction was stopped with 0.3 M NaOH and the absorbance at 405 nm was measured with a plate reader. ALP activity was normalized to construct cellularity (9).

4.2.11. Calcium Content Assay

The acid-soluble calcium content of MSC-seeded scaffolds was used to quantify mineralized matrix deposition, which is a late-stage marker of osteogenic differentiation (9). An established colorimetric assay was used to quantify calcium content based on the color change that occurs when a calcium chelating agent (Arsenazo III, Diagnostic Chemicals, Oxford, CT) binds to free calcium in an acid solution. Prior to the assay, each construct was removed from the aqueous cell lysate, immersed in 1 mL 1 N acetic acid, and left on a shaker table at 200 rpm overnight to dissolve matrix-bound calcium. The assay was prepared in a 96-well plate as previously described, and absorbance at 650 nm

was read after a 10 min incubation (9). Samples were run in triplicate and diluted to fall within the range of the $CaCl_2$ standards.

4.2.12. Histological Sample Preparation

At each timepoint, n = 1 construct from each group was rinsed twice with PBS and fixed overnight in 5 mL of 10% buffered formalin phosphate. Constructs were then passed through an ascending (70% to 100%) ethanol gradient and stored in 100% ethanol at 4°C. Prior to sectioning, each construct was cut in half using a razor blade, so that cross-sectional images could be obtained. Half was returned to storage in 100% ethanol and the other half was embedded in HistoPrep frozen tissue embedding media (Fisher Scientific, Pittsburgh, PA). Frozen 5 μm thick sections were cut using a cryotome (CM1850, Leica Microsystems, Bannockburn, IL) and mounted on Superfrost Plus glass slides (Fisher Scientific). The slides were incubated at 45°C on a slide warmer for 4-5 days for optimal section adhesion.

4.2.13. Histological Staining and Imaging

To visualize the distribution of mineralized matrix and cells within each construct, sections were rehydrated with water for 1 min and then immersed in von Kossa stain (5% w/w silver nitrate in milliQ water) under UV for 30 min. Residual stain was removed by gentle drop-wise rinsing with water followed by 95% ethanol. Sections were then counter-stained with alcoholic eosin Y (Sigma) for 3 min. Residual eosin was removed by gentle drop-wise rinsing with 95% ethanol. Once dry, stained slides were imaged with a light microscope (Eclipse E600, Nikon, Melville, NY) using an attached video camera (3CCD Color Video Camera DXC-950P, Sony, Park Ridge, NJ) and computer. Light

microscope images were calibrated using the standard two-image method to correct for differences in background lighting and in dark-current effects in the detector (185).

4.2.14. Statistical Analysis

Fiber diameters and porosities are reported as mean ± standard deviation for n = 45 fibers and n = 50 scaffolds, respectively. The average fiber diameter of the top and bottom of each PCL microfiber mesh, along with the average porosity, were compared using a Student's t-test for two independent samples with equal variance ($\alpha = 0.05$) after performing an F-test to validate the assumption of equal variance at 95% confidence. Cellularity, ALP activity, and calcium assay results are reported as mean ± standard deviation for n = 4 constructs. Statistical differences in cellularity, ALP activity, and calcium content amongst groups at each time point, and also within each group over time, were analyzed at 95% confidence using one-way analysis of variance. Multiple pair-wise comparisons were made using the Bonferroni post-hoc analysis method at 95% confidence.

4.3. Results

The two electrospun PCL microfiber meshes fabricated for this study had statistically equivalent mean fiber diameters ($p > 0.05$), as shown in Table 4.1. Although the average porosities of the two meshes were statistically different ($p < 0.05$), the magnitude of the difference was quite small (77.8 ± 2.8% vs. 79.5 ± 3.1%), and so the two meshes were used to generate the PCL scaffolds for this study. Equal numbers of

scaffolds were randomly selected from each mesh. Figure 4.1 shows representative scaffold morphology obtained via SEM at varying magnifications.

Table 4.1 Comparison of fiber diameters and porosites for the two electrospun meshes used for this study.

Parameter for Comparison	Value for Mesh 1	Value for Mesh 2
Fiber Diameter, Top (μm)	9.50 ± 1.57	9.37 ± 2.04
Fiber Diameter, Bottom (μm)	11.58 ± 2.23	11.76 ± 1.79
Porosity (%)	77.8 ± 2.8*	79.5 ± 3.1*

Values are presented as mean ± standard deviation. The sample size was $n = 45$ for fiber diameters from the top and bottom of each mesh, and $n = 50$ scaffolds for PCL mesh porosity. Pairs of values were compared and statistically significant differences ($p < 0.05$) are indicated with a "*."

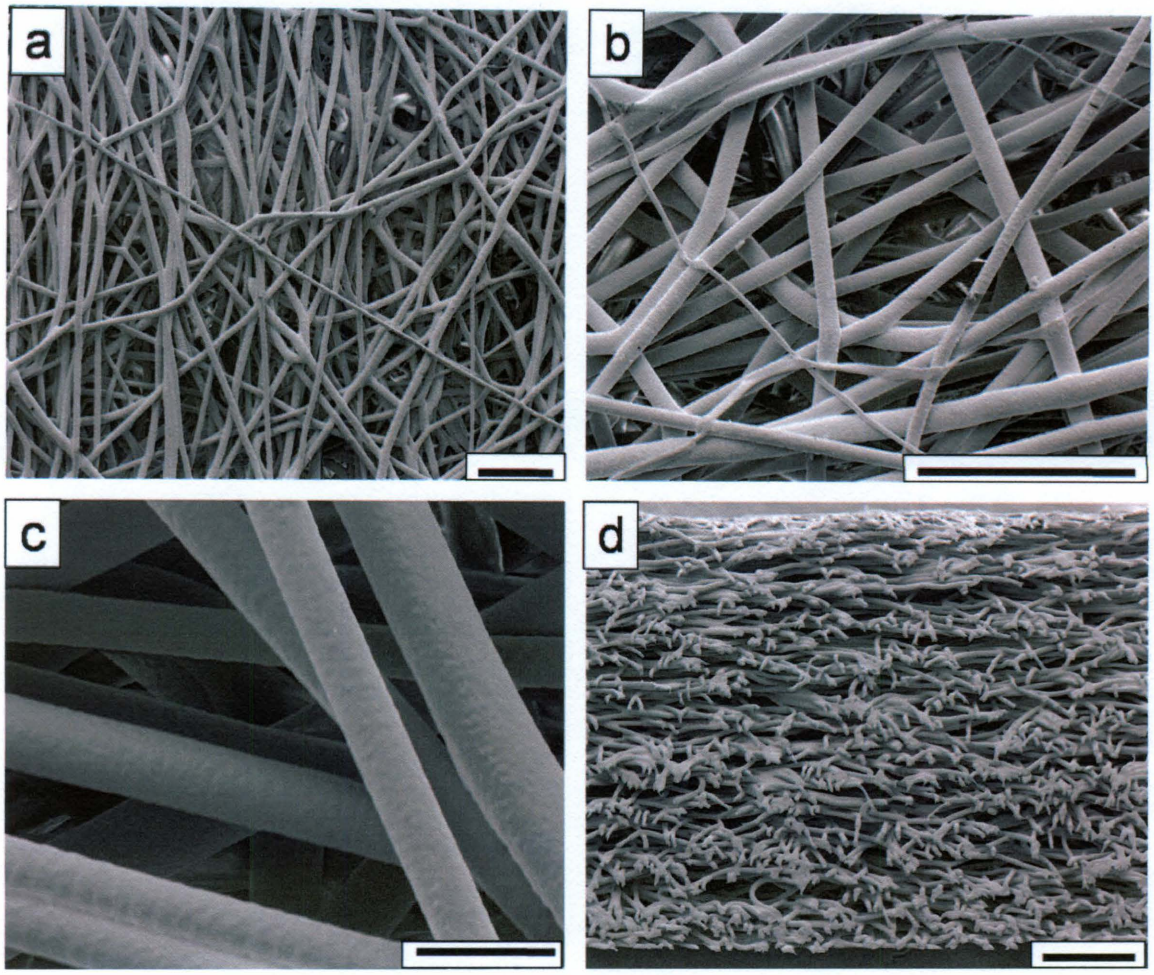

Figure 4.1: Electrospun scaffold morphology.

Electrospun microfibers generated for this study, imaged via SEM at varying magnifications, (a) 200×, (b) 600×, and (c) 2000×. A cross-section through the entire thickness of a representative scaffold is shown in (d), at 120× magnification. Scale bars shown for (a) and (b) represent 100 μm, 20 μm for (c), and 200 μm for (d).

Figure 4.2 depicts the number of cells in the constructs after 4, 8, and 16 days of culture. Most groups had similar cellularity at each timepoint, with a few exceptions. The acellular control ("Acellular") had nearly zero cells/scaffold at all timepoints, as expected. The cellularity of the positive control group ("0 ng/mL TNF +dex") peaked at the earliest timepoint (day 4), at a value significantly higher than the number of cells on the experimental constructs ($p < 0.05$). The number of cells on the positive control constructs subsequently declined (values at all three timepoints differ, $p < 0.05$), such that this group had significantly fewer cells than the other groups at day 16 ($p < 0.05$). The negative control group ("0 ng/mL TNF") followed a similar trend, although no statistical differences were detected between timepoints ($p > 0.05$). In contrast, the lowest dose of TNF-α ("0.1 ng/mL TNF") induced proliferation resulting in a monotonic increase in cellularity (values at all three timepoints differ, $p < 0.05$), with cell numbers for this group exceeding those of all others on days 8 and 16 ($p < 0.05$). The highest dose of TNF-α ("50 ng/mL TNF") also induced proliferation, but cellularity peaked at day 8 and then declined (day 4 and day 16 values both differ from day 8, $p < 0.05$). The middle dose of TNF-α ("5 ng/mL TNF") followed a similar trend, with an apparent peak at day 8 and subsequent plateau, but no statistical differences were detected between timepoints ($p > 0.05$).

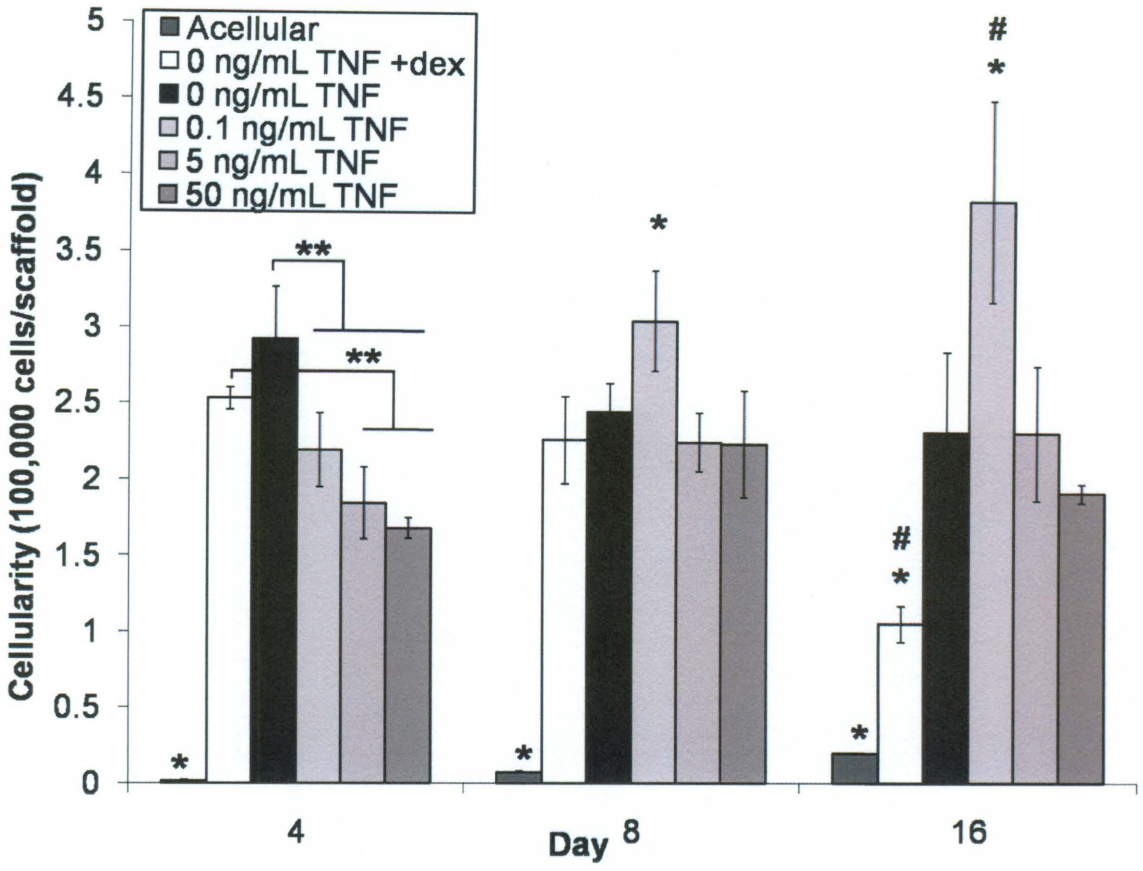

Figure 4.2: Scaffold cellularity over time.

Cellularity of MSC-seeded electrospun PCL scaffolds after 4, 8, and 16 days of culture. Three freeze/thaw/sonication cycles were used to extract dsDNA, which was then quantified with a fluorometric kit and translated to cells/scaffold. Experimental groups were cultured in dexamethasone-free osteogenic media supplemented with 0.1, 5, or 50 ng/mL TNF-α (abbreviated "TNF" in the figure). Three control groups were included: a positive control supplemented with dexamethasone, but no TNF-α ("0 ng/mL TNF +dex"); a negative control cultured without any added dexamethasone ("0 ng/mL TNF"); and an acellular control, where cell-free PCL scaffolds were cultured in dexamethasone-free media ("Acellular"). Each bar represents the mean ± standard deviation for $n = 4$ constructs. Error bars are included for all groups, though they are too small to resolve for "Acellular." Statistical differences ($p < 0.05$) among groups at a single timepoint are indicated by "*" for a group that differs from all other groups, and "**" for a group that differs from only some groups. Changes over time are indicated by "#," meaning that values for that group at each timepoint are significantly different ($p < 0.05$).

Figure 4.3 shows the ALP activity of the constructs on a per cell basis. Dexamethasone induced ALP activity, such that the 0 ng/mL TNF +dex positive control had significantly higher values than all other groups at each timepoint ($p < 0.05$), and showed an increasing trend throughout the study (all timepoints different, $p < 0.05$). Unlike the positive control, the ALP activity of the 0 ng/mL TNF negative control did not change throughout the study (all timepoints similar, $p > 0.05$), although it did appear to be declining by day 16. In contrast, supplementation with TNF-α greatly reduced ALP activity on a per cell basis. The experimental groups had significantly lower ALP activity than both of the MSC-seeded control groups at all timepoints ($p < 0.05$). This suppression appeared dose-dependent on day 4 since 0.1 ng/mL TNF had higher ALP activity than 50 ng/mL TNF ($p < 0.05$), and the value for 5 ng/mL TNF fell between these two. Although the ALP activity of 0.1 ng/mL TNF remained higher than that of the other two experimental groups at all timepoints ($p < 0.05$), these groups showed divergent trends over time. The ALP activity of 0.1 ng/mL TNF peaked at day 8 (all timepoints differ, $p < 0.05$), while 5 ng/mL TNF and 50 ng/mL TNF had monotonically decreasing ALP activity (in each group, all timepoints differ, $p < 0.05$), that was indistinguishable from the acellular group by day 16 ($p > 0.05$). As expected, the acellular control had nearly zero ALP activity at all timepoints.

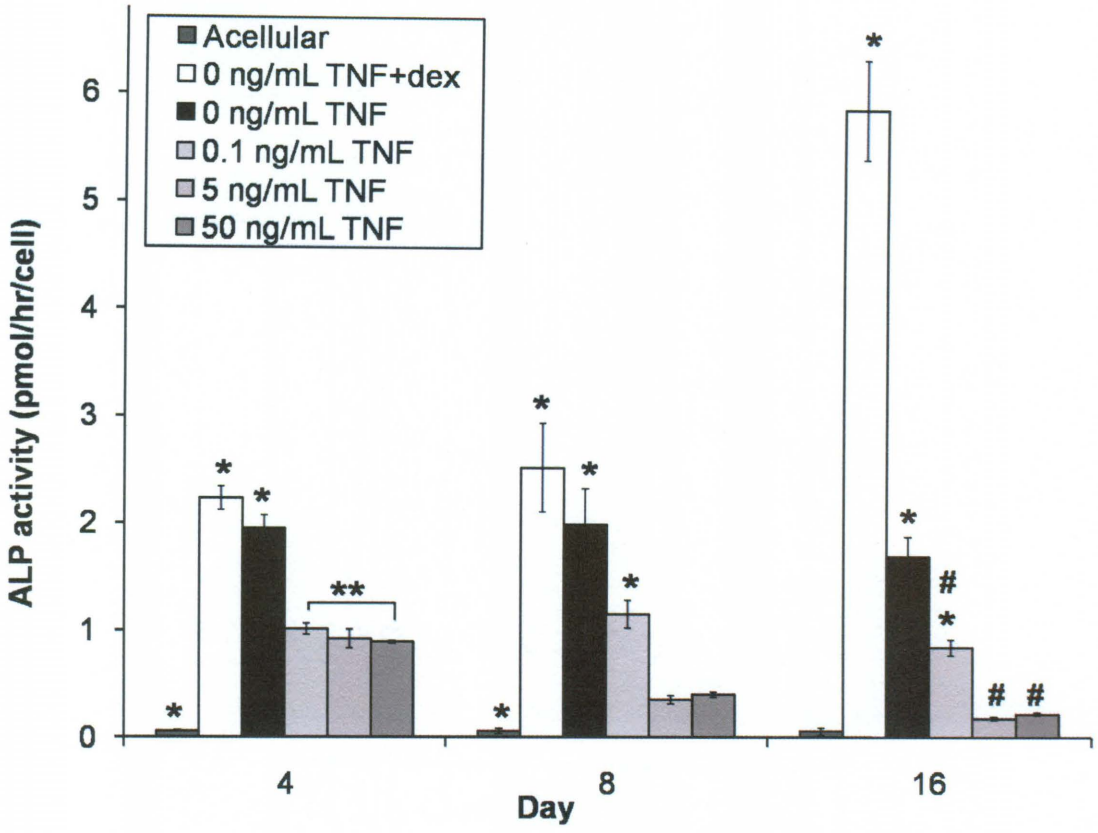

Figure 4.3: Scaffold alkaline phosphatase activity over time.

Alkaline phosphatase (ALP) activity of MSC-seeded electrospun PCL scaffolds after 4, 8, and 16 days of culture. Experimental groups were cultured in dexamethasone-free osteogenic media supplemented with 0.1, 5, or 50 ng/mL TNF-α (abbreviated "TNF" in the figure). Three control groups were included: a positive control supplemented with dexamethasone, but no TNF-α ("0 ng/mL TNF +dex"); a negative control cultured without any added dexamethasone ("0 ng/mL TNF"); and an acellular control, where cell-free PCL scaffolds were cultured in dexamethasone-free media ("Acellular"). Each bar represents the mean ± standard deviation for $n = 4$ constructs. Error bars are included for all groups, though they are too small to resolve in some cases. Statistical differences ($p < 0.05$) among groups at a single timepoint are indicated by "*" for a group that differs from all other groups, and "**" for a group that differs from only some groups. Changes over time are indicated by "#," meaning that values for that group at each timepoint are significantly different ($p < 0.05$).

Figure 4.4 illustrates the acid-soluble calcium content of the constructs after 4, 8, and 16 days of culture. The calcium content of all groups, with the exception of the acellular control, monotonically increased over time. Dexamethasone induced the greatest amount of overall calcium deposition, such that the 0 ng/mL TNF +dex positive control had significantly higher values than all other groups on days 8 and 16 ($p < 0.05$), and showed an increasing trend throughout the study (all timepoints different, $p < 0.05$). TNF-α triggered early mineralized matrix deposition in a dose-dependent manner, such that 5 ng/mL TNF had significantly more calcium on day 4 than the control groups and 0.1 ng/mL TNF ($p < 0.05$), and 50 ng/mL TNF had even more calcium ($p < 0.05$). After day 4, the rate at which calcium was deposited in these constructs declined, while the calcium deposition rate of the controls increased. By day 8, the negative control (0 ng/mL TNF) and 50 ng/mL TNF constructs had similar calcium content ($p > 0.05$), and continued to deposit similar amounts of calcium through day 16 ($p > 0.05$). On both days 8 and 16, the calcium content of 0 ng/mL TNF and 50 ng/mL TNF significantly exceeded that of the other two experimental groups ($p < 0.05$). In fact, the lower doses of TNF-α almost completely suppressed calcium deposition. The mineralized matrix deposition rate of the 5 ng/mL TNF constructs fell to zero after day 4, so that essentially no further calcium was deposited over the course of the study. The calcium content of the 0.1 ng/mL TNF constructs also plateaued; it increased ($p < 0.05$) from a near-zero level on day 4 to a level equivalent to the 5 ng/mL TNF constructs on day 8. Neither group showed any further calcium deposition on day 16 ($p > 0.05$).

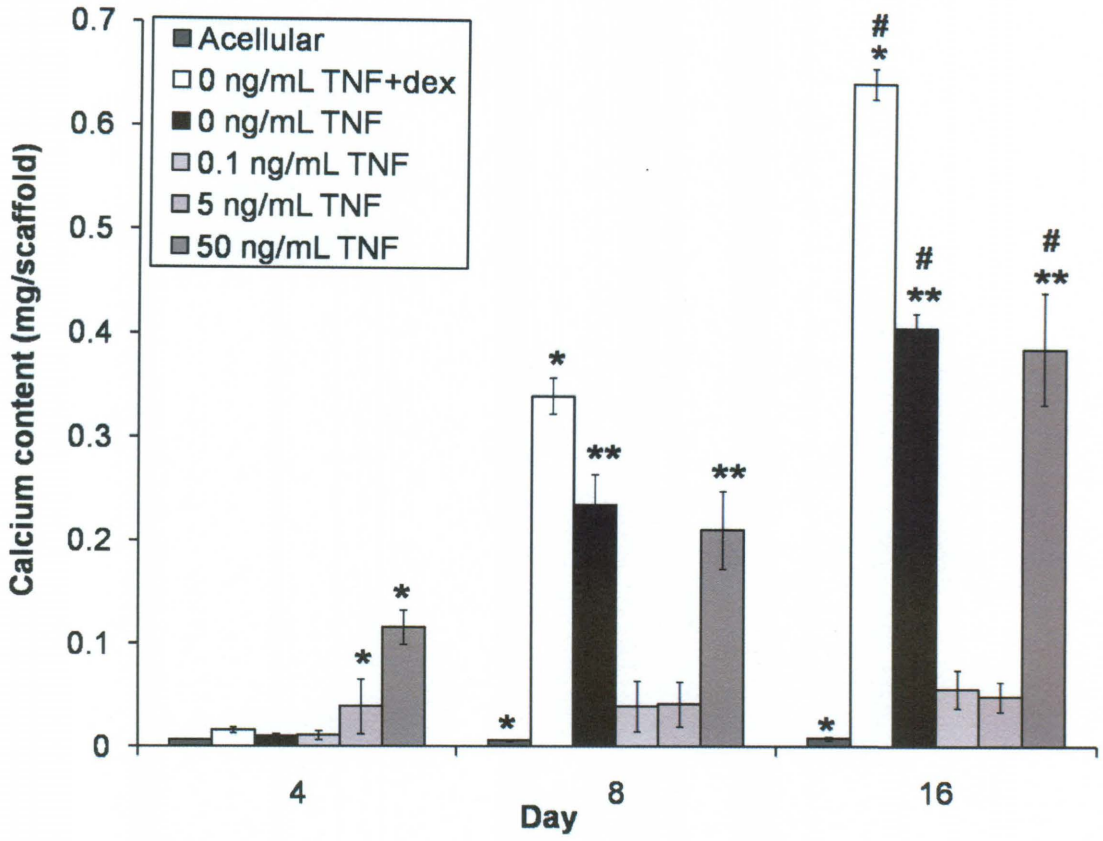

Figure 4.4: Scaffold mineralization over time.

Calcium content of MSC-seeded electrospun PCL scaffolds after 4, 8, and 16 days of culture. Experimental groups were cultured in dexamethasone-free osteogenic media supplemented with 0.1, 5, or 50 ng/mL TNF-α (abbreviated "TNF" in the figure). Three control groups were included: a positive control supplemented with dexamethasone, but no TNF-α ("0 ng/mL TNF +dex"); a negative control cultured without any added dexamethasone ("0 ng/mL TNF"); and an acellular control, where cell-free PCL scaffolds were cultured in dexamethasone-free media ("Acellular"). Each bar represents the mean ± standard deviation for $n = 4$ constructs. Error bars are included for all groups, though they are too small to resolve in some cases. Statistical differences ($p < 0.05$) among groups at a single timepoint are indicated by "*" for a group that differs from all other groups, and "**" for groups that do not differ from each other, but differ from all other groups. Changes over time are indicated by "#," meaning that values for that group at each timepoint are significantly different ($p < 0.05$).

The results of the cellularity and calcium content assays were confirmed qualitatively through histological analysis, shown in Figure 4.5. Sections were stained with von Kossa, which stains mineralized extracellular matrix black, and counter-stained with eosin, which dyes cytoplasmic material and organic matrix components (e.g., collagen) reddish-pink. The highest density of mineralized matrix was observed at the top of the scaffolds, visible as black deposits of varying widths and ~40 μm thickness (blue arrows in Figure 4.5). Consistent with the calcium assay data (Figure 4.4), 50 ng/mL TNF sections stained the darkest with von Kossa on day 4, while 0 ng/mL TNF +dex was the darkest-staining group on days 8 and 16 (Figure 4.5). The presence of the black-stained mineralized matrix made it difficult to discern the cells in sections with high calcium because the matrix was co-localized with cells.

In general, the highest density of cells was observed at the top of the scaffolds. At the earliest timepoint, when the calcium content of all groups was at its lowest, a 5-10 μm thick pink-stained layer of cells and non-mineralized matrix was visible at the top of each section (indicated by yellow arrows), except for the acellular construct (Figure 4.5). Consistent with cellularity (Figure 4.2) and calcium measurements (Figure 4.4), a very thick (~30 μm) reddish-pink layer of cells and (mostly non-mineralized) matrix was observed on the top surface of the 0.1 ng/mL TNF sections on days 8 and 16 (see representative images in Figure 4.5). Cells infiltrated 200-500 μm into each microfiber scaffold; these lower-density collections of cells gave the upper ~200 μm of the section a grayish tint (e.g., day 8 image of 0 ng/mL TNF in Figure 4.5), and/or appeared as grayish threads and speckles amidst the PCL fibers (e.g., yellow arrows in lower half of day 16 image of 0 ng/mL TNF in Figure 4.5). The grayish color of these features is an artifact of

the low magnification (10×) used to capture the images in Figure 4.5. At higher magnification (not shown), these structures were tinted pink, as expected for eosin-stained cells. Mineralized matrix was also deposited on PCL fibers 200-500 μm below the surface, consistent with the depth of cell infiltration. This was particularly evident when comparing the lower portions of the stained sections (e.g., day 16 images of 0 ng/mL TNF +dex, 0 ng/mL TNF, and Acellular in Figure 4.5).

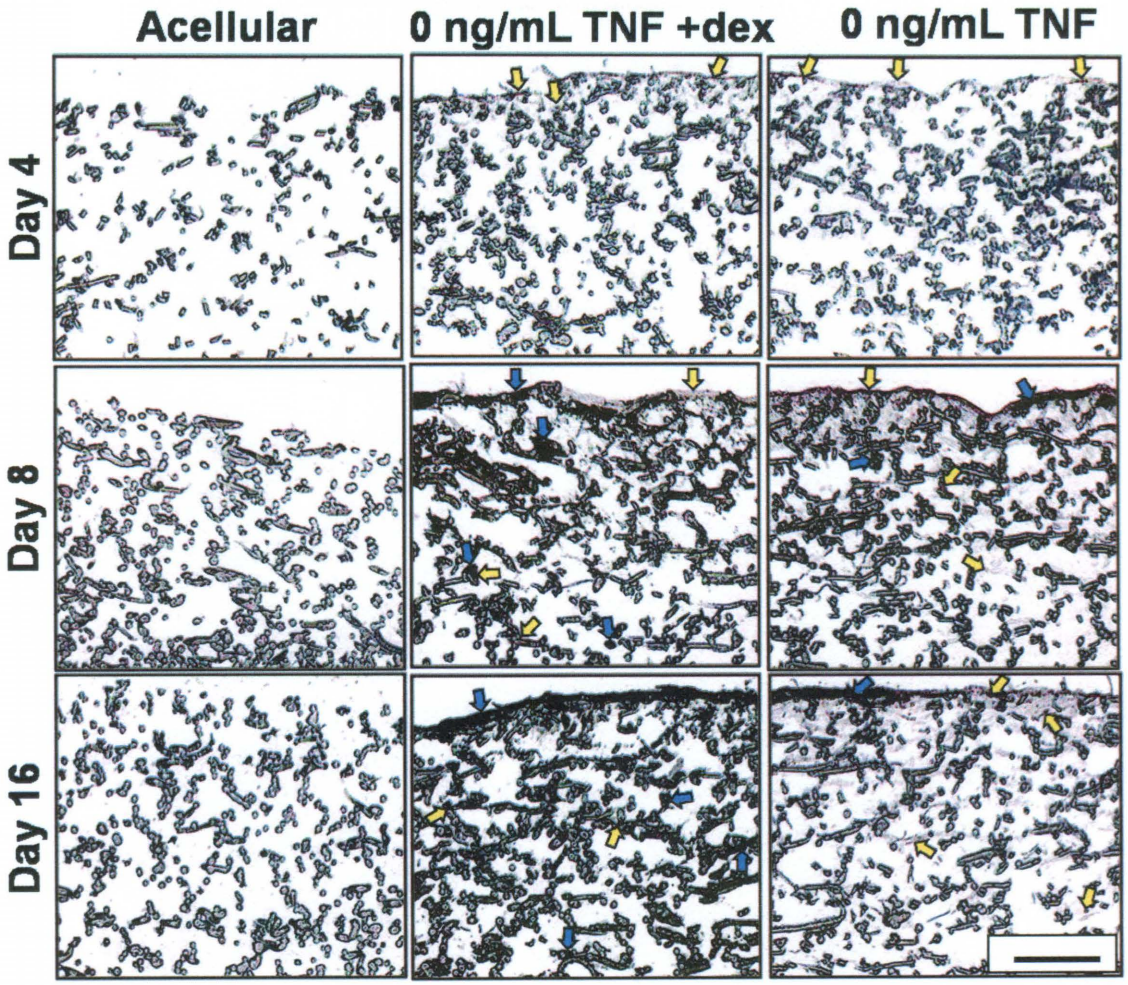

Figure 4.5 – part 1 (continued on next page)

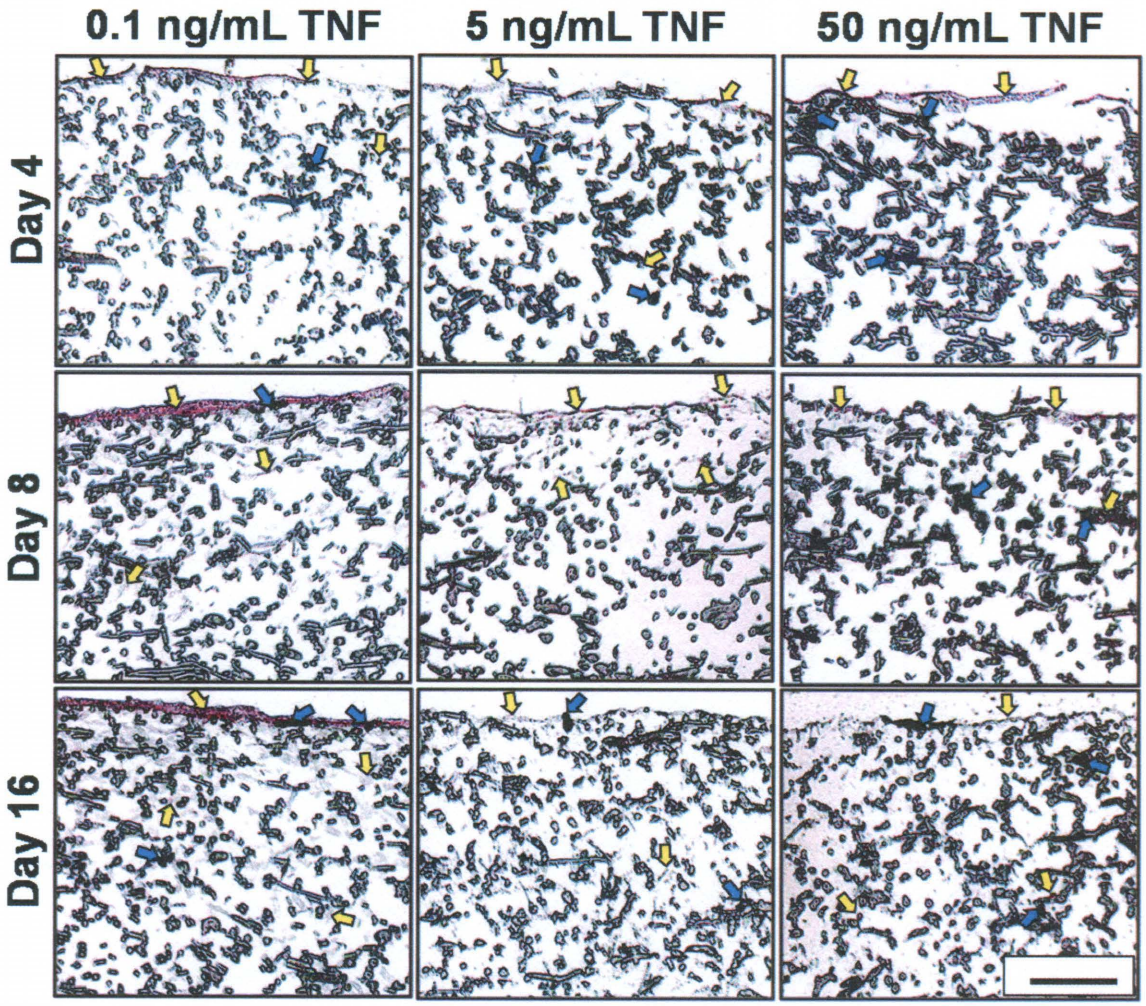

Figure 4.5: Representative histological images from each timepoint.
Representative cross-sectional images (5 μm thick) of stained MSC-seeded electrospun PCL scaffolds after 4, 8, and 16 days of culture. Sections were stained with von Kossa and eosin. Each image shows only the top half of each cross-section, which is where cells (representative examples indicated by yellow arrows) and mineral deposits (representative examples marked with blue arrows) were located. Experimental groups were cultured in dexamethasone-free osteogenic media supplemented with 0.1, 5, or 50 ng/mL TNF-α (abbreviated "TNF" in the figure). Three control groups were included: a positive control supplemented with dexamethasone, but no TNF-α ("0 ng/mL TNF +dex"); a negative control cultured without any added dexamethasone ("0 ng/mL TNF"); and an acellular control, where cell-free PCL scaffolds were cultured in dexamethasone-free media ("Acellular"). Images were captured at 10× original magnification. Scale bar in lower right corner represents 200 μm and applies to all images.

4.4. Discussion

The goal of this study was to determine the effect of TNF-α dose on MSC osteogenic differentiation in a 3D biodegradable microfiber mesh scaffold. The lowest TNF-α concentration (0.1 ng/mL) for this study was selected because it approximates the physiologic level of TNF-α measured in wound fluid from patients with severe bone injuries (67). The medium (5 ng/mL) and high TNF-α concentrations (50 ng/mL) were selected based on previous studies demonstrating differential effects on the 2D osteogenic differentiation of MSCs (158, 160, 162). We found that continuous delivery of a low dose (0.1 ng/mL) of recombinant rat TNF-α suppressed osteogenic differentiation of rat MSCs over 16 days. In contrast, continuous delivery of a higher dose, 5 ng/mL TNF-α, stimulated osteogenic differentiation for a few days, and 50 ng/mL TNF-α resulted in significant mineralized matrix deposition over the course of the study. Our findings suggest that TNF-α stimulates osteogenic differentiation of MSCs, and that this effect can be antagonized by signaling resulting from pre-culture with the anti-inflammatory agent dexamethasone.

An important feature of this study is the use of TNF-α and MSCs from the same species. Recombinant rat TNF-α was used to better model the *in vivo* biology, since the MSCs were from a rat source. Rats were selected in anticipation of future *in vivo* implantation studies to evaluate bone regeneration using an established rat critical size cranial defect model (186). To our knowledge, no other studies have reported on the ALP activity and mineralized matrix deposition of rat MSCs treated with rat TNF-α *in vitro* either in 2D or 3D culture. Several previous studies with rat osteoprogenitors have inter-mingled species; for instance, fetal rat calvarial osteoblasts were treated with recombinant

human TNF-α, resulting in decreased calcium deposition when TNF-α was given during the first two weeks of culture, and no effect if TNF-α administration began thereafter (187, 188). However, inter-species variability in TNF-α is significant, as shown rigorously for humans and mice. Human TNF-α selectively binds to the type 1 TNF receptor on murine MSCs, while murine TNF-α has equal affinity for both type 1 and 2 TNF-α receptors (184). Thus, it is difficult to use the results of these studies to better understand the *in vivo* impact of TNF-α. Additionally, studies using MSCs and TNF-α from the same species have shown divergent effects. Human MSCs treated *in vitro* with human TNF-α for 14-21d showed increased ALP activity and calcium deposition (159, 160), while recombinant murine TNF-α (also delivered for 14-21d) suppressed ALP activity and mineralized matrix deposition of murine MSCs (162, 189). This suggests that species physiology affected our osteogenic marker results.

Our results indicate that unmodified electrospun PCL microfiber meshes support 3D osteogenic differentiation of MSCs. This was not seen in similar *in vitro* studies with titanium microfiber meshes, where scaffolds required a pregenerated bone-like mineralized matrix coating in order to support *in vitro* rat MSC osteogenic differentiation under static conditions, particularly in the absence of dexamethasone (9). In this study, the calcium per construct achieved in the 0 ng/mL TNF +dex positive control constructs after 16 days (Figure 4.4) far exceeds the values reported for MSC-seeded titanium microfiber meshes under similar *in vitro* conditions (644.5 ± 14.9 μg vs. 10-20 μg), and is similar to the net calcium deposition achieved when the titanium microfibers were coated with pregenerated bone-like matrix (9). Similarly, the 407.6 ± 14.1 μg of calcium deposited after 16 days in the absence of dexamethasone (0 ng/mL TNF values in Figure

4.4) exceeds that for both unmodified (~0 μg) and bone-like matrix coated (213.2 ± 13.6 μg) titanium microfiber constructs (9). Several potential explanations for these findings exist. The batch of MSCs used for this study may have had inherently higher capacity for mineralized matrix deposition. This is a less likely explanation, however, since the MSCs from 5 or more rats were pooled to reduce such variability. Additionally, similar high calcium values have been achieved in pilot studies using MSC-seeded PCL scaffolds (results not shown). The hydrophobicity of the PCL microfibers may have played a role by promoting protein adsorption and subsequent cell adhesion, which may have enhanced osteogenic differentiation. PCL was selected for the generation of electrospun microfiber scaffolds because of its biocompatibility and very slow degradation rate, such that scaffolds implanted *in vivo* as a component of a future bone tissue engineering strategy would promote tissue ingrowth and provide structural support within a bone defect, and then later degrade to allow for remodeling of the regenerated bone (179, 182). The variation in fiber size inherent to the generation of electrospun PCL meshes may have been beneficial, compared to the relatively uniform prefabricated titanium meshes. SEM indicated that although largely comprised of ~10 μm diameter fibers, the PCL meshes also contained some smaller fibers (Figure 4.1a,b). Electrospun PCL fibers with sub-micron diameters have been shown to enhance rat MSC adhesion and spreading (179). The results of this study indicate that electrospun PCL microfiber meshes are promising candidates as components of 3D *in vitro* culture systems to better understand the role of inflammatory mediators in MSC osteogenic differentiation.

We capitalized on this finding to culture MSCs in the absence of dexamethasone, which was particularly important as this anti-inflammatory corticosteroid blocks the *in*

vitro effects of TNF-α on osteoblasts (62). Corticosteroids, including dexamethasone, interfere with intracellular TNF-α signaling mainly by binding to and inactivating nuclear factor-κB (NF-κB), a transcription factor (177). TNF-α binding to cell-surface receptors activates NF-κB, which travels from the cell cytoplasm to the nucleus, binds to DNA, and activates specific genes. Antagonizing NF-κB blocks many effects of TNF-α on cells (177). Unlike TNF-α, corticosteroids are not found in the *in vivo* fracture healing microenvironment and have been shown to suppress *in vivo* bone regeneration (104, 177). Thus, the exclusion of dexamethasone from the culture media of all but the positive control group had the benefit of making the 3D culture system described herein a better approximation of *in vivo* bone biology.

However, dexamethasone is commonly used for *in vitro* MSC culture, in combination with ascorbic acid and β-glycerophosphate, due to the resulting significant stimulation of osteogenic markers like ALP activity and mineralized matrix deposition (3, 5, 9). In this study, all three of these supplements were provided to the rat MSCs during the 2D pre-culture expansion period based on previous reports that dexamethasone is necessary to initiate *in vitro* osteogenic differentiation of rat MSCs (3, 9). Dexamethasone supplementation was discontinued once the MSCs were seeded onto the biodegradable PCL microfiber scaffolds, i.e., during the portion of the study involving TNF-α supplementation. The only exception was the 0 ng/mL TNF +dex positive control group, which received continuous dexamethasone supplementation and as a result showed elevated markers of osteogenic differentiation, with the highest level of ALP activity throughout the study ($p < 0.05$; Figure 4.3) and the highest level of calcium deposition on days 8 and 16 ($p < 0.05$; Figure 4.4).

The decrease in cellularity over time observed in the 0 ng/mL TNF +dex positive control (Figure 4.2; values at all three timepoints differ, $p < 0.05$) is consistent with our previous experience with rat MSC osteogenic differentiation on titanium meshes (20 μm fiber diameter) (9) and starch-PCL blend (180 μm fiber diameter) scaffolds (182). Two possible explanations for this decline in measured cellularity over time have been reported. One possibility is that it is an artifact of late-stage osteogenic differentiation of MSCs, which results in increased deposition of mineralized matrix that traps DNA and prevents its detection (9). The 0 ng/mL TNF +dex constructs exhibited high levels of calcium deposition on days 8 and 16 (Figure 4.4), a trend confirmed by von Kossa staining (Figure 4.5). Histology also indicated that calcified matrix co-localized with cells and the (eosin-stained) cell content of the 0 ng/mL +dex constructs appeared to increase over time, particularly from days 4 to 8 (Figure 4.5), suggesting that complete DNA detection may have been impaired by the high mineralized matrix content of these constructs. This mechanism could also be applied to the subtly declining cell counts seen in the dexamethasone-free negative control (Figure 4.2; non-significant decreasing trend for 0 ng/mL TNF constructs, $p > 0.05$), and also to the 50 ng/mL TNF group, where measured cellularity declined significantly from day 8 to day 16 (Figure 4.2; $p < 0.05$); this finding was not seen with the other two doses of TNF-α. At the same time, calcium content of the 0 ng/mL TNF and 50 ng/mL TNF constructs increased significantly (Figure 4.4; all three timepoints differ within each group, $p < 0.05$) and greatly exceeded that for the other two TNF-α doses on days 8 and 16 (Figure 4.4; $p < 0.05$).

Another possible explanation for the decrease in cellularity over time observed in the 0 ng/mL TNF +dex positive control (Figure 4.2; values at all three timepoints differ, p

< 0.05) is a direct effect of dexamethasone, which is known to support MSC proliferation in some cases and inhibit it in others. Factors influencing this effect include dexamethasone dose and duration, as well as MSC species and stage of osteogenic differentiation (3). Under this theory, the subtle decline in cellularity seen for the 0 ng/mL TNF (Figure 4.2; non-significant decreasing trend, $p > 0.05$) and 50 ng/mL groups (Figure 4.2; significant decline from days 8-16, $p < 0.05$) would be attributable to end-stage osteogenic differentiation of the MSCs, associated with cessation of cell proliferation, decreased early-stage markers (in this study, ALP activity shown in Figure 4.3; non-significant decreasing trend for 0 ng/mL TNF, $p > 0.05$, and significant decreasing trend for 50 ng/mL TNF, $p < 0.05$), and elevated late-stage markers (here, mineralized matrix deposition in Figure 4.4; significant increasing trends for 0 ng/mL TNF and 50 ng/mL TNF, $p < 0.05$). In contrast, the substantial decrease in cell content of the 0 ng/mL TNF +dex constructs (Figure 4.2; cellularity lower than all other groups except acellular on day 16, $p < 0.05$) would be the combined result of terminal MSC differentiation into osteoblasts and a direct effect of dexamethasone on cellularity. Further studies are required to distinguish between these two possibilities.

Overall, no adverse effect of 0.1 – 50 ng/mL TNF-α on cell viability was seen over the course of 16 days, consistent with recent reports for 2D *in vitro* MSC cultures in dexamethasone-free osteogenic media (159, 160). Although cell counts in the experimental constructs were lower than in the controls on day 4 ($p < 0.05$), this difference was no longer present by day 8 (Figure 4.2). The monotonic increase in cellularity over time for 0.1 ng/mL TNF constructs (Figure 4.2; values at all three timepoints differ, $p < 0.05$) is consistent with proliferation recently reported for human

MSCs encapsulated in 3D poly(ethylene glycol)-based hydrogels and exposed to recombinant human TNF-α for 14 days in the presence of dexamethasone (163). This increase in proliferation was suggested to indicate that TNF-α inhibits osteogenic differentiation of human MSCs, particularly when combined with data indicating that TNF-α suppressed ALP activity of human MSCs in the hydrogels (163). However, it is likely that these published results reflect the combined, opposing effects of TNF-α and dexamethasone delivery.

In this study, the divergent effects of low and high doses of TNF-α on markers of MSC osteogenic differentiation likely arose from the relative balance between dexamethasone- and TNF-α-related signaling early in 3D culture. Our results for the 0.1 ng/mL TNF constructs suggest that TNF-α inhibited osteogenic differentiation, but the data for the 50 ng/mL TNF group suggest the opposite. Previous studies have reported one result or the other, but never a combination of the two findings as in our case. The most likely explanation is a residual effect of the dexamethasone that was used as a supplement during the MSC *in vitro* pre-culture period. Corticosteroids, including dexamethasone, are internalized by cells and bind to an intracellular receptor, so the *in vitro* effects of dexamethasone can persist for up to 2 weeks after its removal from the environment (3, 177). Thus, despite the separation in the delivery of dexamethasone and TNF-α during MSC culture, our results suggest that intracellular signals arising from the two agents interacted and impacted MSC osteogenic differentiation.

The 7-day pre-culture period used for the rat MSCs in this study typically results in committed osteoprogenitor cells that are not yet mature osteoblasts (132). By day 4 of our study, TNF-α had reduced ALP activity (Figure 4.3; $p < 0.05$) and increased

mineralized matrix deposition (Figure 4.4; $p < 0.05$) in a dose dependent manner. However, this effect was not maintained over the course of 16 days for lower doses of TNF-α. The ALP and calcium data for the 0.1 ng/mL TNF group indicate suppressed osteogenic differentiation over the course of 16 days. Both osteogenic markers were significantly lower than the values for positive and negative control groups throughout the study (ALP activity suppressed, $p < 0.05$ in Figure 4.3; calcium content reduced, $p < 0.05$ in Figure 4.4). When considered together with the cellularity data, where the 0.1 ng/mL constructs showed a monotonic increase in cell content (Figure 4.2; all three timepoints differ, $p < 0.05$), these data are consistent with previous reports of simultaneous delivery of dexamethasone and TNF-α, which stimulated an immature, proliferative phenotype in human MSCs (163). In contrast, the highest dose of TNF-α had the opposite effect on MSCs; cell content remained fairly constant throughout the study (Figure 4.2), while mineralized matrix content increased monotonically (Figure 4.4; all three timepoints differ, $p < 0.05$), consistent with progression towards terminal osteogenic differentiation and with previous reports of human MSCs treated with human TNF-α in the absence of dexamethasone (159, 160). The 5 ng/mL TNF constructs showed a similar pattern, with constant cellularity (Figure 4.2), declining ALP activity (Figure 4.3; all three timepoints differ, $p < 0.05$), and significantly elevated mineralized matrix content on day 4 (Figure 4.4; exceeds all groups except 50 ng/mL TNF, $p < 0.05$). However, mineralized matrix deposition appeared to halt after day 4 for this group, so that the values on days 8 and 16 were equivalent to those of the 0.1 ng/mL TNF constructs (Figure 4.4; $p > 0.05$). Thus, the lowest dose of TNF-α may have only been sufficient to cancel out the effects of dexamethasone, halting MSC osteogenic

differentiation, while the higher doses were able to also exert a TNF-α-related effect on the MSCs, resulting in increased calcium deposition.

Our findings of increased mineralized matrix deposition triggered by TNF-α delivery in the absence of dexamethasone are supported by several studies in a variety of cell types. TNF-α delivered for 28d in the absence of dexamethasone promoted odontoblastic differentiation and increased mineralized matrix deposition of dental pulp cells (161). Increased calcium deposition *in vitro* has also been reported for vascular-derived cells treated with TNF-α in the absence of dexamethasone (190). In addition, human MSCs treated *in vitro* with human TNF-α for 14-21d showed increased calcium deposition in the absence of dexamethasone (159, 160). However, a similar study in murine MSCs indicated that recombinant murine TNF-α suppressed ALP activity and mineralized matrix deposition regardless of the presence of dexamethasone (162, 189), which serves as a reminder that species physiology also impacted our results. Overall, our results suggest that the pro-inflammatory cytokine TNF-α stimulates *in vitro* mineralized matrix deposition by MSCs, a late-stage marker of osteogenic differentiation, and that this effect is likely antagonized by the anti-inflammatory agent dexamethasone. Future studies will expand on this exciting finding to establish the optimal time period for delivery and, ultimately, whether TNF-α can be used as a more physiologically realistic replacement to the traditional osteogenic supplement dexamethasone.

4.5. Conclusions

This study demonstrated that the pro-inflammatory cytokine TNF-α stimulates mineralized matrix deposition, a late stage marker of osteogenic differentiation, when

delivered continuously to MSCs cultured in 3D electrospun PCL microfiber meshes. By day 4 of our study, TNF-α had reduced ALP activity, an early marker of osteogenic differentiation, and increased mineralized matrix deposition in a dose dependent manner. However, this effect was not maintained over the course of 16 days for lower doses of TNF-α. Continuous delivery of 0.1 ng/mL of TNF-α induced proliferation and suppressed osteogenic markers in MSCs over 16 days, an effect that likely arose from the antagonism of TNF-α by anti-inflammatory signaling induced by the corticosteroid dexamethasone, which was used as an osteogenic supplement during *in vitro* MSC pre-culture. In contrast, continuous delivery of a higher dose, 5 ng/mL TNF-α, stimulated osteogenic differentiation for a few days, and 50 ng/mL TNF-α resulted in significant mineralized matrix deposition over the course of the study. This suggests that the lowest dose of TNF-α was only sufficient to cancel out the effects of dexamethasone, halting MSC osteogenic differentiation, while the higher doses were able to also exert a TNF-α-related effect on the MSCs, resulting in increased calcium deposition. Based on these results we conclude that TNF-α stimulates osteogenic differentiation, and that its effects on MSCs can be blocked by the presence of anti-inflammatory agents like dexamethasone.

Chapter 5

Effect of Temporally Patterned TNF-α Delivery on *In Vitro* Osteogenic Differentiation of Mesenchymal Stem Cells

5.1. Introduction

Craniofacial bone is a dynamic tissue that is constantly resorbed and renewed, and has the remarkable capacity to regenerate. However, this regenerative process, which is dependent on adequate temporal and spatial distribution of molecular and cellular signals, fails in bone defects above a critical size, resulting in impaired or completely absent osseous union (41). The limitations of current surgical reconstruction techniques have stimulated interest in tissue engineering. Informed by cell biology research, efforts to date have focused on inducing bone regeneration via delivery of various bioactive molecules,

particularly osteogenic factors. However, recent insight into the critical role of pro-inflammatory cytokines, particularly tumor necrosis factor-α (TNF-α), in bone healing has heralded a new direction in the rational design of bone tissue engineering constructs (191).

TNF-α is best known for its key roles in regulating acute inflammation, systemic immune responses, and osteoclast-mediated bone resorption. However, recent studies have unveiled another important role in priming bone renewal. Expression of TNF-α rises immediately following bone injury, and is elevated again in later stages of bone remodeling (38, 59, 104). Absence of this TNF-α signaling impairs *in vivo* bone fracture healing in a mouse model, delaying endochondral ossification, but it has no effect on skeletal development, suggesting that TNF-α plays a unique role in post-natal osteogenesis (1, 2). Motivated by this significant impact on *in vivo* bone regeneration, we previously examined the effect of varying TNF-α doses on *in vitro* osteogenic differentiation of mesenchymal stem cells (MSCs). We demonstrated that continuous delivery of 50 ng/ml TNF-α to mesenchymal stem cells (MSCs) stimulates mineralized matrix deposition, a marker of osteogenic differentiation (14).

This work built upon this previous finding and explored the effects of temporal variations in TNF-α delivery on MSC osteogenic differentiation. MSCs were cultured in 3D biodegradable electrospun poly(epsilon-caprolactone) (PCL) scaffolds for 4-16 days and exposed to continuous, early, intermediate, or late TNF-α delivery. The early and late patterns mimicked the biphasic pattern of TNF-α signaling observed *in vivo* after bone fracture (see Figure 2.1) (104). The goal of this study was to investigate the effects of

early, intermediate, late, and continuous temporal patterns of TNF-α delivery on MSC osteogenic differentiation.

5.2. Methods and Materials

5.2.1. Experimental Design

This study had a three-factor design with 2 preculture conditions ("+dex" vs. "-dex"), 4 TNF-α delivery periods ("Continuous," "Early," "Intermediate," and "Later"), and 3 time points, as depicted in Figure 5.1. All experimental groups received the same concentration (50 ng/ml) of TNF-α during the various delivery periods. Negative control groups consisted of MSCs (either +dex or -dex precultured) on PCL scaffolds cultured in -dex media without TNF-α. The positive control consisted of +dex precultured MSCs that continued to receive +dex media following seeding onto PCL scaffolds. Due to the large number of groups in this study, the design was repeated twice; the MSCs for each trial were obtained from independent isolations, and (n = 4) scaffolds per group per timepoint were included in each trial.

5.2.2. Electrospun Scaffold Generation

Electrospun PCL meshes were prepared according to an established protocol (14). The PCL (Lactel, Pelham, AL) had a number-average molecular weight (M_n) of 72,100 ± 1400 Da and polydispersity index (M_w/M_n) of 1.60 ± 0.02, determined via gel permeation chromatography (Phenogel Linear Column with 5 μm particles, Phenomenex, Torrance, CA; Differential Refractometer 410, Waters, Milford, MA) using a calibration curve generated with polystyrene standards (Fluka, Switzerland). An 18 w/w% solution of PCL

in 5:1 (by vol) chloroform:methanol was loaded into a 10 ml syringe and positioned in a previously described electrospinning apparatus (14, 179). A 16 gauge blunt-tip needle (Brico Medical Supplies, Inc., Metuchen, NJ) was attached to the syringe such that the needle tip was 33 cm from a glass collecting plate placed in front of the system's grounded copper plate. A voltage difference of 33 kV was applied to the needle tip and the PCL solution was pumped out of the needle tip at 40 ml/h using a syringe pump.

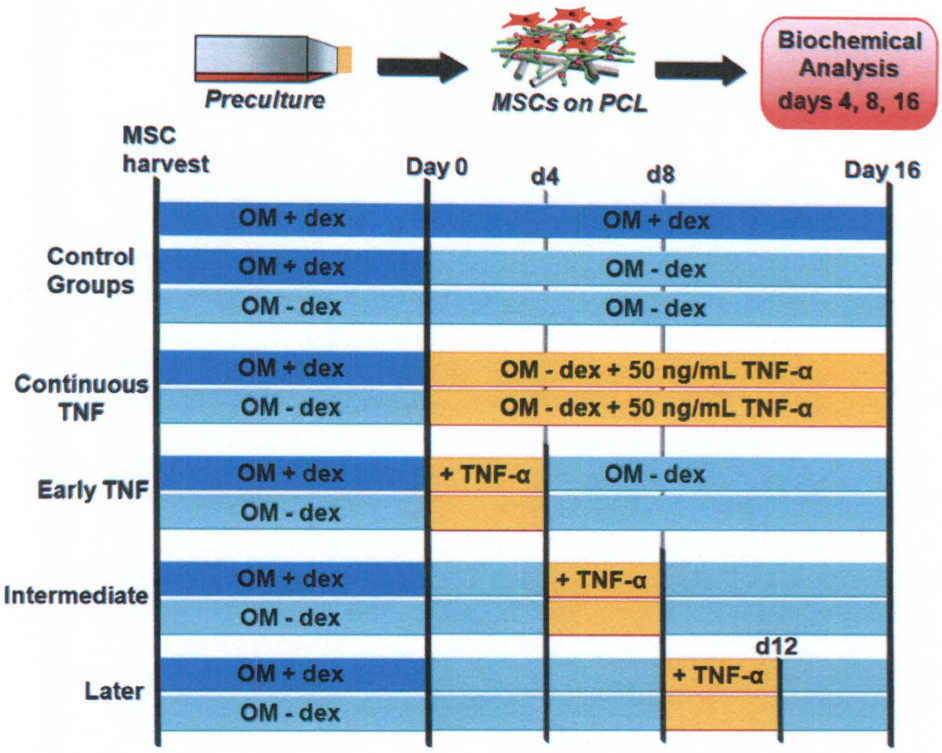

Figure 5.1: Schematic of TNF-α temporal variation study.
OM = Osteogenic Media (α-MEM, 10% v/v fetal bovine serum, 50 μg gentamicin/ml, 1.25 μg amphotericin-B/ml, 10 mM β-glycerophosphate, 50 μg/ml ascorbic acid) either with or without 10^{-8} M dexamethasone ("+dex" vs. "-dex").

Scaffolds with 8 mm diameter were cut from the resulting electrospun PCL meshes using an arch punch (C.S. Osborne & Co., Harrison, NJ). The thickness of each scaffold was measured using digital micro-calipers (Mitutoyo, Aurora, IL) and, for

consistency with previous work (14), scaffolds with thickness 0.90-1.10 mm were used for the study. For each MSC isolation, (n = 2-3) electrospun PCL meshes were required to obtain a sufficient number of scaffolds for the study. Each batch of meshes was prepared on the same day using the same lot of PCL and the same electrospinning parameters. Scaffolds were stored under an inert nitrogen atmosphere at -20°C in a non-defrosting freezer to prevent degradation prior to use.

5.2.3. Scaffold Characterization

For each electrospun mesh, (n = 3) scaffolds were mounted onto aluminum stubs, sputter-coated with 30 nm of gold, and imaged using scanning electron microscopy (SEM) (FEI Quanta 400 Environmental, Hillsboro, OR) at a 7.31 kV accelerating voltage and 3.0 spot size. Predefined coordinates on each scaffold were imaged and the diameters of (n = 45 fibers) from the top and (n = 45 fibers) from the bottom of each mesh were measured using an established protocol (14, 179). The porosity of n = 50 scaffolds from each mesh was determined via an established gravimetric analysis protocol (14, 179) (detailed in Methods of previous chapter).

5.2.4. Mesenchymal Stem Cell Isolation

All MSC isolations were approved by the Rice University Institutional Animal Care and Use Committee and adhered to the National Institutes of Health guidelines. For each of the two independent trials described in the Experimental Design, MSCs were isolated from the pooled femoral and tibial bone marrow of 8 male syngeneic Fischer 344 rats weighing 150-175 g, according to established methods (8, 9). Bone marrow suspensions from each rat were split into two portions and were cultured in either +dex or

-dex media for 7 days. Both types of media consisted of α-MEM (Sigma, St. Louis, MO) with 10% v/v fetal bovine serum (Gemini Bio-Products, West Sacramento, CA), 50 μg/ml gentamicin, 1.25 μg/ml amphotericin-B, 10 mM β-glycerophosphate, and 50 μg/ml ascorbic acid (all from Sigma). The +dex media also contained 10^{-8} M dexamethasone (Sigma). Culture media was changed on days 1, 3, and 5 to remove non-adherent cells. As in previous studies, the adherent cells were designated as "mesenchymal stem cells," based on the established osteogenic potential of this cell population under appropriate *in vitro* conditions (3, 14, 183).

Although the fetal bovine serum used in this study was from the same manufacturer (Gemini) as that used in the previous study (previous chapter; (14)), it was derived from a different serum lot and was found to affect MSC differentiation as well as response to TNF-α. Thus, the previous TNF-α dosage study (14) was repeated with the new serum to establish a baseline for comparison of the results of the temporal patterning study. MSCs for this TNF-α dosage study were isolated from (n = 5) rats and all procedures were performed as previously described (14) (see Methods of previous chapter).

5.2.5. TNF-α Reconstitution and Dilution

Recombinant rat TNF-α (R&D Systems, Minneapolis, MN) was reconstituted at 50 ng/μl on the day of scaffold seeding using sterile phosphate-buffered saline (PBS) containing 0.1 w/w% bovine serum albumin (Sigma), according to the manufacturer's instructions. For experiments, 4 μl of TNF-α stock solution were added to 4 ml of media used for construct culture, resulting in the desired 50 ng/ml TNF-α.

5.2.6. Scaffold Seeding and Culture

Prior to MSC seeding, the scaffolds were sterilized via exposure to ethylene oxide gas for 14h and prewet using a decreasing ethanol gradient (from 100% to 70%), according to established protocols (14, 179). The ethanol was exchanged with sterile milliQ water, and then with -dex media. The next day, the scaffolds were press-fit into seeding cassettes, placed into ultra-low attachment 6-well plates (1 cassette/well) (Corning Incorporated Life Sciences, Lowell, MA), and seeded with MSCs.

For seeding, nearly confluent MSCs were lifted from the cell culture flasks with 0.25% trypsin/EDTA (Gibco, Carlsbad, CA), counted with a hemocytometer, centrifuged, and resuspended at 1.25 million cells/ml in -dex osteogenic media. 0.2 ml of the resuspended MSCs were added drop-wise to each scaffold, which had already been press-fit into a seeding cassette.

After waiting 4h to allow for MSC attachment to the scaffolds, each well was filled with 8 ml of -dex media and the relevant groups were supplemented with either 10^{-8} M dexamethasone or 50 ng/ml TNF-α (according to the design shown in Figure 5.1). After 24h, the constructs were removed from the seeding cassettes and transferred to new ultra-low attachment 6-well plates for the duration of the study. The wells were filled with 4 ml of -dex media, supplemented with dexamethasone or TNF-α as appropriate, and media were changed every two days thereafter.

5.2.7. Cellularity, Alkaline Phosphatase Activity, and Calcium Content Assays

For each of the two independent trials of the TNF-α temporal study, on days 4, 8, and 16, (n = 4) scaffolds from each group were removed, rinsed twice with 4 ml of PBS,

and flash-frozen in 1 ml of sterile milliQ water using liquid nitrogen. The cells were lysed using three consecutive freeze/thaw/sonication cycles (10 min at -80°C, 10 min at 37°C, 10 min sonication). The double-stranded DNA content of each resulting cell lysate solution was quantified using the fluorometric PicoGreen assay (Molecular Probes, Eugene, OR) and then converted to the number of cells per construct (9, 14). The alkaline phosphatase (ALP) activity of the cell lysates was quantified using an established colorimeteric assay based on the rate of conversion of the colorless substrate *p*-nitrophenyl phosphate disodium salt hexahydrate (Sigma), to a yellow product, *p*-nitrophenol (9, 14). Next, each construct was removed from the aqueous cell lysate, immersed in 1 ml 1 N acetic acid, and left on a shaker table at 200 rpm overnight to dissolve matrix-bound calcium. Calcium content was quantified using an established colorimetric assay that is based on a calcium chelating agent (Arsenazo III; Genzyme Diagnostics PEI, Charlottetown, Prince Edward Island, Canada) that changes color upon binding to free calcium in an acid solution. Samples and standards were run in triplicate for all assays. Samples were diluted as necessary to fall within the range of the standards for each assay. A detailed experimental procedure for each of these biochemical assays is provided in the previous chapter and has also been published (9, 14).

5.2.8. Histological Sample Preparation and Analysis

At the final timepoint, $n = 1$ construct from each of the three control groups and from the two "continuous" TNF-α groups was rinsed twice with PBS and fixed overnight in 5 ml of 10% buffered formalin phosphate. Constructs were then passed through an ascending (70% to 100%) ethanol gradient and stored in 100% ethanol at 4°C. Prior to sectioning, each construct was cut in half (so that cross-sectional images could be

obtained) and embedded in HistoPrep (Fisher Scientific, Pittsburgh, PA). Frozen 5 μm thick sections (CM1850 cryotome, Leica Microsystems, Bannockburn, IL) were mounted on Superfrost Plus slides (Fisher Scientific) and incubated at 45°C on a slide warmer for 4-5 days according to an established protocol for optimal section adhesion (14).

Sections were rehydrated and then stained with von Kossa (5% w/w silver nitrate in milliQ water) under UV for 30 min. The slides were rinsed with water followed by 95% ethanol and then alcoholic eosin Y (Sigma) was applied as a counter-stain for 3 min. Excess eosin was removed with 95% ethanol. The slides were allowed to air dry, and then imaged with a light microscope (Eclipse E600, Nikon, Melville, NY) equipped with a camera (3CCD Color Video Camera DXC-950P, Sony, Park Ridge, NJ) and attached to a computer. Light microscope images were calibrated using the standard two-image method to correct for differences in background lighting and in dark-current effects in the detector (185).

5.2.9. Statistical Analysis

Fiber diameters and porosities are reported as mean ± standard deviation for n = 45 fibers and n = 50 scaffolds, respectively. The average fiber diameter of the top and bottom of each PCL microfiber mesh, along with the average porosity, were compared at 95% confidence using one-way analysis of variance. For the temporal variation study, the biochemical assay results are reported as mean ± standard deviation for n = 8 constructs (n = 4 constructs from each of two independent trials). The cellularity, ALP activity, and calcium content data from each of the two trials were combined and analyzed as a randomized complete block design at 95% confidence using two-way analysis of variance. Each trial was set as a block. Multiple pair-wise comparisons were made using

the Bonferroni post-hoc analysis method at 95% confidence. For the TNF-α dosage study, the cellularity, ALP activity, and calcium content values represent the mean ± standard deviation for $n = 4$ constructs from each group at each timepoint. The data were compared using one-way analysis of variance with 95% confidence.

5.3. Results and Discussion

5.3.1. Scaffold Morphology

The morphology of representative scaffolds from each study is shown in Figure 5.2, imaged via SEM at varying magnifications. The average fiber diameter and porosity of each mesh used in this study is listed in Table 5.1. With the exception of the second repetition of the temporal TNF-α study ("Trial 2" in Table 5.1), the PCL microfiber meshes generally had statistically equivalent mean fiber diameters ($p > 0.05$), as shown in Table 5.1. For the second repetition of the temporal study, one mesh had a slightly higher than average fiber diameter (~11 μm). Although nearly every mesh had a statistically unique porosity, the magnitude of the differences was quite small, with the values ranging from 78.8 ± 1.4% to 84.9 ± 0.9% across all meshes.

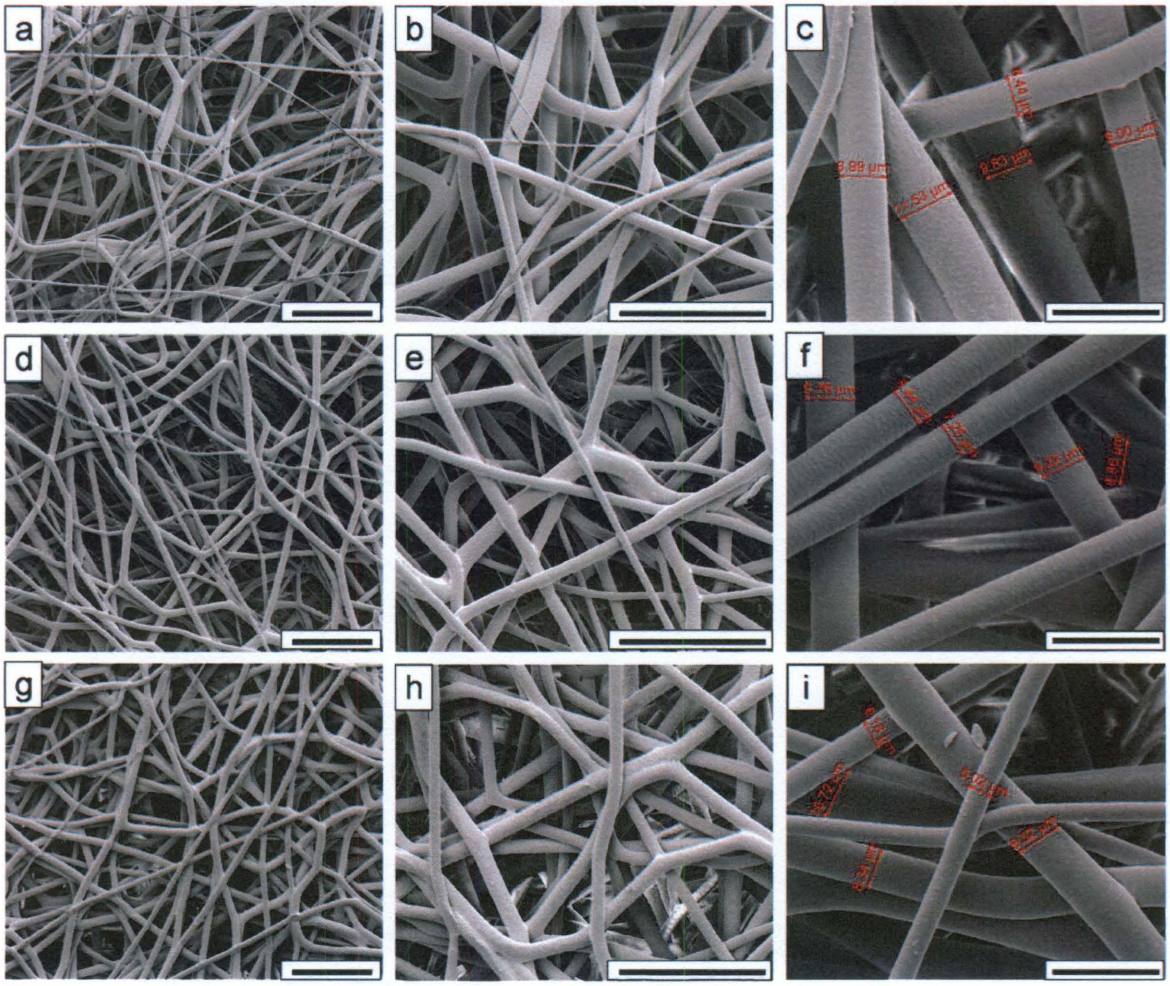

Figure 5.2: Morphology of representative scaffolds via SEM.

Representative electrospun PCL meshes generated for this study, imaged via SEM at varying magnifications, (a,d,g) 300×, (b,e,f) 600×, and (c,f,i) 2000×. Scaffolds shown in the top (a-c) and middle (d-f) rows are from the meshes used for the first and second repetitions of the temporal study, respectively. The bottom row (g-i) depicts scaffolds used for the TNF-α dosage study described in this chapter. Scale bars shown for (c,f,i) are 20 μm. All other scale bars 100 μm.

Table 5.1 Comparison of fiber diameters and porosites of the electrospun meshes used for this study.

Parameter	Temporal Trial 1			Trial 2		Repeat of Dosage Study		
	Mesh 1	*2*	*3*	*4*	*5*	*Mesh 6*	*7*	*8*
Fiber Diameter, Top (μm)	10.0 ± 1.0	9.6 ± 1.5	9.9 ± 1.5	11.1 ± 1.1*	9.0 ± 1.3**	8.9 ± 1.9**	8.6 ± 1.9**	8.3 ± 1.8**
Fiber Diameter, Bottom (μm)	10.7 ± 1.2	10.0 ± 1.9	11.2 ± 2.0	15.9 ± 1.9*	12.5 ± 1.4**	11.0 ± 1.6	10.4 ± 1.2	12.0 ± 1.7**
Porosity (%)	80.1 ± 1.6	84.4 ± 1.0*	83.9 ± 1.4*	78.8 ± 1.4*	81.7 ± 0.9*	80.4 ± 2.6	83.3 ± 1.0*	84.9 ± 0.9*

Values are presented as mean ± standard deviation. The sample size was $n = 45$ for fiber diameters from the top and bottom of each mesh, and $n = 50$ scaffolds for porosity. For each parameter, * indicates values that significantly differ from all other values ($p < 0.05$), while ** indicates groups of values that differ from all other values ($p < 0.05$), but not from each other.

5.3.2. Construct cellularity

Figure 5.3 depicts construct cellularity at each timepoint. The positive control group (+dex preculture/+dex culture/0 ng/mL TNF), the +dex precultured negative control group (+dex/-dex/0 ng/mL TNF), and the +dex precultured continuous TNF-α group (+dex/-dex/50 ng/mL TNF for days 0-16) (Figure 5.3) in this study had analogous groups in the previous study (0 ng/mL TNF +dex, 0 ng/mL TNF, and 50 ng/mL TNF, respectively; Figure 4.2). For all three groups, the number of cells on the scaffolds at day 4 in this study (Figure 5.3) was approximately half of the previous value (Figure 4.2). This difference can be attributed to the change in the batch of fetal bovine serum used as

a supplement in the culture medium, which in turn affected the attachment, proliferation, and/or survival of MSCs on the PCL scaffolds.

The cellularity of the positive control group (+dex/+dex/0 ng/mL TNF) followed a similar trend to that seen in the previous study (Figure 4.2), with a dramatic drop in cell number on day 16. This group had significantly fewer cells than any other group on day 16 ($p < 0.05$)[6]. In contrast, the negative (+dex/-dex/0 ng/mL TNF) control group showed a peak in cellularity on day 8 (Figure 5.3) that was not observed in the previous study (Figure 4.2).

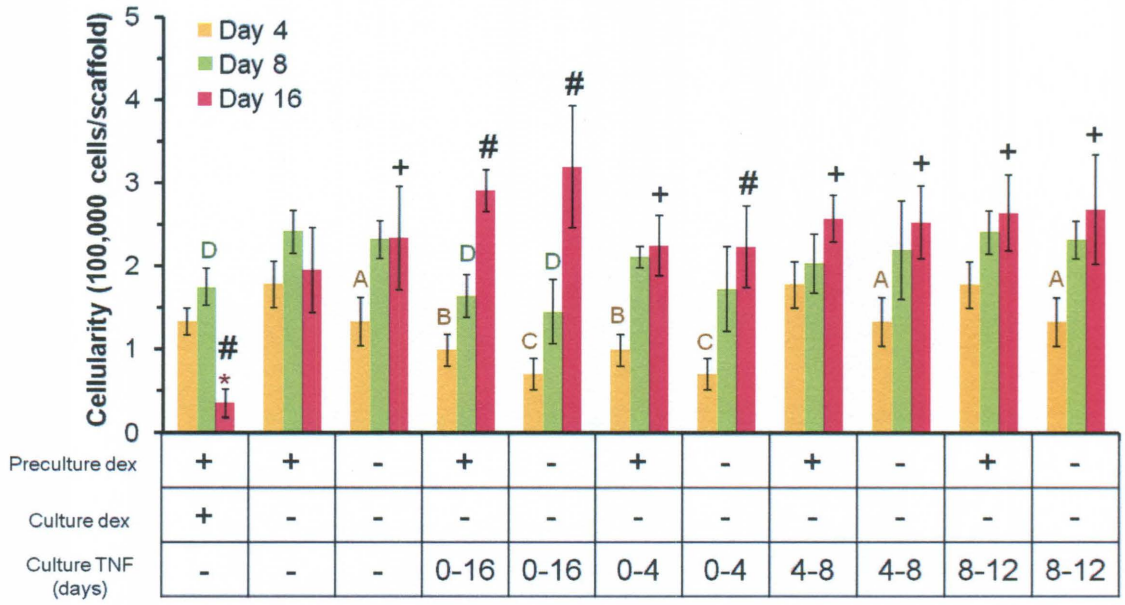

Figure 5.3: Scaffold cellularity with various TNF-α temporal patterns
MSCs precultured with osteogenic supplements ("preculture +dex") and dexamethasone-naïve MSCs ("preculture -dex") were seeded on PCL scaffolds and cultured for 16 days in dexamethasone-free media ("culture -dex"; the only exception is the positive control). Experimental groups were exposed to continuous (days 0-16), early (days 0-4), intermediate (days 4-8), or later (days 8-12) delivery of 50 ng/ml TNF-α. Each bar

[6] Note that an acellular control was not included in this study because no significant biochemical activity was seen for the acellular constructs in the previous study.

represents the average ± standard deviation of (n = 8) scaffolds per group at each timepoint. For each timepoint, letters (A-D) indicate statistically equivalent ($p > 0.05$) groups. Groups that are not marked with the same letter differ significantly ($p < 0.05$). Also, groups marked with * differ from all other groups at that timepoint ($p < 0.05$). For each group, # indicates that values at each timepoint for this group differ ($p < 0.05$), while + indicates that the day 16 value differs from day 4 value ($p < 0.05$).

The continuous TNF-α group (+dex/-dex/50 ng/mL TNF from days 0-16) showed a monotonic increase in cellularity over days 4-16, a trend not observed in the previous study (Figure 4.2), but observed for all groups receiving TNF-α in this study (Figure 5.3), as well as for the dexamethasone-naïve negative control (-dex/-dex/0 ng/mL TNF). Continuous delivery of TNF-α induced elevated cell numbers on day 16 compared to all other groups, although the difference was not statistically significant ($p > 0.05$).

5.3.3. Construct ALP activity

ALP activity was used as an early marker of osteogenic differentiation (Figure 5.4). The positive control (+dex preculture/+dex culture/0 ng/mL TNF), negative (+dex/-dex/0 ng/mL TNF) control, and +dex-precultured continuous TNF-α (+dex/-dex/50 ng/mL TNF for days 0-16) groups had similar trends in ALP activity compared to those previously observed in the TNF-α dosage study (Figure 4.3). Specifically, the positive control group (+dex/+dex/0 ng/mL TNF) showed a monotonic increase in ALP activity, while the +dex precultured continuous TNF-α group (+dex/-dex/50 ng/mL TNF for days 0-16) showed a monotonic decrease in ALP activity. The ALP activity of the +dex precultured negative control group (+dex/-dex/0 ng/mL TNF) remained fairly constant over time (Figure 5.4). Although the trends remained consistent, the change in serum batch caused the magnitude of the ALP activity to increase, which is evident in

comparing the y-axis of Figure 5.4 (maximum value: 50 pmol/hr/cell) to that of Figure 4.3 (maximum value: ~7 pmol/hr/cell).

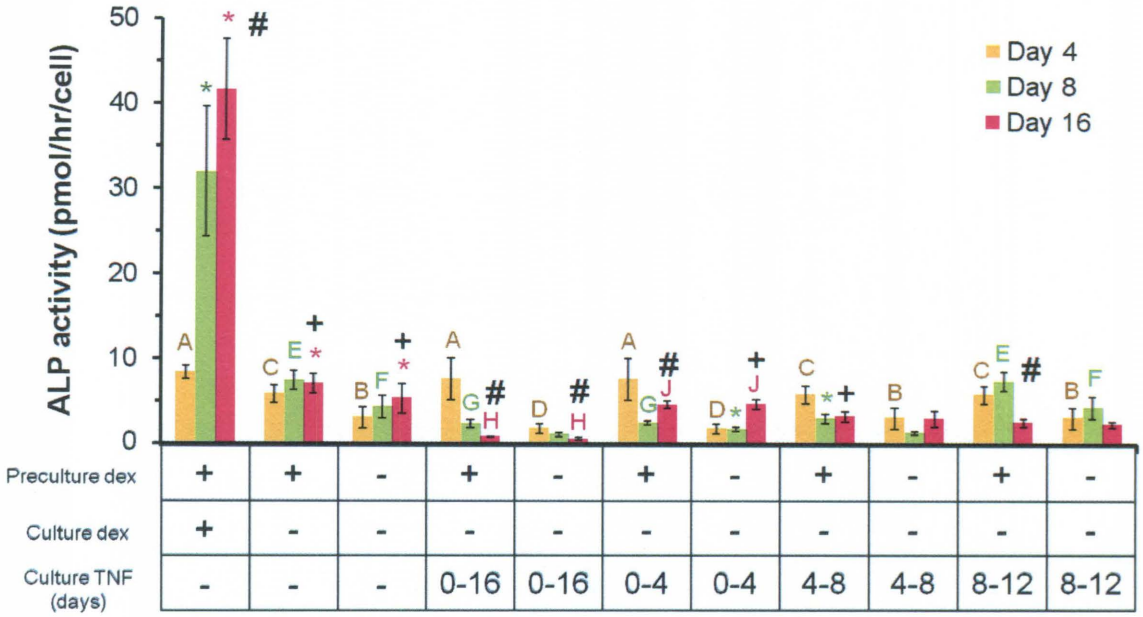

Figure 5.4: ALP activity with various TNF-α temporal patterns
MSCs precultured with osteogenic supplements ("preculture +dex") and dexamethasone-naïve MSCs ("preculture -dex") were seeded on PCL scaffolds and cultured for 16 days in dexamethasone-free media ("culture -dex"; the only exception is the positive control). Experimental groups were exposed to continuous (days 0-16), early (days 0-4), intermediate (days 4-8), or later (days 8-12) delivery of 50 ng/ml TNF-α. Each bar represents the average ± standard deviation of (n = 8) scaffolds per group at each timepoint. For each timepoint, letters (A-J) indicate statistically equivalent ($p > 0.05$) groups. Groups that are not marked with the same letter differ significantly ($p < 0.05$). Also, groups marked with * differ from all other groups at that timepoint ($p < 0.05$). For each group, # indicates that values at each timepoint for this group differ ($p < 0.05$), while + indicates that the day 16 value differs from day 4 value ($p < 0.05$).

TNF-α delivery suppressed ALP activity in both +dex precultured and dexamethasone-naïve MSCs (Figure 5.4). However, this suppression of ALP activity by TNF-α was reversible; both the +dex and -dex precultured versions of the groups that received "early" (days 0-4) or "intermediate" (days 4-8) TNF-α had significantly higher

($p < 0.05$) ALP activity on day 16 compared to day 8. Continuous delivery of 50 ng/ml TNF-α caused a monotonic decrease in ALP activity (values at all timepoints differ for +dex and -dex preculture groups, $p < 0.05$), which was in stark contrast to the monotonic increase seen in all three control groups (+dex/+dex, +dex/-dex, and -dex/-dex). Consistent with previous results (Figure 4.3), the day 16 ALP activity of the +dex/+dex control group greatly exceeded that of all other groups ($p < 0.05$), with the +dex precultured negative control group (+dex/-dex) having the second highest day 16 ALP activity ($p < 0.05$).

5.3.4. Construct mineralization

Mineralized matrix deposition, shown in Figure 5.5, was used as a late marker of osteogenic differentiation. Since the study of TNF-α dose effects indicated that TNF-α supports continued osteogenic differentiation of MSCs in the absence of dexamethasone (Figure 4.4), this study included experimental and control groups with dexamethasone-naïve MSCs to determine whether TNF-α is sufficient to trigger osteogenic differentiation. However, mineralized matrix deposition was only observed in +dex-precultured cells (+dex preculture differs from -dex preculture, $p < 0.05$) (Figure 5.5; note that the y-axis is plotted on a logarithmic scale), indicating that TNF-α is not sufficient to trigger MSC osteogenic differentiation. This finding is consistent with previous reports of the effects of TNF-α on undifferentiated human MSCs; TNF-α significantly affected the *in vitro* protein expression, proliferation, and migration of the cells, but did not induce any type of differentiation (111, 157).

Consistent with previous results, both TNF-α and dexamethasone supported continued osteogenic differentiation and calcium deposition of +dex precultured MSCs.

As in previous studies (Figure 4.4; "0 ng/mL TNF +dex" group), the +dex/+dex positive control had the highest day 16 calcium content of any group ($p < 0.05$; Figure 5.5). Continuous delivery of TNF-α also significantly ($p < 0.05$) increased mineralized matrix deposition on days 8 and 16 compared to the negative control. TNF-α delivery during days 0-4 and 4-8 also resulted in a slight increase in day 16 calcium content (differ from all other groups but not each other, $p < 0.05$). Although the amount of TNF-α-induced calcium deposition on day 16 was an order of magnitude smaller in this study (+dex/-dex/50 ng/mL TNF for days 0-16; Figure 5.5) than in the previous study (50 ng/mL TNF; Figure 4.4), it significantly exceeded the calcium content of the +dex precultured negative control ($p < 0.05$).

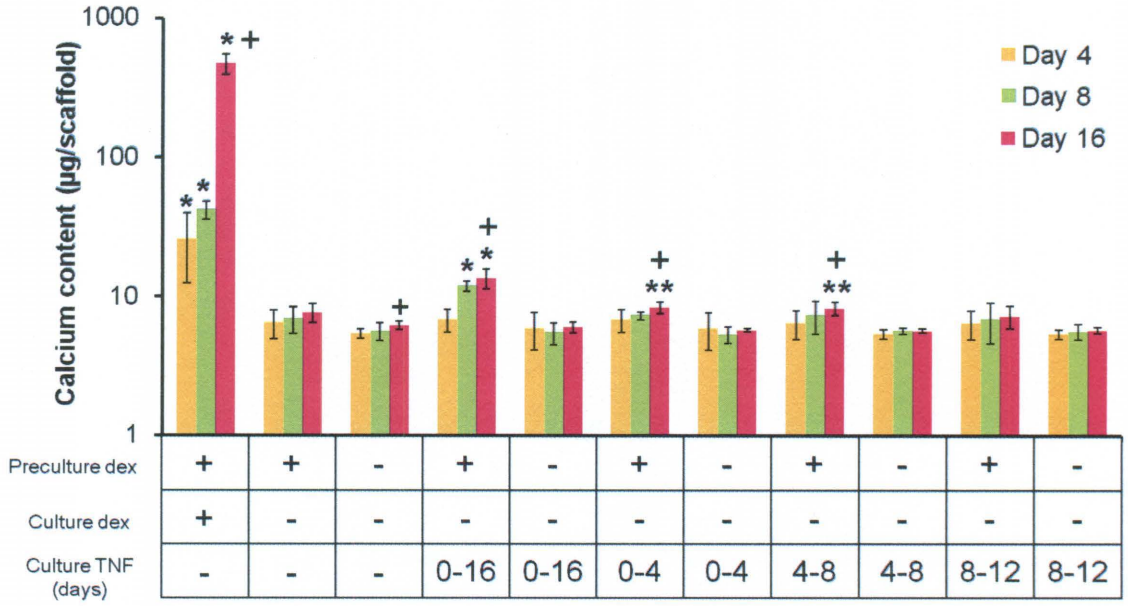

Figure 5.5: Construct mineralization with varying TNF-α temporal patterns
MSCs precultured with osteogenic supplements ("preculture +dex") and dexamethasone-naïve MSCs ("preculture -dex") were seeded on PCL scaffolds and cultured for 16 days in dexamethasone-free media ("culture -dex"; the only exception is the positive control). Experimental groups were exposed to continuous (days 0-16), early (days 0-4), intermediate (days 4-8), or later (days 8-12) delivery of 50 ng/ml TNF-α. Each bar represents the average ± standard deviation of (n = 8) scaffolds per group at each

timepoint. Groups marked with * differ from all other groups at that timepoint ($p < 0.05$). For each group, + indicates that the day 16 value differs from day 4 value ($p < 0.05$).

5.3.5. Cell and mineral distribution by histology

Cellularity and calcium content values were qualitatively confirmed via histological analysis of day 16 constructs using von Kossa, which stains mineralized matrix black, and eosin, which stains cells and non-mineralized matrix reddish-pink (Figure 5.6). Consistent with the calcium assay data (Figure 5.5), the +dex/+dex positive control group stained much darker and contained more calcium deposits (blue arrows) than any other group.

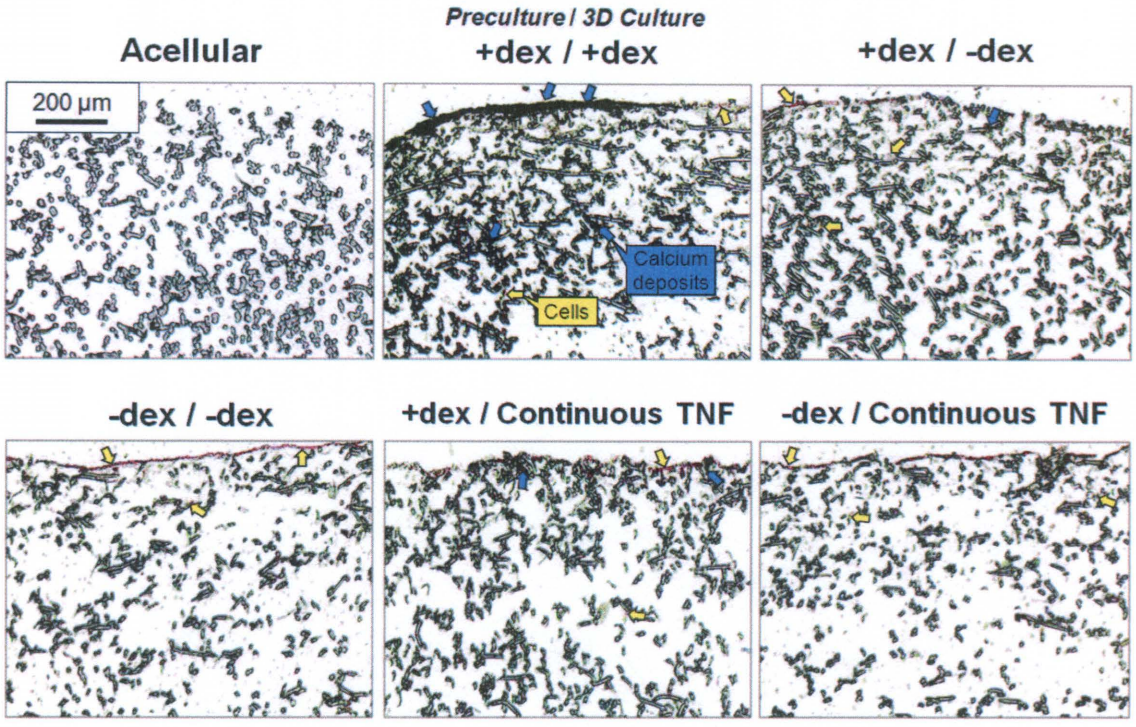

Figure 5.6: Scaffold cell and mineral distribution visualized via histology
Representative cross-sections of MSC-seeded PCL scaffolds after 16 days of culture. MSCs were precultured in complete osteogenic media (+dex) or in dexamethasone-free media (-dex). The positive control (+dex/+dex) continued to receive dexamethasone after MSCs were seeded onto the scaffold. All other MSC/scaffold constructs were cultured in

dexamethasone-free media. Experimental groups shown were continuously supplemented with 50 ng/mL TNF-α (abbreviated "TNF" in the figure). 5 μm thick sections were stained with von Kossa, which stains mineralized matrix black (blue arrows), and eosin, which stains cells and non-mineralized matrix reddish-pink (yellow arrows). An image of an acellular scaffold is included for reference. Images were captured at 10× original magnification. Scale bar in upper left corner represents 200 μm and applies to all images.

The highest concentration of calcium deposits (blue arrows) and cells (yellow arrows) were observed in the top half of each construct (Figure 5.6). A 5-10 μm pink-stained layer of cells and non-mineralized matrix was visible at the top of each section (indicated by yellow arrows), except for the acellular scaffold (Figure 5.6). In some areas, particularly in the +dex/+dex control, the pink color of the cells was obscured by the dark black color of the calcium deposits. As seen previously for similar electrospun PCL scaffolds cultured under static conditions ((14); Figure 4.5), cells infiltrated 200-500 μm into each microfiber scaffold (yellow arrows).

5.3.6. Effect of new serum batch on response to varying TNF-α concentration

Since the cellularity, ALP activity, and calcium content of three groups in this study that were also included in the previous study (previous chapter; (14)) differed in magnitude and also in trends over time, the TNF-α dosage study (14) was repeated with the new serum to establish a new baseline for comparison of the temporal results shown above. Figure 5.7 depicts the cellularity, ALP activity, and calcium content of MSC-seeded scaffolds given varying TNF-α concentrations in media supplemented with the batch of serum used for the temporal results shown earlier in this chapter.

a

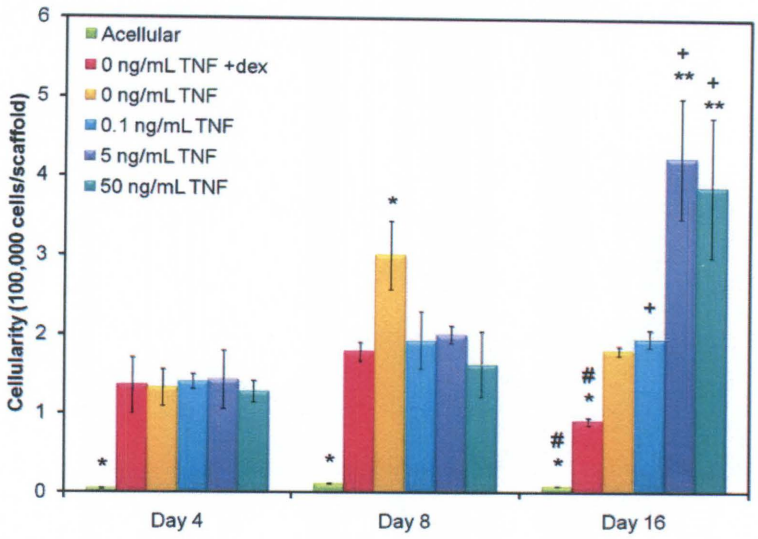

b

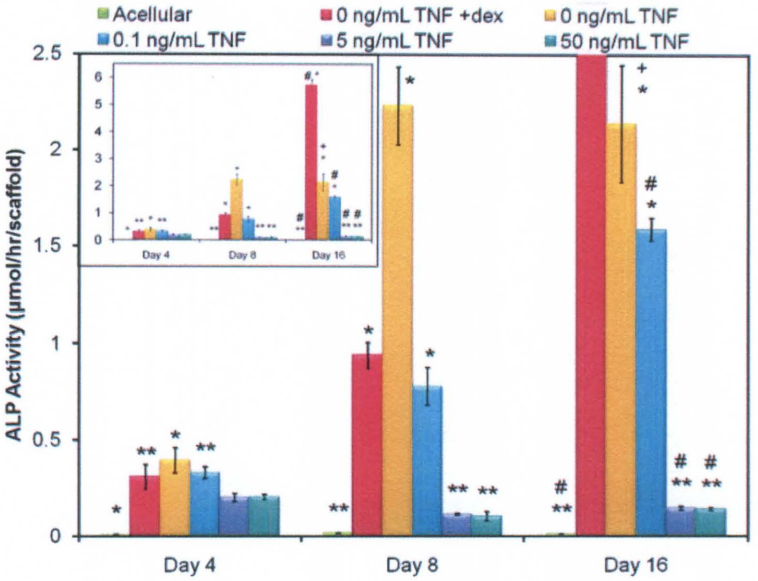

Figure 5.7: Construct cellularity, ALP activity, and calcium content with varying TNF-α concentrations in new serum.

(continued on next page)

c

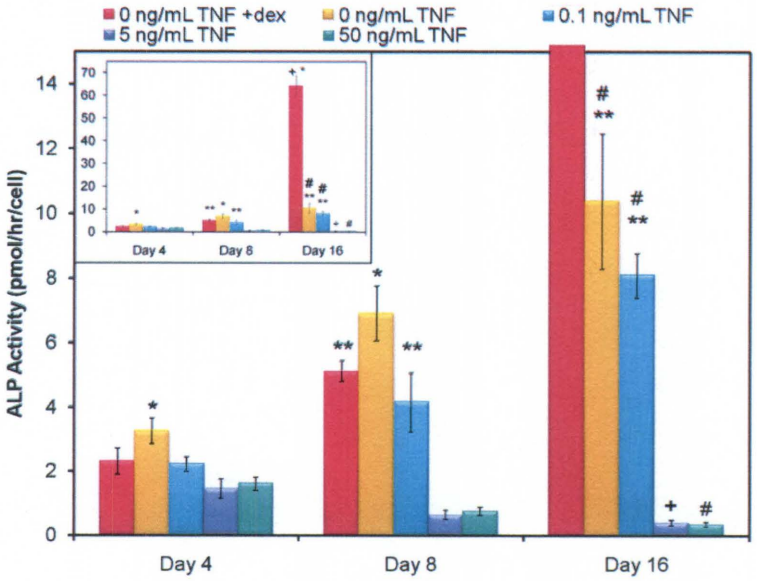

d

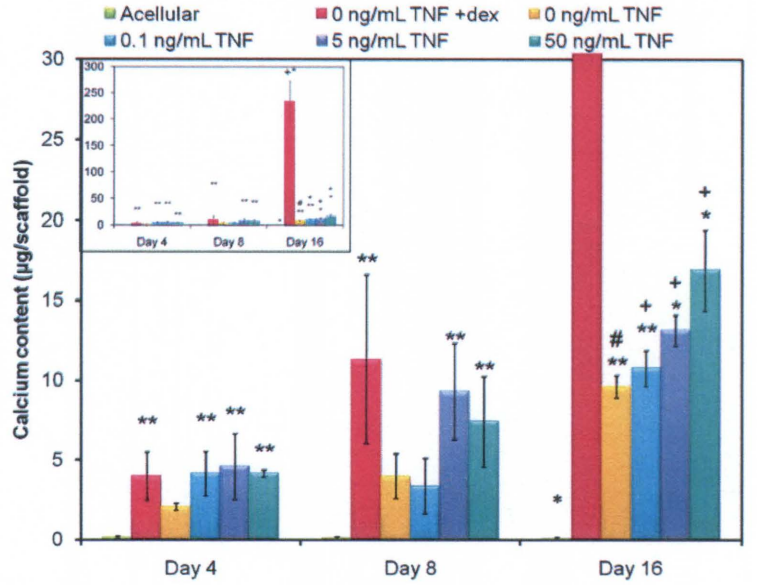

Figure 5.7: Construct cellularity, ALP activity, and calcium content with varying TNF-α concentrations in new serum.

The previously published study examining the effect of varying TNF-α dosage on MSC differentiation (14) was repeated using media supplemented with a different batch of fetal bovine serum. Cellularity over time is shown in (a). ALP activity on a per scaffold basis is shown in (b), while the same data on a per cell basis are shown in (c) with the exception of the acellular group. Calcium content is shown in (d). The insets in (b-d)

depict the full height of the bar for the day 16 positive control (0 ng/mL TNF +dex). Bars represent average ± standard deviation of (n = 4) scaffolds per group at each timepoint. Within a timepoint, groups with * differ from all other groups ($p < 0.05$), while ** differ from all other groups but not each other ($p < 0.05$). On day 16, + indicates that d4 and d16 values of that group differ ($p < 0.05$), while # indicates that values at all timepoints differ ($p < 0.05$).

Figure 5.7a depicts construct cellularity at each timepoint. By comparing Figure 5.7a to Figure 4.2, which shows the same groups cultured in the previous batch of fetal bovine serum, it is evident that the change in the batch of serum affected the attachment, proliferation, and/or survival of the MSCs on the PCL scaffolds. Since serum is derived from blood by removing the cellular components and clotting factors, its composition can vary greatly from batch to batch. Each batch of serum can differ in terms of the concentration of any number of substances, including antibodies, hormones, growth factors, and cytokines. For human MSCs, serum selection often involves an extensive screening process (3), but serum for MSCs from other species is not always subjected to such rigorous screening. These procedures may need to be revised as more complicated *in vitro* cell culture models are developed.

Although the results in Figure 5.7a differ from those in Figure 4.2, they are consistent with the cellularity trends reported earlier in this chapter. Consistent with the results in Figure 5.3, the number of cells on the scaffolds at day 4 in the new serum batch (Figure 5.7a) was approximately half of the previous value (Figure 4.2). As in the previous TNF-α dosage study, most of the groups had similar cell numbers at each timepoint. The acellular constructs ("Acellular") had nearly zero cells at all timepoints, as expected. The positive control ("0 ng/ml TNF +dex") group showed similar patterns in

both studies; the dramatic drop in cellularity at day 16 previously observed for this group in both Figure 4.2 and Figure 5.3 also occurred in this study. In contrast, the cellularity of the negative control group ("0 ng/mL TNF") showed a peak at day 8 that was not observed in the previous study (Figure 4.2), where this group had nearly constant cell numbers. However, this day 8 peak in cellularity was consistent with the trend observed for the analogous group in Figure 5.3 (+dex/-dex/0 ng/mL TNF). The significant monotonic increase in cellularity previously observed in the 0.1 ng/mL TNF group (Figure 4.2) was not seen in this study; instead, a dramatic increase in cellularity from day 8 to day 16 was observed in the 5 and 50 ng/mL TNF groups (Figure 5.7a). This increase is consistent with the change in cellularity of the +dex precultured continuous TNF-α group (+dex/-dex/50 ng/mL TNF for days 0-16) shown in Figure 5.3, confirming that this change in the response to TNF-α resulted from the change in serum.

The ALP activity in response to varying TNF-α concentrations in the new batch of serum is shown in Figure 5.7b,c. Consistent with the findings earlier in this chapter (Figure 5.4), the change in the serum affected the magnitude of ALP activity, but the trends for the groups remained similar. For example, for the three groups with the highest ALP activity on days 8 and 16 (i.e., 0 ng/mL TNF +dex, 0 ng/mL, and 0.1 ng/mL TNF), the ALP activity was at least 2-fold higher on day 8 and 5- to 10-fold higher on day 16 with the new serum batch (Figure 5.7c) compared to the previous serum (Figure 4.3). The ALP activity per cell (Figure 5.7c) was not calculated for the acellular constructs, as their near-zero cellularity would artificially raise the ALP activity values. Instead, the ALP activity per scaffold for the acellular constructs and for all other groups is depicted in Figure 5.7b. For the MSC-seeded constructs, the "per cell" and "per scaffold" ALP

activities followed similar trends since the cellularity of the constructs was fairly constant (Figure 5.7a).

As in the previous study (Figure 4.3) and in the results of the temporal study (Figure 5.4) earlier in this chapter, a dramatic increase in the ALP activity of the 0 ng/mL TNF +dex positive control was seen from days 8-16; this group again had a much higher ($p < 0.05$) ALP activity than all other groups on day 16 (see insets in parts b and c of Figure 5.7 for full size of this bar). Unlike the study with the previous serum batch, where the ALP activity of the 0 ng/mL TNF negative control did not change (Figure 4.3), there was a monotonic increase in ALP activity per cell in this study. The negative control had significantly higher ALP activity than all other groups on days 4 and 8 ($p < 0.05$), and the second-highest value on day 16 ($p < 0.05$). This trend is consistent with the ALP activity of the analogous group (+dex/-dex/0 ng/mL TNF) shown in Figure 5.4.

For both batches of serum, TNF-α suppressed the ALP activity of the MSCs in a dose-dependent fashion. The 0.1 ng/mL TNF group had much higher ALP activity than the other two TNF-α groups at all timepoints (Figure 5.7b,c), with a monotonic increase in ALP activity over time that paralleled that of the negative control group. In contrast, the groups with higher TNF-α dose had monotonic decreases in ALP activity over time, a trend that was also observed in the previous studies (Figure 4.3 and Figure 5.4).

The change in the batch of serum dramatically affected construct mineralization (Figure 5.7d). The new serum batch was selected based on its ability to induce comparable calcium deposition to the previous batch of serum when used as a component of +dex media for MSCs growing in a 2D layer. For both sera, the acellular control showed no mineralization over time and the positive control (0 ng/mL TNF +dex) had

significantly higher ($p < 0.05$) calcium content than all other groups on day 16. However, a comparison of the +dex positive control in Figure 5.7d (maximum y-axis value of 30 μg (inset: 300 μg)) and in Figure 4.4 (maximum y-axis value 700 μg) suggests that the new serum was not equivalent to the previous serum in terms of its impact on MSC osteogenic differentiation in 3D electrospun PCL scaffolds.

The negative control group (0 ng/mL TNF; Figure 5.7) had significantly lower ($p < 0.05$) day 16 calcium content than the 5 and 50 ng/mL TNF groups, which is consistent with the findings for the analogous groups in the study described earlier in this chapter (+dex/-dex/0 ng/mL TNF and +dex/-dex/50 ng/mL TNF for days 0-16; Figure 5.5) but differs from the statistically equivalent mineralization reported in Figure 4.4. This low calcium content for the 0 ng/mL TNF negative control was repeatedly observed in studies in our laboratory, suggesting that the previous study (Figure 4.4) had a unique component that induced this effect.

The new serum had several significant effects on TNF-α-induced construct mineralization. In the previous study (Figure 4.4), TNF-α triggered early dose-dependent mineralized matrix deposition by day 4. In this study (Figure 5.7d), although the day 4 calcium content of all TNF-α groups was equivalent to that seen with dexamethasone, it was significantly higher than that of the negative control ($p < 0.05$). A somewhat similar trend was observed for the analogous groups in Figure 5.5, where the +dex precultured continuous TNF-α group (+dex/-dex/50 ng/mL TNF for days 0-16) had slightly higher calcium content than the +dex precultured negative control (+dex/-dex/0 ng/mL TNF), although in that case the trend was not significant ($p > 0.05$) and the positive control had significantly higher calcium content than all other groups ($p < 0.05$) (Figure 5.5).

By day 8 of the TNF-α dosage study show n in Figure 5.7d, the 0.1 ng/mL TNF group no longer exhibited elevated calcium content, but the 5 and 50 ng/mL TNF groups continued to have calcium values significantly higher than that of the negative control on both days 8 and 16 ($p < 0.05$). Previously (Figure 4.4), both the 0.1 ng/mL TNF and 5 ng/mL TNF groups showed suppressed calcium deposition, which was assumed to reflect the antagonism between residual signaling from the dexamethasone used during MSC preculture (to induce osteogenic differentiation) and the TNF-α delivered during the study (14). However, this suppression was not seen with the current serum, suggesting that the prior suppression may have been attributable to a TNF-α antagonist (e.g., native corticosteroids or soluble TNF-α receptors) present in the serum used for that study.

In summary, the results of this new baseline study indicated that TNF-α stimulates construct mineralization in a dose-dependent fashion. Although the new serum resulted in a variety of changes in the biochemical assay results, the 50 ng/mL TNF group once again had the highest mineralization of all the experimental groups and was thus the appropriate TNF-α concentration to use in the temporal variation study.

To our knowledge, no other studies have examined the temporal effects of TNF-α on MSC osteogenic differentiation. However, several studies have reported that TNF-α causes a dose-dependent increase in mineralized matrix deposition when delivered to osteoprogenitors in media lacking dexamethasone (14, 112, 159-161). While dexamethasone is commonly used in *in vitro* MSC cultures, it is not present in the *in vivo* bone fracture environment; in fact, delivery of corticosteroids impairs bone fracture healing (104). Thus, the results of this study are not only important for understanding the

role of TNF-α in bone regeneration, but are also a useful step toward the development of a more clinically realistic *in vitro* model of the fracture healing microenvironment.

5.4. Conclusions

This study demonstrated that continuous delivery of the pro-inflammatory cytokine TNF-α is the optimal temporal pattern to induce osteogenic differentiation of MSCs cultured in 3D electrospun PCL microfiber meshes. Continuous 16-day exposure to 50 ng/ml TNF-α was compared with early (days 0-4), intermediate (days 4-8), and later (days 8-12) delivery. Since TNF-α has been shown to support continued osteogenic differentiation of MSCs in the absence of dexamethasone, an anti-inflammatory agent that is commonly used to stimulate *in vitro* MSC osteogenic differentiation and is typically required for continued differentiation, this study included experimental and control groups with dexamethasone-naïve MSCs to determine whether TNF-α is sufficient to trigger osteogenic differentiation. Mineralized matrix deposition was not observed in constructs with dexamethasone-naïve MSCs, indicating that TNF-α does not induce osteogenic differentiation of MSCs, but instead stimulates and supports progression toward terminal differentiation.

For MSCs precultured with osteogenic supplements, TNF-α suppressed ALP activity, an early marker of osteogenic differentiation, and stimulated mineralized matrix deposition, a late stage marker of MSC osteogenic differentiation. The results for the brief temporal delivery periods included in this study demonstrated that the TNF-α-induced suppression of ALP activity is reversible once exposure to TNF-α ceases, and that TNF-α stimulates some mineralized matrix deposition when delivered at any time

during the first 8 days of MSC culture. After 16 days of culture, dexamethasone-precultured MSCs that were continuously exposed to TNF-α had the second-highest amount of mineralized matrix deposition. The calcium content of these constructs was significantly greater than that of both negative controls and was exceeded only by the positive control group.

By elucidating the impact of temporal variations in TNF-α delivery, as well as the interplay between TNF-α and the anti-inflammatory osteogenic supplement dexamethasone, our results greatly improve our understanding of the impact of TNF-α on *in vitro* MSC osteogenic differentiation. These findings will facilitate the design of future *in vitro* and *in vivo* experiments to probe the interplay of TNF-α with other growth factors and cytokines typically present at the site of bone injury and regeneration, which will ultimately enable the design of new strategies to rationally control TNF-α signaling and stimulate bone regeneration.

Chapter 6

The Interplay of Bone-Like Extracellular Matrix and TNF-α Signaling on *In Vitro* Osteogenic Differentiation of MSCs

6.1. Introduction

Inflammation is an immediate response to bone injury, and a growing body of evidence indicates that the signaling cascades initiated during the week-long acute inflammatory response play a critical role in priming bone regeneration (105, 108, 191). Bone fracture alters the expression of over 6000 genes, including genes encoding inflammatory cytokines as well as a variety of growth factors (30). Together with growth factors, fracture-induced inflammatory mediators promote regeneration, e.g., by promoting angiogenesis and guiding mesenchymal stem cell (MSC) differentiation (105,

108, 191). Several cytokines, including tumor necrosis factor alpha (TNF-α), interleukin-6 (IL-6), and stromal cell-derived factor-1 (SDF-1), have been shown to directly modulate the migration of MSCs *in vivo* (109-112).

Further studies into the impact of TNF-α on MSC osteogenic differentiation have been motivated by the recognition of its important role during *in vivo* bone regeneration. TNF-α expression increases immediately after bone injury, returning to baseline after a few days, and is elevated again in later stages of bone remodeling (38, 59, 104). In an animal model lacking TNF-α, fracture healing was severely impaired and bone formation was delayed by several weeks (1, 2). In an *in* vivo fracture healing model, repeated local injections of TNF-α in the first few days after injury resulted in significantly increased fracture callus mineralization four weeks later (112).

While exciting, these results have also highlighted the need for more realistic *in vitro* models of the fracture healing environment. *In vitro* studies of the effects of TNF-α on osteogenic differentiation have been complicated by the fact that two supplements typically used to stimulate *in vitro* MSC osteogenic differentiation, dexamethasone and ascorbic acid, antagonize TNF-α signaling (14, 62, 158). In fact, when added to this typical osteogenic medium, TNF-α had the opposite effect of that seen *in vivo* – it suppressed *in vitro* MSC osteogenic differentiation (162, 163). One strategy to overcome this limitation has been to preculture MSCs in osteogenic supplements and then administer TNF-α afterwards. In the absence of dexamethasone, TNF-α has been shown to stimulate dose-dependent increases in the alkaline phosphatase (ALP) activity and mineralized matrix deposition, which are, respectively, early and late markers of osteogenesis (14, 112, 159-161).

In a continued effort to better model the function of TNF-α in the fracture healing microenvironment, this study investigated the interplay of bone-like extracellular matrix (ECM) and TNF-α on MSC osteogenic differentiation. Although the bone ECM is mainly composed of mineralized deposits, the fracture microenvironment contains a hematoma rich in molecular signaling sources including: insoluble macromolecules (e.g., collagen), soluble proteins (including growth factors and cytokines), as well as proteins and receptors on the surfaces of neighboring cells (105, 192). Our laboratory has previously described a method to coat microfiber meshes with bone-like, mineralized ECM containing an array of osteogenic growth factors (6, 9, 180). The presence of preformed bone-like ECM has been shown to transform osteoconductive microfiber scaffolds into osteoinductive materials (6, 7, 9-11).

To create a more realistic *in vitro* model of the injured bone microenvironment and to elucidate the interplay of TNF-α and bone-like ECM, this study investigated the impact of varying doses of TNF-α delivered to osteogenically differentiating MSCs cultured on 3D biodegradable microfiber scaffolds containing pregenerated bone-like ECM. The objective of this study was to determine the impact of bone-like ECM on the concentration and temporal pattern of TNF-α delivery that enhances *in vitro* osteogenic differentiation of MSCs.

6.2. Methods and Materials

6.2.1. Experimental Design

The study design required the culture of two separate batches of MSCs on each electrospun poly(ε-caprolactone) (PCL) scaffold: one batch to generate the bone-like extracellular matrix (ECM), and a second batch for the actual experiment (Figure 6.1)

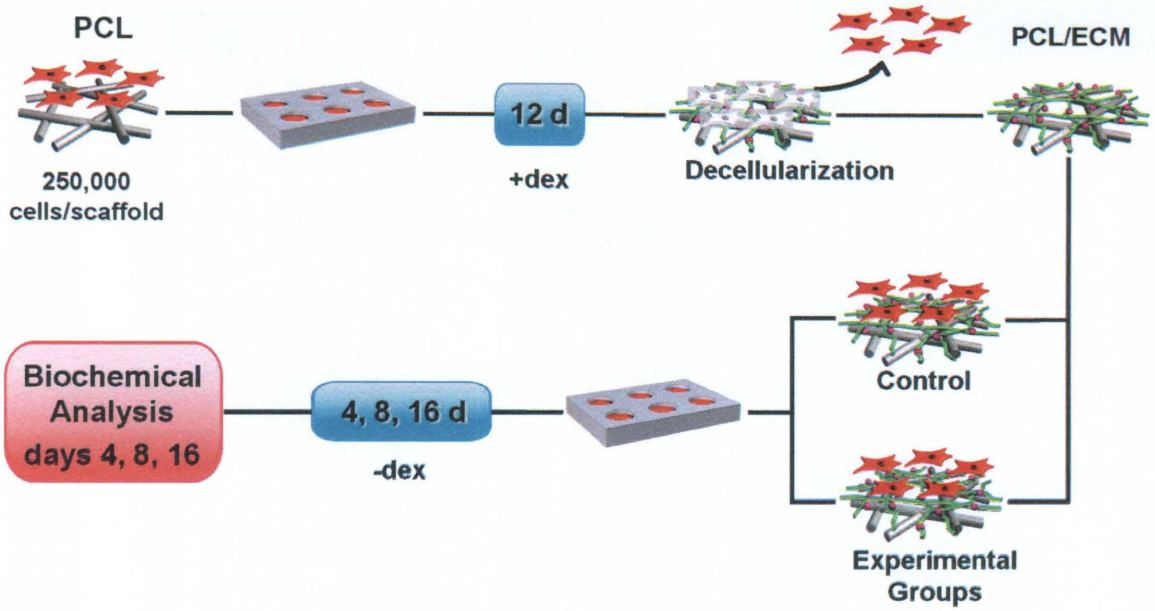

Figure 6.1: Overall study design using pregenerated bone-like ECM. Mesenchymal stem cells (MSCs) were isolated from rat bone marrow and cultured on electrospun PCL scaffolds in the presence of dexamethasone (+dex) and complete osteogenic media, which has been shown to stimulate production of bone-like ECM. These MSCs were removed and then replaced with a second batch of freshly isolated MSCs, which were subjected to the experimental conditions shown in Figure 6.2

A design with 7 groups and 3 time points was used to evaluate the impact of pregenerated bone-like ECM on the optimal TNF-α dose for rat MSC osteogenic differentiation (Figure 6.2). Based on the previous findings (see previous chapter) of very low TNF-α-induced mineralization under the current culture conditions, we selected

continuous TNF-α delivery as a temporal pattern because it triggered the highest amount of mineralization (other than the positive control) in the temporal variation study (see Figure 5.5). The three experimental groups received varying concentrations of TNF-α (0.1 ng/ml, 5 ng/ml, 50 ng/ml), that were identical to those in previous studies of MSCs on plain PCL scaffolds (see previous two chapters and (14)).

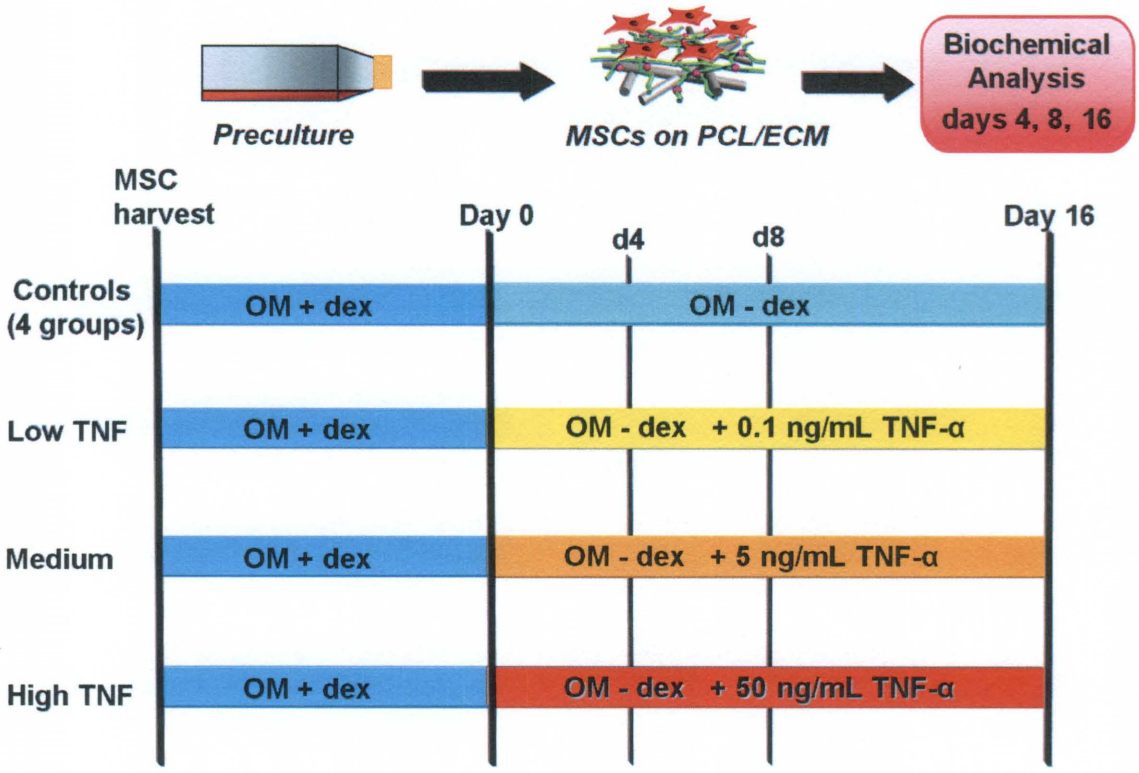

Figure 6.2: Schematic of study design for ECM and TNF-α interplay.
The four control groups consist of two negative controls seeded with MSCs precultured in "+dex" media (as shown) or in "-dex" media; a positive control seeded with MSCs precultured in "+dex" media that continued to receive dexamethasone during days 0-16, and a group of acellular PCL/ECM scaffolds. OM = Osteogenic Media (α-MEM, 10% v/v fetal bovine serum, 50 μg gentamicin/ml, 0.5 μg amphotericin-B/ml, 10 mM β-glycerophosphate, 50 μg/ml ascorbic acid) either with or without 10^{-8} M dexamethasone ("+dex" vs. "-dex").

Four control groups were included: a positive control seeded with MSCs precultured in complete (+dex) osteogenic media that continued to be supplemented with dexamethasone during the study; two negative controls cultured in dexamethasone-free media that differed in terms of the MSCs seeded (one group had MSCs precultured in +dex osteogenic media and the other had MSCs precultured in -dex media); and a group of acellular PCL/ECM scaffolds that were "cultured" in -dex media. This final group was included because similar ECM-coated scaffolds have been previously shown to undergo non-cell-specific scaffold calcium accumulation (11).

6.2.2. Electrospun PCL preparation

Electrospun PCL meshes were generated according to an established protocol (14). The PCL (Lactel, Pelham, AL) had a number-average molecular weight (M_n) of 59,000 ± 800 Da and polydispersity index (M_w/M_n) of 2.01 ± 0.03, determined via gel permeation chromatography (Phenogel Linear Column with 5 μm particles, Phenomenex, Torrance, CA; Differential Refractometer 410, Waters, Milford, MA) and a calibration curve generated from polystyrene standards (Fluka, Switzerland). A 10 ml syringe was loaded with an 18 w/w% solution of PCL in 5:1 (by vol) chloroform:methanol, fitted with a 16 gauge blunt-tip needle (Brico Medical Supplies, Inc., Metuchen, NJ), and positioned in the electrospinning apparatus so that the needle tip was 33 cm from a glass collecting plate placed over the system's grounded copper plate. A detailed description of this electrospinning apparatus has been published previously (14, 179). A voltage difference of 33 kV was applied to the needle tip and to a copper ring placed 4 cm from the needle tip. The PCL solution was pumped out of the needle at 40 ml/h using a syringe pump

until a ~1mm thick electrospun mesh was generated. All scaffolds used in this study were derived from two electrospun meshes.

Scaffolds with 8 mm diameter were cut from the meshes using biopsy punches (Miltex, York, PA). The thickness of each scaffold was measured using digital micro-calipers (Mitutoyo, Aurora, IL) and, for consistency with previous work (previous chapters as well as (14)), scaffolds with thickness 0.90-1.10 mm were used for the study. To prevent degradation or changes to the scaffold surface, electrospinning was performed two days prior to MSC seeding, which allowed just enough time to sterilize and prewet the scaffolds.

6.2.3. Scaffold Characterization

Scaffolds (n = 3) from each of the two electrospun meshes used in this study were mounted onto aluminum stubs, sputter-coated with 20 nm of platinum, and imaged using scanning electron microscopy (SEM) (FEI Quanta 400 Environmental, Hillsboro, OR) at a 7.0 kV accelerating voltage and 2.5 spot size. Predefined coordinates on each scaffold were imaged and the diameters of (n = 45 fibers) from the top and (n = 45 fibers) from the bottom of each mesh were measured using an established protocol (14, 179). The porosity of n = 50 scaffolds from each mesh was determined via an established gravimetric analysis protocol (14, 179).

6.2.4. Preparation of ECM-Coated Scaffolds

All MSC isolations were approved by the Rice University Institutional Animal Care and Use Committee and adhered to the National Institutes of Health guidelines. Two batches of cells were required for this study (see Figure 6.1) and were obtained from

separated MSC isolations. MSCs were isolated from the pooled femoral and tibial bone marrow of male syngeneic Fischer 344 rats weighing 150-175 g, according to established methods (8, 9). The MSCs from the first isolation (n = 8 rats) were used to generate the bone-like ECM. The bone marrow suspensions from this isolation were cultured in 75 cm^2 cell culture flasks using +dex complete osteogenic media: α-MEM (Gibco, Carlsbad, CA) with 10% v/v fetal bovine serum (Gemini Bio-Products, West Sacramento, CA), 50 μg/ml gentamicin, 0.5 μg/ml amphotericin-B, 10 mM β-glycerophosphate, 50 μg/ml ascorbic acid, and 10^{-8} M dexamethasone (Sigma, St. Louis, MO). As in previous studies, the medium was changed after one day and the non-adherent cells removed. The adherent cells were designated as "mesenchymal stem cells," based on the established osteogenic potential of this cell population under appropriate *in vitro* conditions (3, 14, 183). Thereafter, media was changed every two days. MSCs were cultured for a total of 7 days until nearly confluent and then seeded onto PCL scaffolds.

Prior to MSC seeding, and immediately after being punched from freshly electrospun meshes, the PCL scaffolds were sterilized via exposure to ethylene oxide gas for 14h and prewet using a decreasing ethanol gradient (from 100% to 70%), according to established protocols (14, 179). The ethanol was exchanged with sterile milliQ water, and then with sterile +dex media. The scaffolds (in media) were stored at 37°C overnight. The next day, the scaffolds were press-fit into sterile seeding cassettes and placed into ultra-low attachment 6-well plates (1 cassette/well) (Corning Incorporated Life Sciences, Lowell, MA) for seeding.

On the day of seeding, the nearly confluent MSCs were detached with 0.25% trypsin/EDTA (Gibco, Carlsbad, CA), counted with a hemocytometer, centrifuged, and

resuspended at 1.25 million cells/ml in +dex osteogenic media. 0.2 ml of the resuspended MSCs were added drop-wise to each seeding cassette containing a press-fit scaffold.

After a 4h attachment period, each well was filled with 8 ml of +dex media. After 24h, the constructs were moved to fresh ultra-low attachment 6 well plates containing 4 ml of fresh +dex media (1 scaffold/well). The constructs were cultured for 12 days total, with media changes every two days.

After 12 days, all scaffolds were removed from the media and rinsed twice with 4 ml of phosphate-buffered saline (PBS). For baseline calcium measurements, (n = 4) constructs were each placed into 1 ml of sterile milliQ water and flash-frozen. These constructs were stored at -20°C in a non-defrosting freezer until the day 4 timepoint, when they were decellularized and their calcium content was quantified in parallel to that of the day 4 samples. The remaining constructs were immediately decellularized according to an established protocol (9) to create the PCL/ECM scaffolds that were used for the experiment. Briefly, the scaffolds were placed in 1.5 ml sterile milliQ water, flash-frozen, and stored at -20°C overnight. The next day, the scaffolds were thawed at 37°C for 10 min, rinsed twice with 2 ml PBS, and then placed in 1.5 ml fresh sterile milliQ water. Aseptic techniques were used for all steps. The entire freeze (this time using liquid nitrogen for 10 min)/thaw (37°C for 10 min)/rinsing cycle was repeated two more times, and then the (now decellularized) PCL/ECM scaffolds were press-fit into sterile seeding cassettes. Each seeding cassette was placed into the well of a sterile ultra-low attachment 6-well plate (Corning) for MSC seeding.

6.2.5. MSC Isolation for TNF-α Culture

On the sixth day of ECM pregeneration, a new batch of MSCs were isolated from the pooled femoral and tibial bone marrow of (n = 6) male syngeneic Fischer 344 rats weighing 150-175 g, according to established methods (8, 9). The bone marrow suspensions from each rat were split into two portions and cultured in either +dex or -dex media (equivalent to +dex media except that it lacks dexamethasone) in fresh 75 cm^2 culture flasks. As for the previous isolation, non-adherent cells were removed after 24h and the MSCs were cultured for 7 days total.

On the day of seeding, which was the same day that the decellularized PCL/ECM scaffolds were prepared, the nearly confluent MSCs were detached with 0.25% trypsin/EDTA (Gibco, Carlsbad, CA), counted with a hemocytometer, centrifuged, and resuspended at 1.25 million cells/ml in -dex osteogenic media. The cells that had been precultured in -dex media were lifted and resuspended separately from those precultured in +dex media. For the MSCs precultured in -dex media, 0.2 ml of the cell suspension were added to (n = 13) PCL/ECM scaffolds; this was the -dex/-dex control group (see Figure 6.2). For the acellular group, (n = 13) PCL/ECM scaffolds were press-fit into seeding cassettes but were not seeded with any MSCs. The remaining PCL/ECM scaffolds were seeded with +dex-precultured cells (0.2 ml cell suspension/scaffold, corresponding to 0.25 million cells/scaffold).

After allowing 4h for cell attachment, each well was filled with 8 ml of -dex media and the relevant groups (see Figure 6.2) were supplemented with either dexamethasone (to achieve a 10^{-8} M concentration) or 4 μl/well of the appropriate TNF-α stock solution.

6.2.6. TNF-α Reconstitution and Dilution

Recombinant rat TNF-α (R&D Systems, Minneapolis, MN) was reconstituted at 100 ng/μl on the day of scaffold seeding using sterile PBS containing 0.1 w/w% bovine serum albumin (Sigma), according to the manufacturer's instructions. The stock solution was then further diluted to prepare 0.1 ng/μl, 5 ng/μl, and 50 ng/μl stock solutions. For experiments, 4 μl of TNF-α stock solution were added to 4 ml of media used for construct culture, resulting in the desired 0.1 ng/ml, 5 ng/ml, or 50 ng/ml TNF-α.

6.2.7. Cellularity, Alkaline Phosphatase Activity, and Calcium Content Assays

On days 4, 8, and 16 of the culture of the second batch of MSCs on PCL/ECM (see Figure 6.1), (n = 4) scaffolds from each group were removed, rinsed twice with 4 ml of PBS, and flash-frozen in 1 ml of sterile milliQ water using liquid nitrogen. The cells were lysed using three consecutive freeze/thaw/sonication cycles (10 min at -80°C, 10 min at 37°C, 10 min sonication). The DNA content of each resulting cell lysate was quantified using the fluorometric PicoGreen assay (Molecular Probes, Eugene, OR) and then converted to the number of cells per construct (9, 14). The alkaline phosphatase (ALP) activity of the cell lysates was quantified using an established colorimeteric assay based on the rate of conversion of the colorless substrate p-nitrophenyl phosphate disodium salt hexahydrate (Sigma), to a yellow product, p-nitrophenol (9, 14). Next, each construct was transferred into 1 ml 1 N acetic acid and left on a shaker table at 200 rpm overnight to dissolve matrix-bound calcium. Calcium content was quantified using an established colorimetric assay that is based on the Arsenazo III calcium chelating agent (Genzyme Diagnostics PEI, Charlottetown, Prince Edward Island, Canada). Samples and

standards were run in triplicate for all assays. Samples were diluted as necessary to fall within the range of the standards for each assay. A detailed experimental procedure for each of these biochemical assays is provided on pages 58-59 and has also been published (9, 14).

6.2.8. Sample Preparation for Histology and SEM

At the final timepoint, $n = 1$ construct from each of the seven groups was rinsed twice with PBS and cut in half with a sterile razorblade. One half of each construct was prepared for SEM via fixation in 2.5% glutaraldehyde (Sigma) overnight and then dehydration through an ascending ethanol gradient (70% to 100%). The samples were air-dried overnight, mounted on aluminum stubs, coated with platinum, and imaged with SEM as described above (see "Scaffold Characterization").

The other half of each construct was fixed overnight in 5 ml of 10% buffered formalin phosphate (Fisher Scientific, Pittsburgh, PA), passed through an ascending ethanol gradient (70% to 100%), and embedded in HistoPrep (Fisher Scientific) overnight at room temperature. Frozen 5 μm thick sections were cut with a cryotome (CM1850, Leica Microsystems, Bannockburn, IL), placed on Superfrost Plus slides (VWR, Radnor, PA), and incubated at 45°C on a slide warmer for 4-5 days to achieve optimal section adhesion (14).

On the day of histological staining, the sections were rehydrated with water. The slides were then flooded with von Kossa stain (5% w/w silver nitrate (Sigma) in milliQ water) and kept under an ultraviolet (UV) lamp for 30 min. The slides were rinsed with water and then 95% ethanol. Alcoholic eosin Y (Sigma) was applied as a counter-stain for 3 min. The slides were rapidly dehydrated and cleared with 95% ethanol, and then

imaged with a light microscope (Eclipse E600, Nikon, Melville, NY) equipped with a camera (3CCD Color Video Camera DXC-950P, Sony, Park Ridge, NJ) and image-capture software. Light microscope images were calibrated using the standard two-image method to correct for differences in background lighting and in dark-current effects in the detector (185).

6.2.9. Statistical Analysis

Fiber diameters and porosities are reported as mean ± standard deviation for n = 45 fibers and n = 50 scaffolds, respectively. The average fiber diameter of the top and bottom of each PCL microfiber mesh, along with the average porosity, were compared using a Student's t-test for two independent samples with equal variance ($\alpha = 0.05$) after performing an F-test to validate the assumption of equal variance at 95% confidence. Cellularity, ALP activity, and calcium assay results are reported as mean ± standard deviation for n = 4 constructs. Statistical amongst groups at each time point, and also within each group over time, were analyzed at 95% confidence using one-way analysis of variance. Multiple pair-wise comparisons were made using the Bonferroni post-hoc analysis method at 95% confidence.

6.3. Results and Discussion

6.3.1. Electrospun PCL morphology

The morphology of representative scaffolds from this study is shown in Figure 6.3, imaged via SEM at varying magnifications. The top surfaces of the PCL microfiber meshes, which were seeded with MSCs, had statistically equivalent mean fiber diameters

($p > 0.05$), as shown in Table 6.1. However, one mesh had a slightly higher mean fiber diameter at the bottom (~14 μm). Despite this minor differences, the two electrospun PCL microfiber meshes fabricated for this study had statistically equivalent mean porosities ($p > 0.05$) (Table 6.1).

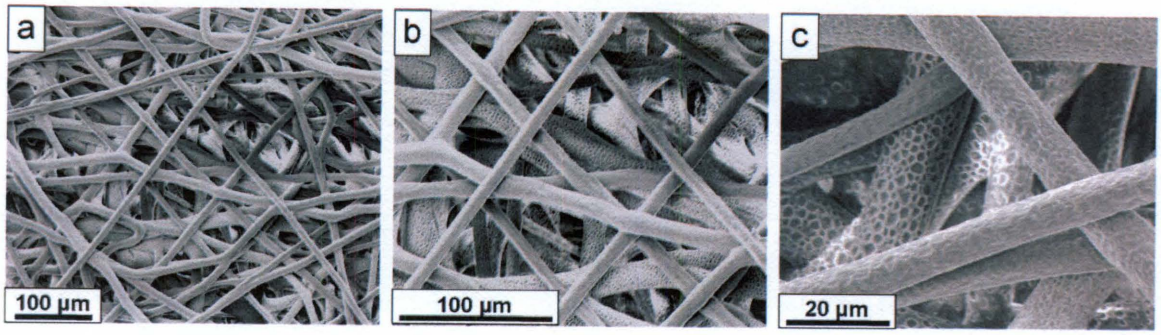

Figure 6.3: Representative scaffold morphology via SEM.
Representative scaffolds from the electrospun PCL meshes generated for this study, imaged via SEM at varying magnifications, (a) 300×, (b) 600×, and (c) 2000×. Scale bars for (a,b) are 100 μm, while the scale bar (c) is 20 μm.

Table 6.1 Comparison of fiber diameters and porosites for the two electrospun meshes used for this study.

Parameter for Comparison	Value for Mesh 1	Value for Mesh 2
Fiber Diameter, Top (μm)	10.9 ± 2.0	11.8 ± 1.2
Fiber Diameter, Bottom (μm)	11.3 ± 1.4*	13.6 ± 2.4*
Porosity (%)	80.6 ± 2.1	80.1 ± 2.0

Values are presented as mean ± standard deviation. The sample size was $n = 45$ for fiber diameters from the top and bottom of each mesh, and $n = 50$ scaffolds for PCL mesh porosity. * indicates pairs of values that significantly differ ($p < 0.05$).

6.3.2. PCL/ECM construct cellularity

Figure 6.4 depicts the construct cellularity at each timepoint. When the same treatment groups were cultured on plain PCL (Figure 5.7a), all groups had similar day 4 and day 8 cellularity, with the exception of the +dex-precultured negative control (0 ng/mL TNF), which had a much higher cell count than all other groups on day 8.

In contrast, the presence of bone-like ECM suppressed the proliferation of the negative control groups (0 ng/mL TNF and 0 ng/mL TNF (pre: -dex) in Figure 6.4) compared to plain PCL (+dex/-dex and -dex/-dex, respectively, in Figure 5.3). The cellularity of the positive control was fairly similar on both PCL/ECM and plain PCL, and the acellular constructs ("Acellular") had nearly zero cells at all timepoints, as expected.

On PCL/ECM, MSCs supplemented with TNF-α had slightly higher day 4 and day 8 cell counts, and much lower day 16 values (Figure 6.4), compared to the analogous groups on plain PCL scaffolds (Figure 5.7a). The presence of bone-like ECM, combined with TNF-α, appears to have stimulated MSC proliferation at the early timepoints, and slowed proliferation between days 8-16 (Figure 6.4).

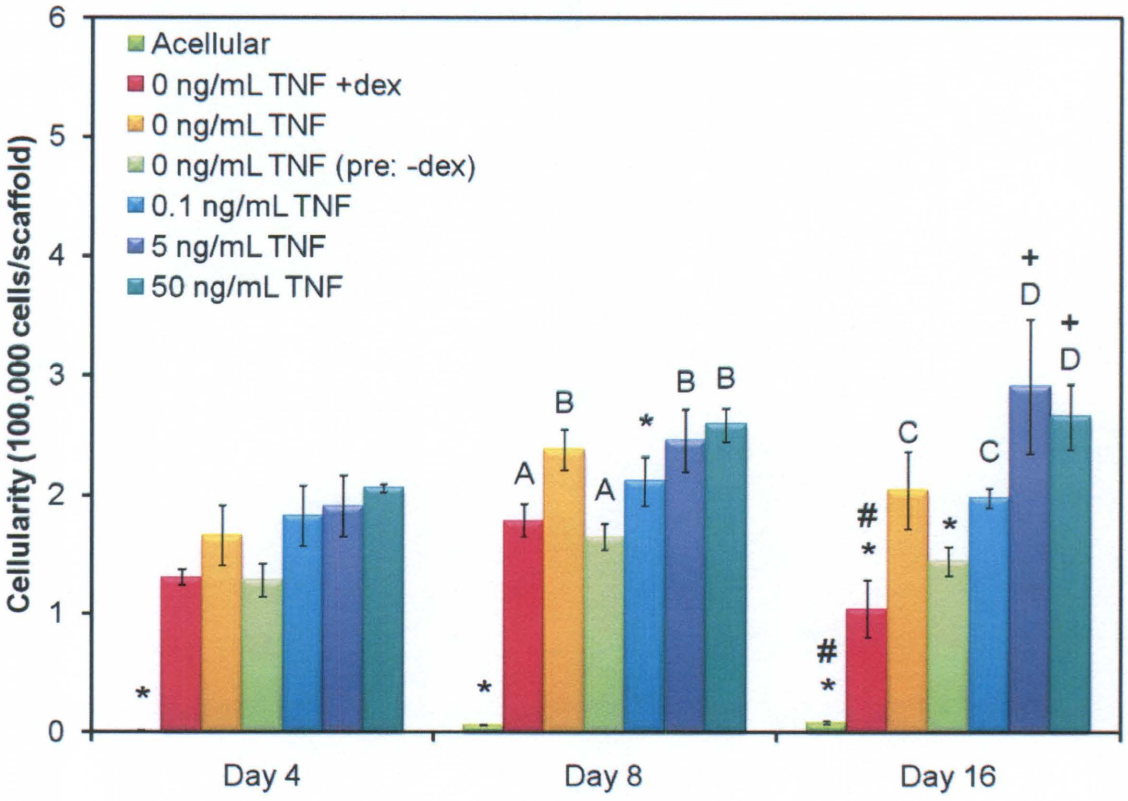

Figure 6.4: MSC cell count on preformed ECM and varying TNFα dose

Scaffolds with pregenerated bone-like ECM (PCL/ECM) were seeded with MSCs precultured in +dex media (except for the group designated "(pre: -dex)," which was seeded with MSCs precultured in -dex media). Experimental groups were exposed to varying TNF-α doses. The control groups included acellular PCL/ECM, a positive control cultured in +dex media (0 ng/mL +dex), and two negative controls cultured in -dex media (0 ng/mL TNF) containing MSCs precultured in either +dex or -dex media (the latter is denoted with "pre: -dex"). Bars represent average ± standard deviation of (n = 4) scaffolds per group at each timepoint. Within a timepoint, groups with * differ from all other groups ($p < 0.05$), while letters A-D indicate groups that differ from all other groups but not groups with the same letter ($p < 0.05$). On day 16, + indicates that d4 and d16 values of that group differ ($p < 0.05$), while # indicates that values at all timepoints differ ($p < 0.05$).

6.3.3. PCL/ECM construct ALP activity

The presence of preformed ECM greatly increased the ALP activity of all groups by several fold, which is particularly evident in comparing the y-axis of Figure 6.5b (maximum value: 55 pmol/hour/cell) to that of Figure 5.7c (maximum value 15 pmol/hour/cell). The most prominent change was in the acellular constructs, which had much higher ALP activity on PCL/ECM (Figure 6.5a) compared to plain PCL (Figure 5.7b), despite near-zero cellularity (Figure 6.4). The ALP detected on the acellular PCL/ECM constructs likely reflects ALP secreted by the first batch of MSCs, which generated the ECM. Studies of native rat bone have shown that ALP exists in both a membrane-bound form, on the external surface of osteoblasts, and also as a free extracellular enzyme localized near the collagen fibers of mineralizing osteoid (193). It is likely that the values for the acellular group in Figure 6.5 reflect the activity of this latter "free" ALP, since nearly complete decellularization of the PCL/ECM was achieved (Figure 6.4).

In contrast to the monotonic increasing trends observed on plain PCL for the negative control groups (see "+dex/-dex" and "-dex/-dex" in Figure 5.4), as well as for the 0.1 ng/mL TNF group (see group with same name in Figure 5.7c), the ALP activity per cell for each of these groups on PCL/ECM was fairly constant on days 4-8 and then slightly increased by day 16 (see "0 ng/mL TNF," "0 ng/mL TNF (pre: -dex)," and "0.1 ng/mL TNF" groups in Figure 6.5b).

Aside from the change in the magnitude of the ALP activity values, the positive control group (0 ng/mL +dex) and the 5 and 50 ng/mL TNF groups had the same trends in ALP activity on plain PCL and on PCL/ECM: a monotonic increase in ALP activity

for the positive control, and a monotonic decrease for the 5 and 50 ng/mL TNF groups. On both plain PCL (Figure 5.7b) and PCL/ECM (Figure 6.5a), the ALP activity per scaffold for the 5 and 50 ng/mL TNF groups was indistinguishable from that of the acellular constructs on days 8 and 16, suggesting that the increased ALP values on PCL/ECM were due to the extracellular ALP, which was not affected by TNF-α.

a

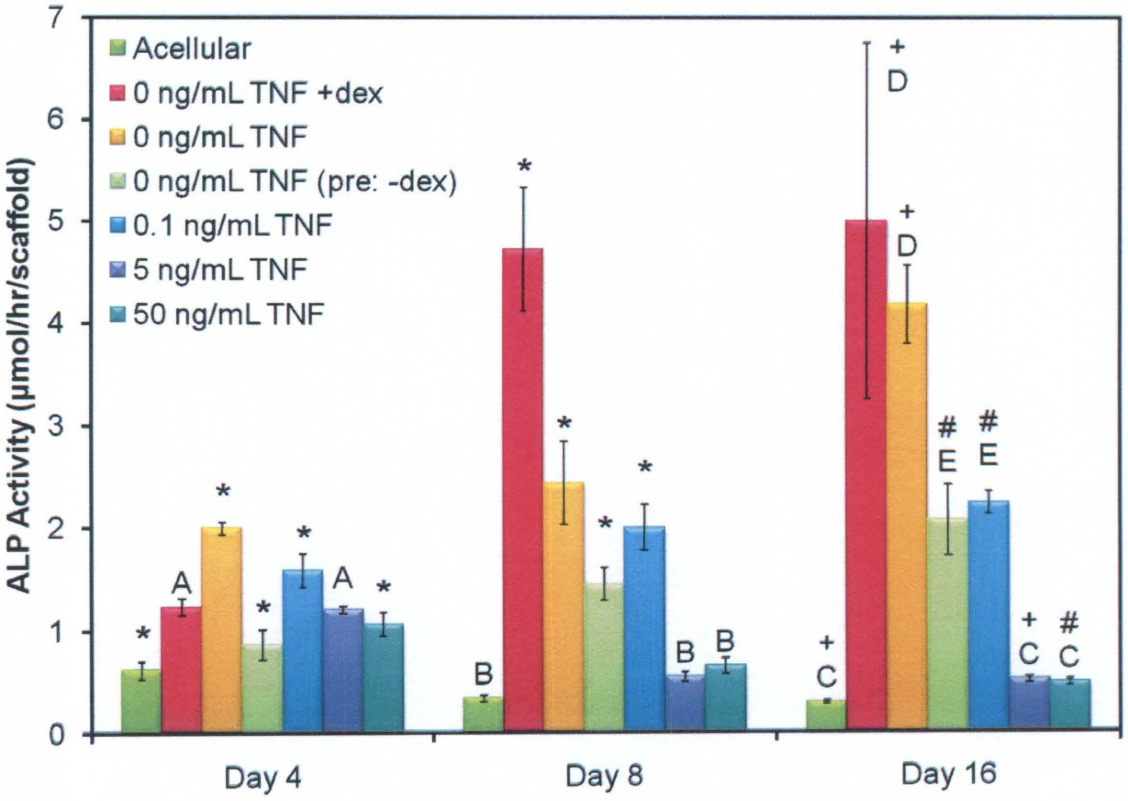

Figure 6.5: ALP activity of MSCs on preformed ECM with varying TNF-α dose – continued on next page.

b

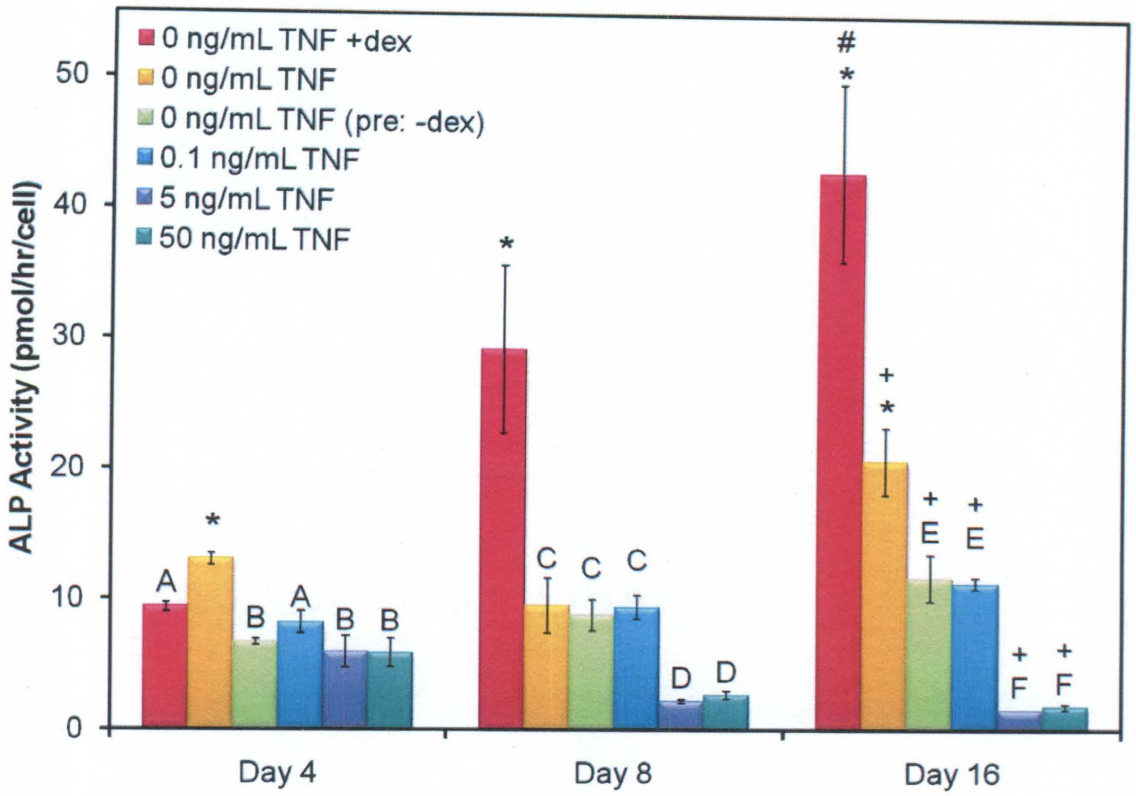

Figure 6.5: ALP activity of MSCs on preformed ECM with varying TNF-α dose
Scaffolds with pregenerated bone-like ECM (PCL/ECM) were seeded with MSCs precultured in +dex media (except for the group designated "(pre: -dex)," which was seeded with MSCs precultured in -dex media). ALP activity on a per scaffold basis is shown in (a), while the same data on a per cell basis is shown in (b) with the exception of the acellular group. Experimental groups were exposed to varying TNF-α doses. The control groups included acellular PCL/ECM, a positive control cultured in +dex media (0 ng/mL +dex), and two negative controls cultured in -dex media (0 ng/mL TNF) containing MSCs precultured in either +dex or -dex media (the latter is denoted with "pre: -dex"). Bars represent average ± standard deviation of ($n = 4$) scaffolds per group at each timepoint. Within a timepoint, groups with * differ from all other groups ($p < 0.05$), while letters A-F indicate groups that differ from all other groups but not groups with the same letter ($p < 0.05$). On day 16, + indicates that d4 and d16 values of that group differ ($p < 0.05$), while # indicates that values at all timepoints differ ($p < 0.05$).

6.3.4. PCL/ECM construct mineralization

The baseline calcium content of the PCL/ECM was 140 ± 13 μg Ca^{2+}/scaffold, which is indicated by the dashed line in Figure 6.6. Comparison to the analogous study on plain PCL scaffolds (Figure 5.7d) indicates that the presence of pregenerated ECM stimulated a huge increase in the calcium values of all groups.

The presence of ECM caused the acellular constructs to accumulate calcium at a rapid, linear rate (~23 μg/day). This phenomenon has been previously reported for PCL microfiber scaffolds with smaller fiber diameter (~5 μm, compared to ~10 μm in this study) that were coated with ECM generated under similar *in vitro* culture conditions (11). Remarkably, despite the presence of ECM, the dexamethasone-naïve negative control group (0 ng/mL TNF (pre: -dex)) ceased to mineralize between days 4 and 8. Although some calcium deposition occurred between days 8 and 16, this group had the lowest calcium content at the final timepoint ($p < 0.05$). This type of negative control was not included in the previous study of PCL/ECM (11), which only included a negative control with MSCs precultured in +dex media (analogous to the "0 ng/mL TNF" group in Figure 6.6). The low calcium content of the "0 ng/mL TNF (pre: -dex)" negative control indicates that the presence of dexamethasone-naïve cells and/or the ECM secreted by these cells inhibited the non-cell-specific calcium accumulation of the pregenerated ECM. This suggests that the dexamethasone-naïve (0 ng/mL TNF (pre: -dex)) constructs may be a superior negative control compared to acellular PCL/ECM, since all other groups also contain cells, which would also presumably reduce non-cell-specific calcium accumulation.

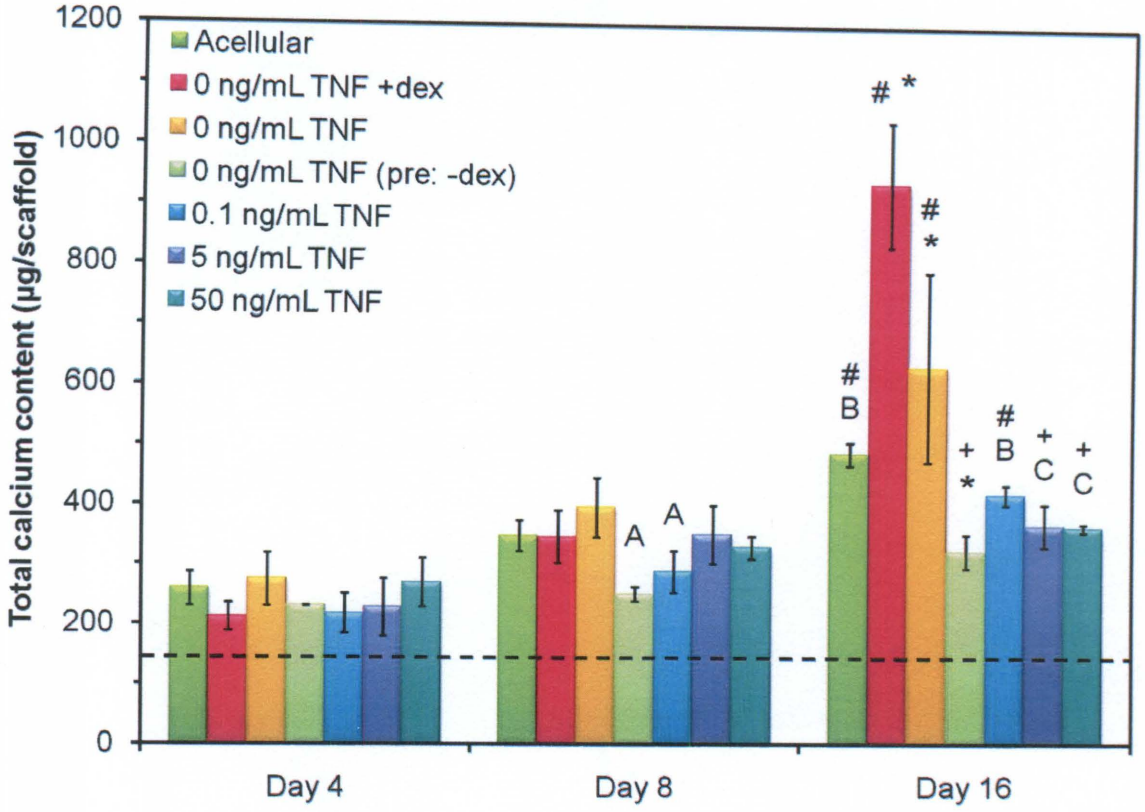

Figure 6.6: MSC calcium deposition on PCL/ECM with varying TNF-α dose
The baseline calcium content of the PCL scaffolds with pregenerated bone-like ECM (PCL/ECM) was 140 ± 13 µg Ca^{2+}/scaffold, which is indicated by the dashed line. PCL/ECM scaffolds were seeded with MSCs precultured in +dex media (except for the group designated "(pre: -dex)," which was seeded with MSCs precultured in -dex media). Experimental groups were exposed to varying TNF-α doses. The control groups included acellular PCL/ECM, a positive control cultured in +dex media (0 ng/mL +dex), and two negative controls cultured in -dex media (0 ng/mL TNF) containing MSCs precultured in either +dex or -dex media (the latter is denoted with "pre: -dex"). Bars represent average ± standard deviation of (n = 4) scaffolds per group at each timepoint. Within a timepoint, groups with * differ from all other groups ($p < 0.05$), while letters A-C indicate groups that differ from all other groups but not groups with the same letter ($p < 0.05$). On day 16, + indicates that d4 and d16 values of that group differ ($p < 0.05$), while # indicates that values at all timepoints differ ($p < 0.05$).

The +dex-precultured negative control (0 ng/mL TNF) constructs had slightly higher calcium content than the positive control group (0 ng/mL TNF +dex) at both of the

early timepoints ($p > 0.05$; Figure 6.6), which greatly differed from the pattern observed on plain PCL (Figure 5.7d) where the positive control had much greater calcium content at all timepoints ($p < 0.05$). By day 16, the calcium content of both the positive control (0 ng/mL TNF +dex) and the +dex-precultured negative control (0 ng/mL TNF) exceeded that of the acellular PCL/ECM constructs ($p > 0.05$; Figure 6.6). A similar pattern was observed in the previous study of ECM-coated 5 μm PCL microfibers, although the pattern of per cell ALP activity in that study differed from that shown in Figure 6.5b in that both groups exhibited peak ALP activity on day 8 (11).

The presence of pregenerated ECM greatly altered the calcium deposition in response to varying doses of TNF-α. In the analogous study on plain PCL (Figure 5.7d), all doses of TNF-α stimulated day 4 calcium deposition that was greater ($p < 0.05$) than that of the negative control (0 ng/mL TNF) and equivalent to that of the positive control group (0 ng/mL TNF +dex). In that same study, from days 4-8, the higher TNF-α doses (5 and 50 ng/mL TNF) continued to stimulate calcium deposition that exceeded that of the negative control ($p < 0.05$) and was equivalent to that seen with dexamethasone (0 ng/mL +dex), although by day 16 the positive control group had much higher calcium content ($p < 0.05$) than the TNF-α groups (Figure 5.7d). In contrast, on PCL/ECM, the highest dose of TNF-α (50 ng/mL TNF) resulted in day 4 calcium content that was slightly higher than that of the positive control ($p = 0.08$), but equivalent to that of the +dex-precultured negative control (0 ng/mL TNF) and the acellular constructs (Figure 6.6). On day 8, as seen on plain PCL, the constructs exposed to higher doses of TNF-α (5 and 50 ng/mL TNF) had equivalent calcium content to the positive control (0 ng/mL +dex). However, in contrast to plain PCL, this calcium content was also equivalent to that

of the +dex-precultured negative control (0 ng/mL TNF) and yet significantly exceeded ($p < 0.05$) the calcium deposition of the 0.1 ng/mL TNF group. Thus, comparing the day 8 calcium values on plain PCL (Figure 5.7d) and PCL/ECM (Figure 6.6) indicates that the presence of ECM reduced the impact of both dexamethasone and the higher doses of TNF-α. This may reflect complex signaling from the ECM molecules. SEM imaging (Figure 6.7) and histology (Figure 6.8) confirmed that cells and matrix coated the surfaces of the scaffolds and also penetrated into the pores between the PCL fibers.

The difference between TNF-α effect on MSCs cultured on plain PCL and on PCL/ECM constructs was most evident at the final timepoint. TNF-α caused a dose-dependent increase in day 16 calcium content on plain PCL ($p < 0.05$; Figure 5.7d), and a dose-dependent decrease in calcium content on PCL/ECM ($p < 0.05$; Figure 6.6). The dose-dependent decrease seen in this study differs from the results of previous studies of osteoprogenitors cultured *in vitro* and exposed to TNF-α in the absence of dexamethasone; in those studies, TNF-α stimulated a dose-dependent increase in mineralized matrix deposition (14, 112, 159-161). However, with the exception of one study (14), in which MSCs were cultured on 3D plain PCL microfiber meshes, all of these other studies involved delivery of TNF-α to cells cultured in 2D (112, 159-161). Thus, the effects noted in this study likely reflect the interplay of the 3D bone-like ECM and TNF-α.

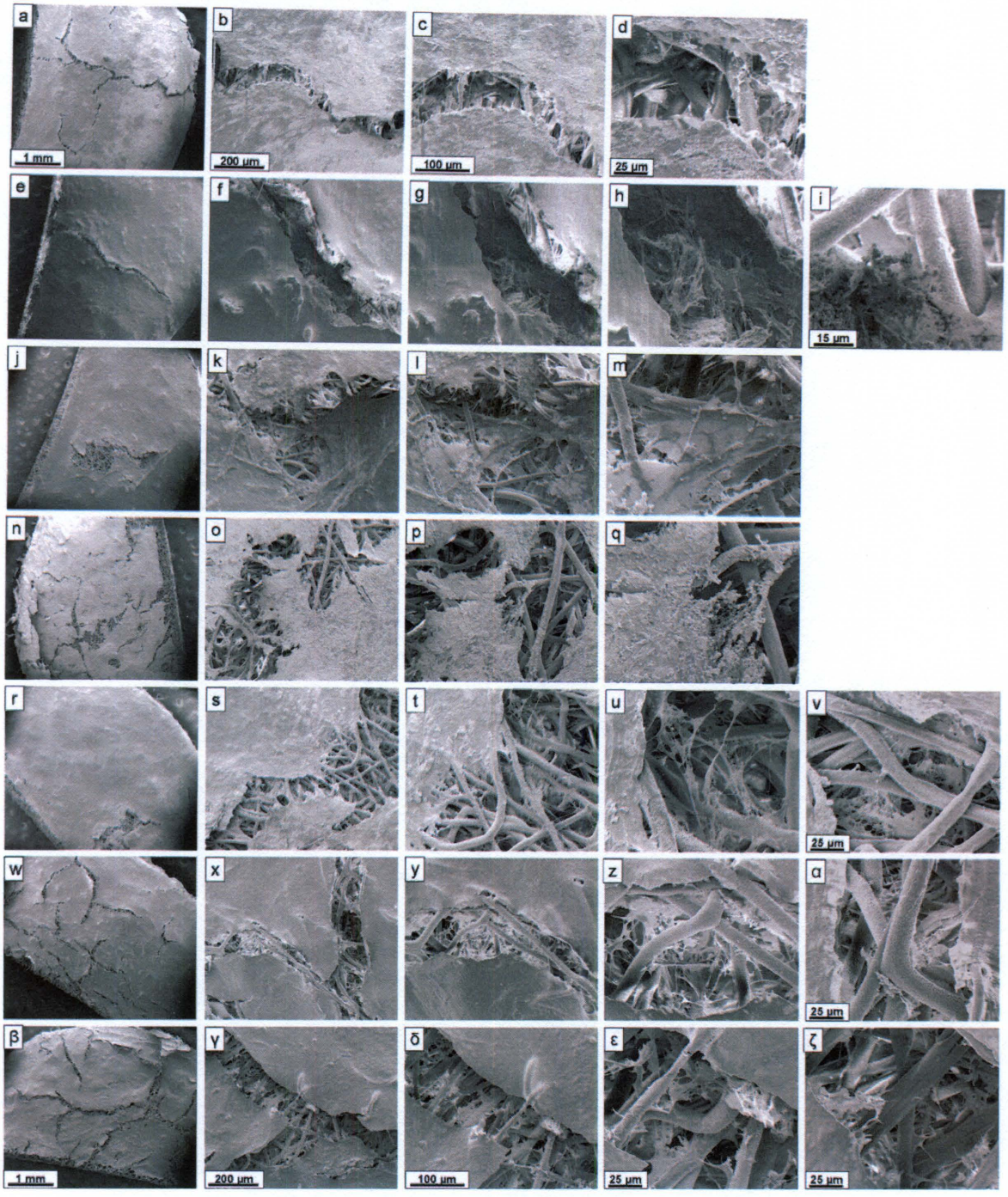

Figure 6.7: Surface morphology of PCL/ECM after 16 days of culture

On the final day of the study, the surface of one half of a representative scaffold from each group was imaged via SEM. Images in each row are from the same group, and images in each column have the same magnification (with the exception of the right-most column). Specifically, the images depict: (a-d) the positive control (0 ng/mL +dex in other Figures); (e-i) the negative control cultured in -dex media (0 ng/mL TNF); (j-m) the negative control seeded with dexamethasone-naïve MSCs and cultured in -dex media (0

ng/mL TNF (pre: -dex)); and (n-q) acellular PCL/ECM (Acellular). The final three rows of images depict the experimental groups cultured with varying doses of TNF-α: (r-v) 0.1 ng/ml, (w-α) 5 ng/ml, and (β-ζ) 50 ng/ml. The original magnification of the images in the columns (from left to right) is: 34× (scale bar is 1 mm), 200× (scale bar is 200 μm), 400× (scale bar is 100 μm), 1000× (scale bar is 25 μm). The images in the final column were taken at 1000× (scale bar is 25 μm), except for (i) which was taken at 2000× (scale bar is 15 μm). For all columns except for the right-most column, the scale bars at the top and bottom of each column apply to all images within that column.

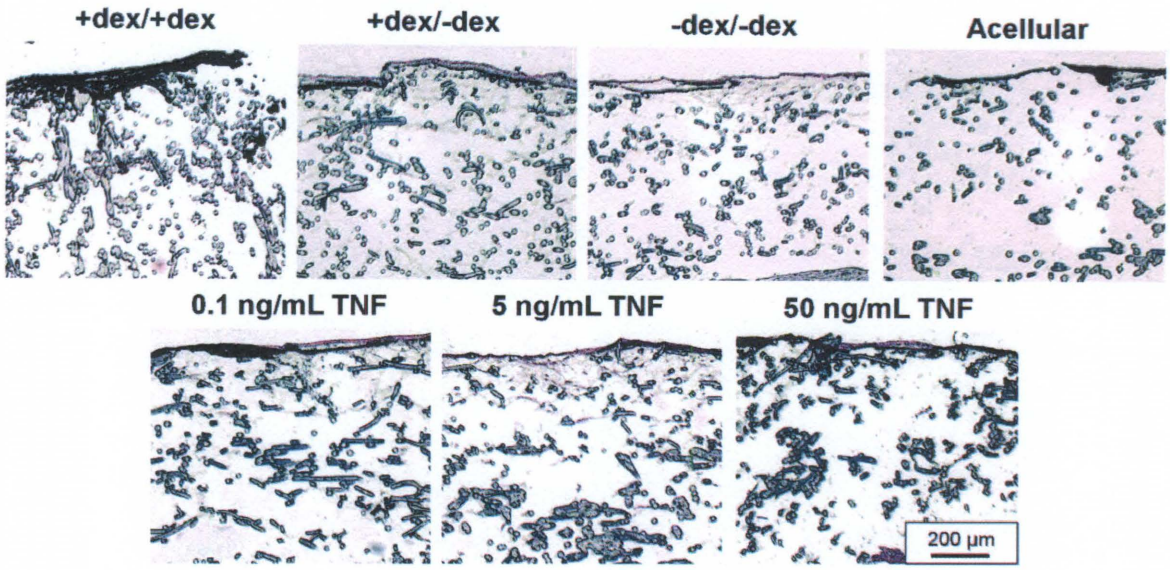

Figure 6.8: Construct cell and mineral distribution visualized by histology
Representative cross-sections of MSC-seeded PCL/ECM scaffolds after 16 days of culture. MSCs were precultured in complete osteogenic media (+dex) or in dexamethasone-free media (-dex). The positive control (+dex/+dex) continued to receive dexamethasone after MSCs were seeded onto the scaffold. All other MSC/scaffold constructs were cultured in dexamethasone-free media. Experimental groups shown were continuously supplemented with 0.1, 5, or 50 ng/ml TNF-α (abbreviated "TNF" in the figure). 5 μm thick sections were stained with von Kossa, which stains mineralized matrix black (blue arrows), and eosin, which stains cells and non-mineralized matrix reddish-pink (yellow arrows). Images were captured at 10× original magnification. Scale bar in the lower right corner represents 200 μm and applies to all images.

As previously observed in a similar 3D culture system containing biodegradable microfibers coated with bone-like ECM (11), MSCs cultured on PCL/ECM continued to undergo osteogenic differentiation and deposit mineralized matrix in the absence of dexamethasone (Figure 6.6 and Figure 6.8). This is remarkable because dexamethasone is typically required for *in vitro* osteogenic differentiation of MSCs (4). However, since corticosteroid signaling is not involved in *in vivo* bone regeneration, and may even inhibit fracture healing (128, 191), our findings suggest that culture on 3D PCL/ECM constructs is a better model of *in vivo* MSC osteogenic differentiation.

The findings of this study with respect to TNF-α may be a reflection of the fact that PCL/ECM constructs are a more realistic model of the *in vivo* fracture microenvironment. Although TNF-α signaling is critical for *in vivo* bone regeneration (1), the distinct temporal pattern of its expression cannot be ignored (see Figure 2.1). In murine models, TNF-α signaling peaks 24h following bone injury, returns to baseline levels after a few days, and then rises again several weeks later (59). In a recent study of a fracture healing model, daily local injections of TNF-α during the first two days after bone fracture significantly increased fracture callus mineralization four weeks later (112). However, chronic exposure to high levels of TNF-α has damaging effects on *in vivo* fracture healing, including decreased bone volume and reduced bone mechanical strength (120). The pattern of mineralized matrix deposition seen on PCL/ECM is consistent with these *in vivo* findings. At early timepoints, high doses of TNF-α did not adversely affect calcium content. However, 16 days of continuous TNF-α delivery caused a dose-dependent decrease in mineralized matrix deposition (Figure 6.6). These results for TNF-α highlight the exciting potential of PCL/ECM constructs as a more clinically realistic *in*

vitro culture model to improve our understanding of the *in vivo* effects of various cytokines.

6.4. Conclusions

This study demonstrated that continuous delivery of the pro-inflammatory cytokine TNF-α over 16 days reduces mineralized matrix deposition, a late stage marker of osteogenic differentiation, when delivered to MSCs cultured in 3D electrospun PCL microfiber meshes coated with pregenerated bone-like ECM ("PCL/ECM"). As previously observed in a similar 3D culture system, MSCs cultured on PCL/ECM continued to undergo osteogenic differentiation and deposit mineralized matrix in the absence of dexamethasone. Exposure to TNF-α for 4-8 days caused a dose dependent decrease in cell-specific ALP activity, which is an early marker of osteogenic differentiation, and did not adversely affect mineralized matrix deposition. However, continuous TNF-α delivery over 16 days markedly reduced calcium deposition compared to the untreated control group. These results simulate the *in vivo* response to TNF-α, where brief, highly regulated signaling stimulates bone regeneration, while prolonged signaling has damaging effects on bone. Thus, this study underscores the exciting potential of PCL/ECM constructs as a more clinically realistic *in vitro* culture model to improve our understanding of the impact of various cytokines on MSC osteogenic differentiation, which will ultimately facilitate the design of new tissue engineering strategies to rationally control inflammation and promote bone regeneration.